DISSERTATION

INVESTIGATION INTO THE MECHANISMS OF BONE LOSS IN A SHEEP MODEL OF OSTEOPOROSIS

Submitted by

Katherine T. Bisazza

Department of Clinical Sciences

In partial fulfillment of the requirements

For the Degree of Doctor of Philosophy

Colorado State University

Fort Collins, Colorado

Spring 2024

Doctoral Committee:

Advisor: Jeremiah T. Easley

Russell V. Anthony
Kirk McGilvray
Laurie R. Goodrich
Bradley B. Nelson

ABSTRACT

INVESTIGATION INTO THE MECHANISMS OF BONE LOSS IN A SHEEP MODEL OF OSTEOPOROSIS

Osteoporosis is the most common metabolic bone disease in humans and the leading cause of fragility fractures in the aging population. Given the invasiveness of researching bone diseases in people, appropriate animal models are essential to both build our understanding of the disease as well as examine novel therapeutics. While small animals and rodents are more commonly used as models in bone research, large animal models offer the ability to perform robust, long-term studies on bone quality with higher translational impact. Ovariectomized sheep are a well-established large animal model for osteoporosis because of the comparable bone size and microarchitecture that is shared with humans. While the ovariectomized sheep has been utilized for decades as a model for the study of bone, many gaps in the model characterization remain. Based on results from a preliminary literature search, we developed study objectives and hypotheses to expand upon current knowledge gaps in the characterization of the sheep model of osteoporosis. In order to test these aims, we performed a single 12-month *in vivo* study utilizing sixteen ewes. Osteoporosis was induced experimentally in ten of these ewes via ovariectomy followed by a 24-week regimen of high dose corticosteroids, while six ewes were used as healthy seasonal controls.

In our first aim, we compared the bone density and microarchitectural changes in the osteoporotic animals as compared to healthy controls over the course of a year. Dual-energy x-

ray absorptiometry (DXA) scans revealed significant bone density loss in the osteoporotic animals in both the lumbar spine and tibia as compared to control animals. We also noted significant microarchitectural changes in iliac crest bone biopsies of osteoporotic animals as indicated by micro-computed tomography (microCT), including decreased bone volume fraction, trabecular thickness, and trabecular number, as well as increased trabecular spacing. Additionally, we compared the use of quantitative computed tomography (QCT) and DXA to measure bone mineral density and correlated those findings with microarchitectural parameters in the osteoporotic animals. We demonstrated superior QCT sensitivity and specificity to subtle bone changes in the lumbar spine as compared to DXA, as well as demonstrated a higher correlation of QCT with iliac crest biopsy microarchitectural changes.

The second aim of our study was to explore the systemic and clinical impacts of osteoporosis model development in our ten sheep compared to the healthy control animals. To test this aim, we collected blood, bone marrow, and body weights throughout the course of the year-long study. Osteoporotic animals demonstrated significant impacts to hematology and serology blood levels over the course of model development, primarily at 3 and 6-months when corticosteroids were at peak use. In particular, we note significant reductions in monocytes, lymphocytes, and eosinophils at 3-months with accompanying neutrophilia, as well as an increase in platelet count and volume. We also observed an increase in serum phosphorus and electrolytes, decrease in kidney enzymes and total protein, and an increase in select liver enzymes at 3 and 6-months in the same animals. Serum cortisol and estradiol were significantly depleted at 3 and 4-months, respectively, in the osteoporotic animals. However, estradiol levels were maintained to control levels for the remainder of the study. All these changes indicate

disruptions to multiple physiologic systems over the course of osteoporosis induction in sheep which may highlight the acute effects of administering high-dose glucocorticoids.

In the third and final aim of this study, we investigated the morphometrical and proteomic changes in the bone of sheep following osteoporosis induction over the course of a year. Histomorphometry of iliac crest bone biopsies revealed decreases in trabecular bone area in osteoporotic model animals compared to healthy controls, while negligible differences were observed in cortical bone morphometry. Initial global untargeted proteomic outputs identified a total of 4,765 proteins from the iliac bone biopsy samples, 909 of which were determined to be differentially expressed over the course of model development in our osteoporotic sheep. Pathway analysis of differentially expressed proteins (DEPs) revealed unique enriched pathways at all time points. Enrichment of biological processes such as monocyte differentiation, metabolic processes, regulation of chromosome condensation, and immune responses were noted throughout osteoporosis development. When comparing the 909 DEPs between time points, we identified seven downregulated proteins shared between all time points as compared to baseline in the osteoporotic animals (CTR9, INPP5D, CDK6, PPP2R5C, NUP133, ITPRIPL1, W5PH60_SHEEP). Pathway analysis of these shared proteins revealed enrichment of p53 signaling, mRNA surveillance, sphingolipid signaling, and P13K-Akt signaling pathways. This study was the first to report on the proteomic changes of bone in conjunction with morphometry assessments in a sheep model of osteoporosis.

All three of our described experiments allowed us to successfully fill in some of the knowledge gaps in the characterization of a large animal model of osteoporosis by further

assessing both macro and micro changes in ovariectomized and steroid-dosed sheep over the course of a year. Large animal preclinical models offer researchers the ability to compare bone changes in the same animals over time, allowing for a more comprehensive insight into the progression of postmenopausal and age-related bone loss. Understanding the mechanisms driving bone loss and systemic changes in osteoporosis disease progression could aid in future cellular therapy research and investigation of novel pathway targets for osteoporosis treatment in humans.

ACKNOWLEDGEMENTS

I would like to start by thanking my committee members, Drs. Laurie Goodrich, Brad Nelson, Russ Anthony, and Kirk McGilvray. I am forever grateful that you continued to challenge me with the hard-hitting, important questions, while also extending grace when I did not know the answer. Your guidance has shaped how I critically evaluate the data that I and others produce. But more importantly, you have taught me to not become attached to a single way of thinking. I don't doubt that I will continue to learn from your wisdom for years to come. I would like to also extend my sincere gratitude to everyone in the PSRL and TMI who helped carry out the pivotal sheep study that carried my dissertation results. Specifically, I would like to acknowledge the assistance of Cat Hersh, Emma Starkebaum, Lisa Mangin, Myranda Woolly, and all the anesthesia and animal care staff and students who worked so diligently to provide the highest quality care of the animals during this year-long study. You are a prime example of how the power of a team makes all the difference in scientific research.

I am forever grateful for the team of PSRL graduate mentors and students that was built during my tenure as a graduate student. When I first started this program, there were no other students and mentors with whom I could share this experience. I want to acknowledge the PSRL mentors who helped guide me over the years, including Drs. Linsey Burton, Holly Stewart, and Brad Nelson. Thank you always providing thoughtful feedback when I presented data and for offering assistance when I got stuck on a method that didn't seem to be working. You made it easy to ask for help and seek advice when I couldn't find a solution. Emily Van Zeeland and Andres Bonilla – words cannot describe how having you as graduate student cohorts has

completely changed my graduate experience. You brought lightness, silliness, and comradery to a program that was admittedly isolating until your arrival. Being around you made me realize that you can, in fact, work hard while also having fun. I am so lucky that I had the chance to grow alongside you both over the past few years and can't wait to see where your scientific journeys take you next. I also want to extend my sincere gratitude to Dr. Katie Sikes, who, throughout this whole process, showed me nothing but constant care and support. Thank you for being my sounding board week after week, and always being willing to listen to my concerns and offer wise advice. You helped pull me out of a troublesome time in my research and helped me navigate the tougher years of my graduate career. The dissertation I finished with would not be what it is if not for you and I am eternally grateful for your guidance and friendship.

Thank you for the endless support of my parents, Dean and Eileen, as well as my stepmom Tracey, my late stepdad Tom, and my brother and sister, Anthony and Maggie. You have all shown me nothing but love and support over the past six years. Thank you for your grace and understanding while I navigated balancing work, research, and family, admittedly not always equally. This experience has not been without its difficulties, but I'm so lucky to have such a sturdy support system in my family. I share the fruits of my hard work with you. I would like to especially acknowledge my mom, who has always been, without fail, by my side during the most challenging times of my graduate training, even while navigating her own career and life challenges. Thank you for always lending an ear and reassuring me of my capabilities when I wasn't sure of myself. You are truly my inspiration.

Finally, I would like to take a moment to acknowledge my primary advisor, Dr. Jeremiah Easley, without whom none of this would be possible. Thank you for taking a chance on me and never giving up on this process. Your unending support and belief in my abilities throughout my graduate training has carried me through the past six years as a student. Thank you for always bringing your relentless optimism and empathy to each discussion, and for always being willing to try new things when I've run into a roadblock. Being the first PSRL grad student undoubtedly came with certain "learning opportunities" for us both. But you always lifted me up and made me feel successful when all I could think of was how I fell short. I am forever grateful for your trust in me as we navigated this process together, and I have grown exponentially both as a researcher and as a person because of you. There are certainly few people in this world like you. "When you want to go far, go together."

TABLE OF CONTENTS

CHAPTER 1:
OSTEOPOROSIS AND THE OVARIECTOMIZED EWE

1.1 Introduction

Osteoporosis is a complex disease resulting from a multitude of environmental and genetic factors, affecting over 200 million people worldwide [1]. As the most prevalent metabolic bone disorder, osteoporosis is the leading cause of fractures in the elderly population [2]. A hip breakage can be detrimental to lifestyle and patient autonomy, and can even significantly increase the likelihood of early death in these patients. Osteoporosis not only causes fragility fractures, but it can also contribute to a slew of comorbidities resulting from poor bone quality. Orthopedic surgical repairs, such as rotator cuff tendon reattachment [3], spinal fusion [4], and fracture fixation [5] have a much poorer prognosis of healing in patients with osteoporotic bone.

1.1.1 Pathophysiology of Osteoporosis

Skeletal bone is dynamic, constantly turning over throughout our lifetime and replacing old microdamaged bone with new mineralized bone [6]. By the time we reach our late 20's, we will have reached our peak bone mass. The remainder of our lives then becomes a battle to prevent bone loss. Bone remodeling is a complex but well-balanced process that follows five main phases. First, osteoclastic precursors are recruited to the site of bone remodeling ("Activation"), followed by osteoclast-mediated bone mineral degradation of the bony surface ("Resorption"). Following resorption, cytokines switch the mechanism to bone formation by activating osteoblasts ("Reversal") which synthesize an osteoid matrix and collagen deposition mineralizes to form new bone ("Formation"). Finally, osteoblasts undergo apoptosis and bone

formation is halted ("Termination") [7]. Osteoporosis results from an imbalance between bone formation and bone resorption, resulting in poor bone quality over time.

There are two main forms of osteoporosis, each with distinguishing etiologies: primary and secondary. Primary osteoporosis results from natural aging processes, such as loss of gonadal production of estrogen or age-related senescence of bone cells [7]. Secondary osteoporosis results from a known cause other than age, such as taking certain medications, other primary diseases, and limb disuse [8]. Although the clinical outcome between these two forms of osteoporosis is the same, the mechanism by which they cause bone loss is different. Postmenopausal osteoporosis is the most common form of primary osteoporosis, and it is estimated that approximately one third of postmenopausal women will experience at least one fragility fracture due to osteoporotic bone in their lifetime [9]. It was initially hypothesized in the 1940s that bone loss in women following menopause was primarily caused by the defective bone formation function of cells. However, further research later demonstrated that postmenopausal bone loss was actually caused by rapid bone resorption rather than decreased bone formation [7]. Estrogen plays several key roles in bone regulation by directly and indirectly inhibiting bone resorption. Cytokines involved in activating osteoclastogenesis, such as interleukin-1 (IL-1), IL-6, and tumor necrosis factor (TNF), are suppressed by estrogen in order to prevent excessive resorptive activity [7, 10, 11]. Additionally, estrogen actively inhibits receptor activated nuclear-kappa (RANK) and RANK ligand (RANKL) indirectly by activating osteoprotegerin (OPG), which acts as a soluble ligand for RANK [7, 12]. Following menopause, the body's main source of estrogen is depleted, and thus the regulatory effects of bone resorption are dampened. Bone loss initially occurs in trabecular bone during the first 4-8 years following menopause, followed

by a persistent and slower loss in both trabecular and cortical bone during later years [11]. This first phase of osteoporosis typically results in an average of 10% trabecular bone loss [11].

Glucocorticoid-induced osteoporosis (GIOP) is the most common form of secondary osteoporosis. Glucocorticoids are regularly used to treat a wide array of autoimmune and inflammatory disorders, including rheumatoid arthritis and chronic obstructive pulmonary disease (COPD). Epidemiological studies show that up to 4.6% of postmenopausal women are prescribed glucocorticoids to treat a variety of other conditions [13]. However, patients who are prescribed synthetic glucocorticoids, such as prednisone and prednisolone, are associated with a significantly increased risk of hip and vertebral fractures [14]. It has been shown that patients who are administered glucocorticoids for longer than 6-months are at a significantly greater risk of developing osteoporosis [15]. Contrary to postmenopausal osteoporosis, GIOP causes a "low-turnover" form of osteoporosis resulting from decreased bone formation secondary to impaired osteoblastic differentiation and function rather than impairment to bone resorption [16, 17]. Patients who experience a GIOP fracture often show higher bone density reading than those with postmenopausal osteoporosis, making it difficult to diagnose based solely on clinical bone scanning [16]. Supraphysiologic levels of glucocorticoids suppress serum bone formation markers, such as osteocalcin (OC), alkaline phosphatase (ALP), and procollagen type I N-terminal propeptide (P1NP) [17]. Glucocorticoids induce PPAR-gamma2, which plays a key role in adipogenesis by opposing Wnt/beta-catenin signaling, therefore inhibiting osteoblastogenesis [18]. Glucocorticoid administration also inhibits osteoblast-driven synthesis of type I collagen, a major component of the bone extracellular matrix (ECM), resulting in a decrease in the bone matrix available for mineralization [18].

1.1.2 Diagnosis and Treatment of Osteoporosis

Osteoporosis is diagnosed according to two main factors: bone density and fracture history. The prevalence of disease varies depending on whether it is defined by one factor or the other. Typically, individuals are formally diagnosed with osteoporosis either when their bone mineral density (BMD) T-score is less than -2.5 as compared to the healthy population, or if the patient has a history of at least one previous fragility fracture [19, 20]. Fragility fractures are defined as a bone fracture resulting from minimal force, such as falling from standing height. While BMD and fracture history are arguably two of the most important factors in predicting fracture risk, many other variables contribute to bone fragility in osteoporosis. Lifestyle variables, such as excessive consumption of alcohol, smoking, and lack of exercise, as well as genetic factors, all play a role in predisposing a patient to bone loss [21]. The Fracture Risk Assessment Tool (FRAX) was developed by the World Health Organization to predict an individual's propensity for hip or major osteoporotic fracture based on all of these established risk factors [22]. Additionally, serum biomarkers of bone resorption and formation can act as an additional predictive method of bone health. Serum levels of osteogenic markers, such as OC, ALP, and PINP, as well as resorptive markers, including N-terminal/C-terminal crosslinking telopeptides of type I collagen (CTX, ICTP) and deoxypyridinoline (DPD), can serve as useful indirect measurements of bone activity [23].

Poor bone quality and low bone density are a result of many different variables, making osteoporosis a difficult disease to not only diagnose, but also to treat. Factors such as pre-screening bone scans, fracture history, and age play a significant role in determining how a

patient should be treated [24, 25]. Pharmacological treatments are typically separated into one of two categories based on mechanism of action: antiresorptive, which are drugs that target osteoclast-mediated bone resorption (i.e., bisphosphonates), or anabolic, which are drugs that stimulate osteoblasts to form new bone (i.e., teriparatide) [22, 24]. Bisphosphonates are the most common first-line pharmaceutical treatment in the prevention of osteoporotic fractures as they are effective at progressively increasing patient bone density over time [24]. However, rare but serious adverse events, such as osteonecrosis of the jaw and atypical femoral fractures, have been reported in patients undergoing long-term bisphosphonate treatment [26]. Although several medications are approved for both the treatment and prevention of osteoporotic fractures, understanding the bone loss etiology and age of the patient is key in appropriate clinical management. For the treatment of postmenopausal osteoporosis in individuals with no prior fracture history, bisphosphonates such as alendronate and risedronate, are acceptable as first line options. However, those individuals at higher risk of fracture may be prescribed non-bisphosphonate treatments, such as denosumab or teriparatide, which are more anabolic in mechanism [24]. Osteoporotic fractures can also be prevented by implementing lifestyle changes. Weight-bearing exercises, limiting alcohol consumption, and implementing a daily intake of vitamin D and calcium have all been shown to have long-term beneficial effects on maintaining skeletal microarchitecture [22, 25].

1.2 Animal Models of Osteoporosis

Osteoporosis results from a combination of factors, from genetics and nutrition to lifestyle and age. Since there is not one single cause of osteoporotic bone loss and fragility fractures in humans, any number of methods could be employed in our animal models to

replicate some form of the human condition. It is, however, imperative to acknowledge the population for which the model is intended to represent. This all to say, there is no single "correct" model of osteoporosis and selection of the model is highly dependent on the research objectives.

1.2.1 Regulatory Guidelines for Conducting Preclinical Osteoporosis Studies

Novel drugs intended to prevent or treat osteoporotic fragility fractures must go through a rigorous preclinical assessment in appropriate animal models prior to initiation of human clinical trials. While this is not unlike other pharmaceutical development pathways, there is an emphasis on the preservation of bone quality in addition to the standard safety and toxicity standards for medications intended to treat osteoporosis [27]. In short, preclinical study results must display both the enhancement of bone mass and as well as bone strength. Animal model selection is therefore an essential component in the nonclinical/preclinical evaluation of therapeutics indicated for osteoporosis prevention and treatment. Guidelines published by the Federal Food and Drug Administration (FDA) state that for any nonclinical study intending to assess the quality of bone, "the sponsor should select osteoporosis models that are relevant to the specific clinical indication for which the drug is being developed. For postmenopausal osteoporosis, bone quality studies should be conducted in ovariectomized animals." [28, 29]. It is also recommended that two species be utilized in these bone quality studies. For example, the ovariectomized rat and a larger ovariectomized nonrodent species with more extensive cortical remodeling (i.e., nonhuman primate, sheep, pig, or dog) are commonly used in conjunction with one another [29]. Similarly, the World Health Organization (WHO) provides guidelines highlighting that results acquired from preclinical studies are necessary to further influence the study design for clinical

trials, including determination of the required duration of drug treatment and patient follow-up [27, 30]. While not every animal can perfectly satisfy all study guidelines set forth by the regulatory agencies, as there are inherent limitations with each animal system, comprehensive characterization studies of our animal models are important and necessary references for the osteoporosis research community. Research outcomes are meaningful only if they are tested in appropriate and clinically relevant models.

1.2.2 Animal Models of Postmenopausal Osteoporosis

Due to the invasiveness of bone research, much of the current concepts surrounding osteoporosis pathophysiology have been extrapolated from animal studies. There are many animal models available to study the different etiologies of osteoporosis. The most commonly accepted method of modeling postmenopausal bone loss is via ovariectomy (OVX), as mentioned in the previous section. This process involves removal of both ovaries and, in turn, the removal of the female body's main source of estrogen synthesis. While this is a canonical way to induce a postmenopausal osteoporosis model, it has limitations in many common animal systems. For example, in mice, it has been observed that the loss of cancellous bone occurs following OVX, but not cortical bone [31]. The rat, on the other hand, does a nicer job at mimicking the human condition of postmenopausal bone loss by exhibiting similar "bone resorption exceeding bone formation" mechanisms [32]. It has been shown that significant bone loss occurs in the proximal tibia metaphysis of the rat in as little as 14 days following OVX, in the femoral neck after 30 days, and in the lumbar vertebrae after just 60 days [31]. However, the two major drawbacks to using a rodent as a model for osteoporosis is the inability for the animals to truly reach skeletal maturity [32], as well as the lack of secondary cortical Haversian bone

remodeling capabilities [33]. The most clinically relevant model to humans may be the nonhuman primate (NHP), as this is the only other species known to experience a true menopause comparable to humans. These animals similarly show high levels of bone turnover accompanied by rapid bone loss over 3 months following OVX [34]. However, ethical considerations, requirement of specialized personnel and facilities, and high cost of animal use all limit the use of NHPs in bone research. Other commonly accepted non-rodent animals include the rabbit and sheep. These animals both present with bone turnover mechanisms more aligned with postmenopausal women and include Haversian cortical remodeling. OVX in the sheep has demonstrated increases in the bone porosity, eroded surfaces, and osteoid surfaces of cortical bone [31]. Additionally, select markers for bone resorption and formation also follow human clinical trends, whereby levels of each are observed to be at the highest levels following 3-4 months following osteoporosis induction [31]. Yet, the bone loss produced by OVX alone in sheep is not typically as severe as what is observed in the rodent model and does not develop sufficient osteoporosis to mimic clinical bone loss in humans. Sheep also display fluctuations in bone density affected by seasonality [35, 36], requiring either the enrollment of a control group or pursuit of a longitudinal study greater than or equal to a year to control for these variations. While OVX is the primary method by which postmenopausal osteoporosis is modeled in animals, select genetic mouse models are also available to model estrogen-driven bone loss. Mice with conditional knockout of estrogen receptor alpha (Esr1) in both osteoclasts and osteocytes can be used to understand the direct mechanism of estrogen on the bone cells *in vivo* [37].

1.2.3 Animal Models of Glucocorticoid-Induced Osteoporosis

To model glucocorticoid-induced osteoporosis (GIOP), animals are typically administered a regimen of high dose corticosteroids such as prednisone or prednisolone. While rodents offer a cost-effective model for researchers, there are limitations to their use in modeling GIOP. Rats and mice display significant phenotypic variability based on the age of the animal, dosage of corticosteroid administration, and duration of treatment [31]. There is also a minimal amount of trabecular loss in rodent models, which is also a notable limitation with their use in OVX-induced osteoporosis, and inconsistent with the human condition [32]. Rabbits, conversely, have been shown to model GIOP similarly to humans, displaying a reduction of both cancellous and cortical bone following administration of prednisolone [31]. Moreover, rabbits display Haversian bone remodeling and therefore can be used to understand impacts of glucocorticoids on the cortical bone [32]. The small bone size and relatively limited amount of cancellous bone present in rabbits does, however, present an inconvenience if utilizing bone densitometry to monitor *in vivo* changes in bone density [32]. In sheep, treatment of glucocorticoids results in a similar GIOP phenotype to humans and allows investigators to also evaluate the surgical treatment of fractures in similarly sized bones [32]. It should be taken into consideration that bone loss is reversed after discontinuation of glucocorticoid treatment in most animal models of GIOP. Additionally, high doses of corticosteroid administration can have detrimental effects on the animal by suppressing the immune system. This is especially a problem in large animal species and highlight the importance of implementing a taper dosing regimen [32].

1.2.4 The Sheep Model of Osteoporosis

As mentioned previously, the ovariectomized sheep is a commonly accepted translational model for osteoporosis research. In the early 1990's, it was observed that removal of the ovaries

by OVX in sheep resulted in a decrease in bone density over time. Following OVX, implantation of an estradiol device was able to return density levels of the animals to normal levels [38, 39]. While the sheep had previously been accepted as a translational large animal model for medical device research in bone [40], this was the first time the sheep was specifically suggested for use in postmenopausal osteoporosis studies [41]. This model has since been widely used for decades as the standard large animal model of postmenopausal bone loss [42, 43]. By the early 2000's, the model had evolved to include multiple methods of induction in addition to OVX to further drive rapid bone loss, including the addition of corticosteroid injections [44, 45] and diet manipulation [46, 47]. Preclinical studies began reporting use of sheep to assess fracture healing in osteoporotic bone [48], as well as to test medical devices indicated for use in osteoporotic patients affected by fracture in the lumbar spine [49-53] and long bones [54-56].

Rising availability of -omics, genomic sequencing, and single-cell laboratory techniques has opened the field of osteoporosis research to investigate not only the cellular and histological manifestations of bone, but also the molecular pathways that drive bone loss. Mouse models have been the standard for deducing genetic effects on bone through knockout and knock-in experimentation, as the mouse genome has been thoroughly researched and annotated. Large animals, on the other hand, have only been able to fill in certain gaps when the mouse fails to recapitulate mechanisms of bone loss observed in humans. While the sheep is a relevant model to assess bone quality, there are gaps that do not allow the sheep to fit within some of the current trends of osteoporosis research. For example, the sheep genome has been vastly under-annotated compared to that of the laboratory mouse, leaving genetic and -omics research in the large animal model sparce. Yet, there is a consistent need for more translatable animal models,

especially in regards to cortical bone remodeling. Additionally, the large animal models offer a way to monitor long-term changes in bone quality using the same animals over time and collect a wide array of biological samples. While the use of large animal models is not always appropriate to answer each research question regarding bone loss, they certainly can be utilized to help answer the larger research question when used in conjunction with small animal models and/or clinical cohort data.

1.3 Literature Review

1.3.1 Search Terms and Database

To determine the knowledge gaps in the characterization of the current sheep model of osteoporosis, a brief literature review was performed on all previously published sheep osteoporosis research studies. The literature review was conducted using the search engine PubMed® (National Library of Medicine, National Center for Biotechnology Information, Bethesda, MD). Search terms "sheep AND osteoporosis" were utilized and all articles were compiled.

1.3.2 Inclusion Criteria

Published studies from all available dates were evaluated in the review and no date ranges were excluded. Articles included were to adhere to the following parameters: 1) randomized-control experimental studies, 2) studies that included female sheep, 3) studies that characterized bone and its changes after experimental intervention (i.e., sheep osteoporosis induction was included in methods descriptions), 4) studies that were performed *in vivo*, and 5) articles available in English. Review articles, editorials, commentaries, studies evaluating only

normal bone (i.e., no interventional bone loss model employed), field observational studies, or any studies performed only using explanted tissues, human clinical tissues, or *in vitro* tissues/cells were excluded from the review.

1.3.3 Overview of Review Findings

A total of 248 articles were retrieved in the initial literature search. Dates of articles ranged from 1966 to 2021. Following removal of studies that did not meet inclusion criteria #1-#4, a total of 116 articles remained. Two additional articles were only available in languages other than English and were therefore also removed. Thus, a total of 114 articles were included in this review (**Table 1.1)**.

1.3.4 Common Methods of Osteoporosis Induction

Approximately 46% of articles listed only a single induction method of osteoporotic bone loss in sheep, while the majority (56%) of articles listed more than one induction method (**Fig. 1.1A-B**). The most common single induction method was unsurprisingly OVX alone (77%). Lesser common single induction methods included diet manipulation (6%), external fixator placement (6%), and using aged/old animals (5%). The least common single induction methods were the use of corticosteroids alone (2%), hypothalamic-pituitary disconnection (HPD) (2%), pinealectomy (2%), and parasitic induction (2%) (**Fig. 1.1A**). Of the combination methods, OVX with corticosteroid administration and diet manipulation was the most commonly used (43%), followed by OVX with steroid administration (16%) and OVX with diet manipulation (13%). Less frequently utilized combination methods included OVX in combination with old age, diet manipulation, and steroid administration (6%), OVX with HPD (6%), and OVX with old age

(5%). The least common combination methods of induction of bone loss were OVX with steroid administration, diet manipulation, and movement restriction (2%), OVX with diet manipulation and movement restriction (2%), OVX with aromatase inhibitor administration (2%), diet manipulation with steroid administration (2%), and OVX with steroid administration and old age (1%) (**Fig. 1.1B**).

1.3.5 Common Experimental Outcomes

To characterize the outcome parameters previously evaluated in studies using the sheep model of osteoporosis, all methods from 114 publications were classified into one of eight categories: 1) bone density and architecture, 2) cellular organization and mineralization, 3) bone strength, 4) clinical pathology, 5) bone composition, 6) progenitor cells, 7) molecular pathway, and 8) co-morbidity analysis. The most frequent outcome categories were investigating bone density and architecture (36%), cellular organization and mineralization (31%), and bone strength (15%) (**Fig. 1.2**). The most common methods utilized were microCT, biomechanics, histology, histomorphometry, and DXA. The least frequently investigated topics were molecular pathways (2%) and co-morbidity analysis (1%) (**Fig. 1.2**).

1.3.6 Discussion

Appropriate selection of an animal model is highly dependent on the research question at hand. Large animal preclinical models offer researchers the ability to compare bone changes in the same animals over time and gather more comprehensive insight into the progression of osteoporotic bone loss. Ovariectomized sheep have been used for decades as a clinically relevant model for postmenopausal osteoporosis by inducing bone loss via similar mechanisms as humans

[42, 43]. However, this method alone does not induce severe and rapid enough bone loss for utilization in certain preclinical scenarios. In this review, we explored the other methods by which bone loss has been experimentally induced in sheep. A combination of induction methods, such as OVX and steroids or OVX and diet manipulation, has been shown to be much more effective at producing low quality bone more comparable to human osteoporotic bone [45, 46, 57, 58]. Aged animals (greater than 7+ years) were commonly used in conjunction with OVX and other methods [39, 48, 59-62]. However, this method may be associated with higher cost needed to house sheep for multiple years prior to initiation of study. More invasive surgical models, such as pinealectomy [63], HPD [64-68], and disuse models using external fixators [69-71] have also been shown to decrease bone density in the sheep. While several methods have been employed to enhance bone loss in sheep, the most severe has been the inclusion of corticosteroids. Few publications have briefly reported on the adverse effects observed following corticosteroid administration in osteoporotic sheep [59, 72, 73], but only one study to date has attempted to comprehensively evaluate the clinical values associated with steroid administration in these animals [74].

Outcome methods in sheep osteoporosis studies typically include standard measures of bone density and structure, such as microCT and DXA, as well as bone strength using biomechanics. Other methods have been employed to evaluate bone composition, including ashing and ToF-SIMS, as well as the cellular composition of bone through the use of histology, scanning electron microscopy (SEM), and other forms of microscopy. In addition to measures directly applied to the bone, outcomes assessing the systemic impact of osteoporosis have been utilized in sheep studies, including evaluation of serum bone biomarker levels, hormone levels,

and urine biomarkers. However, bone marrow pathology, progenitor cell expansion, and *in vitro* cellular characterization have less frequently been evaluated in these studies. While sheep have demonstrated utility in modeling low quality bone for testing of medical devices and bone cements intended for osteoporotic fracture repair, their use in osteoporosis molecular pathway research has been limited. One study previously evaluated the impact of osteoporosis induction on the metabolome in sheep [75], while another investigated RANKL and OPG protein changes in the bone using immunohistochemistry [76]. Vitamin D receptor mechanisms have also been studied in a sheep osteoporosis model through RT-PCR analysis of mRNA expression in the kidney [77]. To our knowledge, no other -omics or genome association studies have been performed using the sheep in the context of osteoporosis research. Co-morbidity analysis has been the least frequently researched topic using sheep osteoporosis models to date, limited only to two studies investigating osteoarthritis and coronary disease in conjunction with osteoporosis development. Given that there are multiple different co-morbidities associated with osteoporosis, this is an area of research that should be expanded upon in the future.

The overall goal of this literature review was to highlight the common outcomes of studies where sheep are utilized to model osteoporosis and the methods by which they are measured in order to inform the objectives and study design of this overall study. While we provided our best attempt to comprehensively report on the published literature for all studies utilizing sheep models of osteoporosis, we acknowledge that there were limitations in this search. Primarily, we used only one set of search terms ("sheep" and "osteoporosis"), limiting the results to papers that explicitly state "osteoporosis" in their publication and therefore possibly excluded publications that utilized alternate terms to "osteoporosis" such as "osteopenia", "low

bone density", and others. Additionally, our use of a single database to complete the search may have also limited the number of papers that fit our inclusion criteria. Further literature reviews using multiple search terms and across several databases are required to comprehensively report on the use of sheep as a large animal preclinical model in osteoporosis research. Through this search, we intended to minimize redundancy in our current study while continuing to add to the literature of comprehensive animal model characterization. Based on the results of our search, we determined that the following areas were lacking in the characterization of the sheep osteoporosis model and required further investigation. First, we note the lack of use of advanced imaging to measure bone density in the sheep lumbar spine. While most studies in the sheep utilize DXA bone scanning to evaluate bone density changes following osteoporosis induction, there are limited studies available which utilize another form of advanced imaging that may more accurately reflect bone density changes in the animals, such as quantitative computed tomography (QCT) or magnetic resonance imaging (MRI). While a handful of studies have utilized peripheral QCT (pQCT) in the sheep model [63, 78, 79], these are limited to use in a peripheral long bone and have not primarily focused on imaging the lumbar spine. Second, we observed the lack of characterization of systemic blood values in the sheep model, including clinical pathology parameters to assess the health of the animals. To our knowledge, only one study has evaluated these parameters, but only two time points were measured and no control animals were included as comparisons [74]. Finally, there have been very few studies investigating the biological and molecular pathways at play in these animals during osteoporosis progression. While one study thus far has characterized the metabolome and lipidome of the osteoporotic sheep model [75], no studies have directly looked at the proteomic changes in the bone tissue of these animals over time. Understanding the molecular pathways involved in

osteoporosis disease progression in the sheep model could aid in future cellular therapy research and lead to novel pathway targets for disease treatment in humans.

1.4 Study Purpose, Aims, and Hypotheses

1.4.1 Overall Study Purpose

There remain challenges with modeling a complex metabolic disease such as osteoporosis. Based on the recommended guidelines set forth by the regulatory bodies, multiple species are essential in the preclinical evaluation of a potential therapeutic's safety and efficacy. Even with known limitations, the sheep has continued to act as a reliable and cost-effective large animal option for preclinical osteoporosis studies. With the emergence of novel, more highly pathway targeted therapeutics, we need clinically-focused animal models for which to answer our research questions. In order to continue to expand upon the use of the sheep model in preclinical studies of bone quality, a more thorough comprehensive characterization of the bone loss mechanisms at play in sheep are required. Additionally, to fill some of the knowledge gaps presented previously in our literature review, the overarching objective of this study was to comprehensively characterize not only bone loss, but the systemic impacts of our model development and downstream pathways at play in our animals. Our goal was to provide information that can be used to inform researchers on the appropriate selection and use of the sheep model for future osteoporosis studies.

1.4.2 Study Aim 1 and Hypothesis

Aim 1: The first aim of this study was to compare advanced imaging techniques to determine bone density in an ovine model of osteoporosis. Specifically, we aimed to both compare bone density and microarchitectural changes over time in an ovine model of

osteoporosis as compared to age-matched control animals, as well as compare two in-life imaging modalities, DXA and QCT, to determine bone density over time.

Hypothesis: We hypothesized that 1) there would be a decrease in bone density and subsequent changes to trabecular microarchitecture following corticosteroid administration in ovariectomized ewes, and 2) QCT would characterize bone density changes over time more accurately than DXA in our sheep model of osteoporosis.

1.4.3 Study Aim 2 and Hypothesis

Aim 2: The second aim of this study was to characterize the clinical and systemic effects of high-dose corticosteroids and estrogen depletion in an ovine model of osteoporosis.

Hypothesis: We hypothesized that systemic impacts, both in clinical presentation and systemic through clinical pathology, would be observed during the process of model development in our study animals compared to age-matched controls, and that any acute changes observed would be primarily due to glucocorticoid administration.

1.4.4 Study Aim 3 and Hypothesis

Aim 3: In our third and final aim, we compared the bone protein and histologic changes over time in an ovine model over 12-months. We assessed the histologic characteristics of the bone through use of histomorphometry and characterized the proteome of sheep bone through global untargeted proteomic analysis.

Hypothesis: We hypothesized that differences in bone histomorphometry would be noted in the osteoporotic sheep as compared to control animals in a similar trend to what was observed using clinical imaging. We then hypothesized that we would observe differences in protein expression over time following osteoporosis induction.

1.5 Figures / Tables

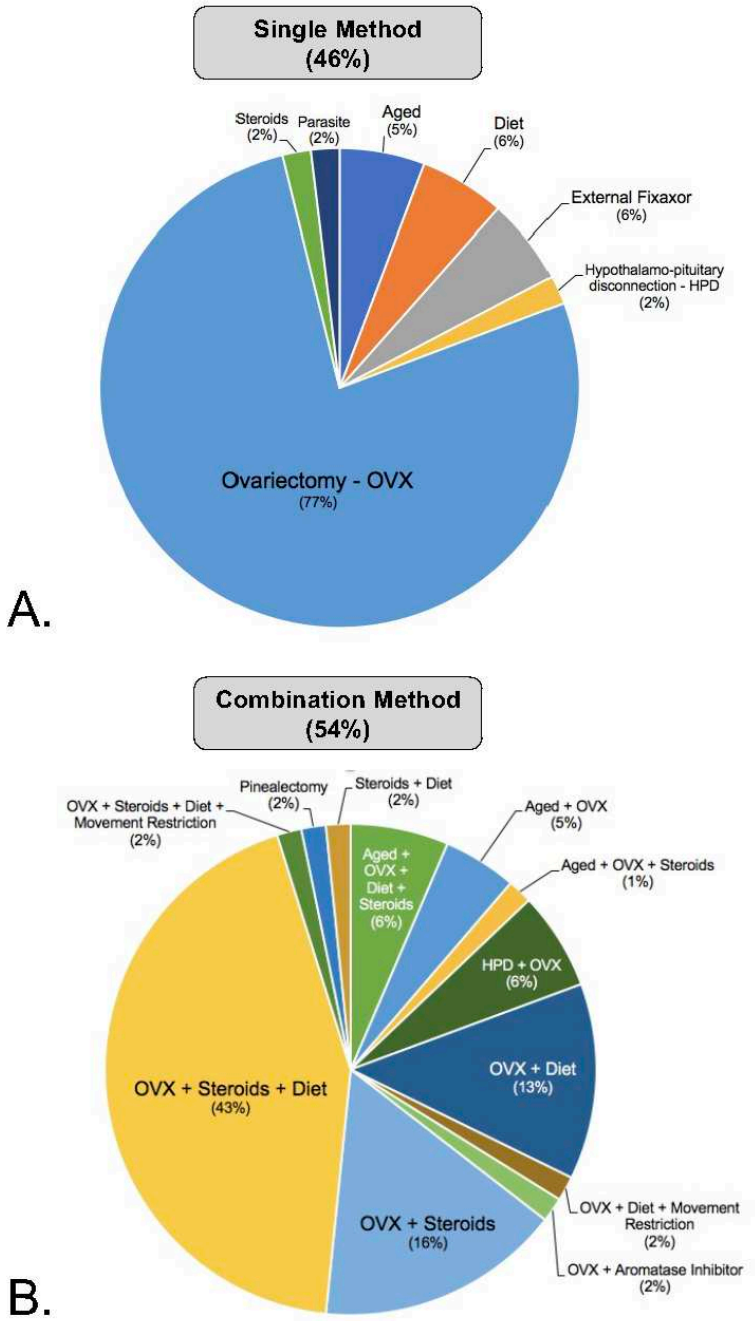

Figure 1.1. Comparison of osteoporosis induction methods in sheep. A) Percentage breakdown of single induction methods where only one intervention was utilized to induce osteoporosis the sheep. B) Percentage breakdown of combination induction methods where more than one intervention was utilized to induce osteoporosis in the sheep.

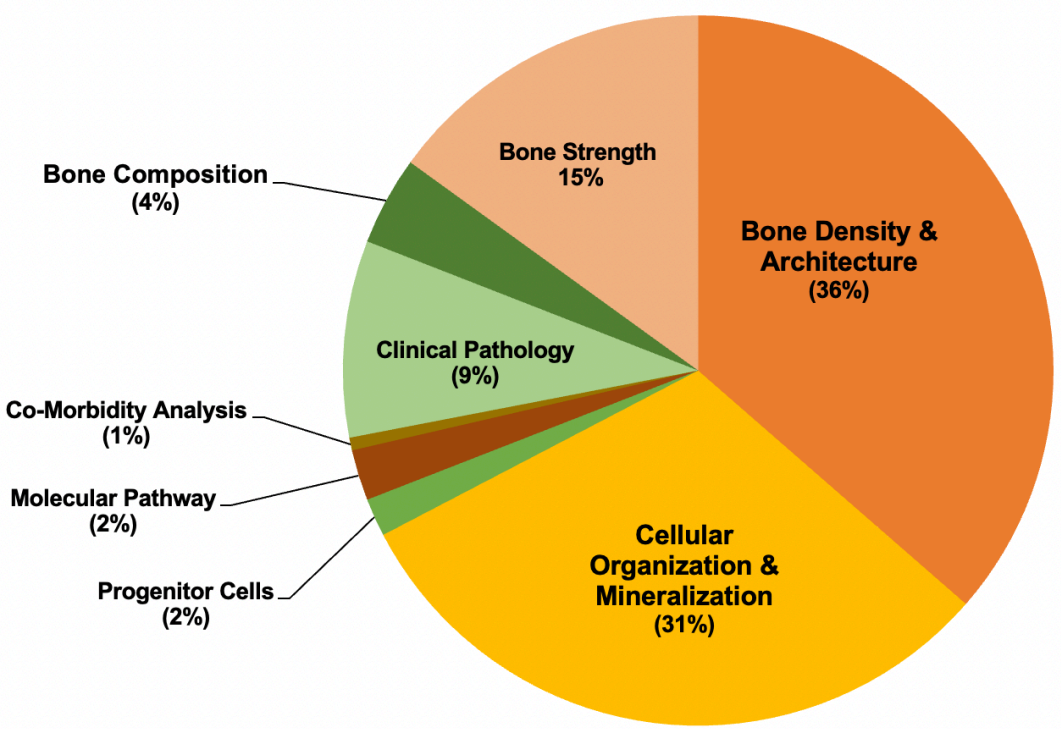

Figure 1.2. Breakdown of all outcome methods reported in the reviewed literature (n=114 publications) where a sheep model of osteoporosis was utilized.

Table 1.1. Summary of Literature Review Publications

Publication PMID	Year	Osteoporosis Model	Induction Method	Outcomes	Comments
35011173	2021	Postmenopausal	OVX + steroids + diet	Serum biomarkers, histology (kidney), RT-qPCR (kidney)	Model characterization; Determine effects on vitamin D and phosphatonin-related genes in the kidney.
33808560	2021	Postmenopausal	OVX + steroids + diet	DXA, microCT, dynamic histomorph, histology	Model development (fracture healing); Combination of OVX alone, OVX + diet, and OVX + steroids + diet depletion.
32296985	2020	Senile	Age 6+ years	DXA, histology, histomorph, biomechanics	Model development; Age related bone loss.
31755105	2020	Bisphosphonate osteonecrosis	OVX	Clinical exam, serum biomarkers, DXA, histomorph, ashing	Model development; Administration of zoledronic acid followed by tooth extraction and dental implantation.
33295580	2020	Postmenopausal	OVX + steroids	MicroCT, histomorph, serum biomarkers, CBC, bone marrow cytology	Model characterization; OVX + steroids only, no OVX only group.
32503480	2020	Glucocorticoid-induced	OVX + steroids	Metabolomics, lipidomics	Metabolism and lipid metabolism; Combination of OVX alone w/ OVX + steroids over 2 months and 5 months.
31678741	2020	Postmenopausal	OVX + steroids + diet	CT, histology, histomorph	Long bone drill hole defect creations and implantation of scaffolds following induction of osteoporosis.
32245019	2020	Postmenopausal	OVX + steroids + diet	QCT, histology, radiographs	Administration of bisphosphonate (trans-7) directly into the rumen.
30715786	2019	Postmenopausal	OVX	DXA, microCT, histology, biomechanics	Mandible defect creation and implantation of titanium implants following induction of osteoporosis.
30445158	2019	Postmenopausal	OVX + steroids + diet	CT, histology	Defect model and implantation of a Ti6Al4V-EL scaffold in the tibia, femur, and humerus following induction of osteoporosis.

Table 1.1. Summary of Literature Review Publications

Publication PMID	Year	Osteoporosis Model	Induction Method	Outcomes	Comments
30965142	2019	Postmenopausal	OVX + steroids + diet	Histology, histomorph	Defect creation and implantation of MBG-PCL graft in tibia, femur, and humerus.
30958193	2019	Postmenopausal	OVX + steroids + diet	DXA, microCT, biomechanics, ToF-SIMS, finite-element analysis	Model characterization; Combination of OVX alone, OVX + diet, OVX + steroids + diet depletion.
29331906	2018	Postmenopausal	OVX + diet	MicroCT, histology, histomorph	Femoral defect model with MSC scaffold following osteoporosis induction.
28485126	2018	Postmenopausal	OVX + steroids	Histology, histomorph, biomechanics	Femoral condyle defect creation and implantation of scaffolds following induction of osteoporosis.
30480061	2018	Postmenopausal	OVX + steroids	Serum biomarkers, DXA, pQCT	Model characterization; pQCT of tibia, DXA of lumbar spine and femur.
30179213	2018	Postmenopausal	OVX + steroids + diet	Bone biopsy, cell isolation, AChE activity assay, BrdU assay, real-time RT-PCR, histomorph	Isolation of MSCs and acetylcholine signaling, collagen expression following administration of donepezil; Combination of OVX alone, OVX + diet, OVX + steroids + diet depletion.
28237183	2017	Postmenopausal	HPD + OVX	Histology, histomorph, biomechanics	Hormone replacement therapy.
28966340	2017	Postmenopausal	OVX + steroids + diet	DXA	Model characterization; T Score control group standard for sheep OVX studies; Combination of OVX alone, OVX + diet depletion, and OVX + steroids + diet depletion.
28618255	2017	Postmenopausal	OVX + steroids + diet	DXA, biomechanics, histology, IHC, dynamic histomorph, confocal microscopy, serum biomarkers, real time RT-PCR	Combination of OVX alone, OVX + diet, OVX + steroids + diet depletion; RANKL-OPG pathway investigation.
27544617	2016	Postmenopausal	OVX	MicroCT, biomechanics, fluorochrome labeled damage quantification	Model characterization.

Table 1.1. Summary of Literature Review Publications

Publication PMID	Year	Osteoporosis Model	Induction Method	Outcomes	Comments
25072801	2016	Postmenopausal	OVX + steroids	MicroCT, histology, biomechanics	Treatment injection of calcium sulfate into vertebral pedicles.
27096794	2016	Postmenopausal	OVX + steroids	Histology, cartilage indentation, biomechanics	N/A
27113550	2016	Postmenopausal	OVX + steroids + diet	DXA, microCT, histology, histomorph, FEA	Vertebral defect model with implantation of rhNELL-1 protein following induction of osteoporosis.
26846710	2016	Bisphosphonate osteonecrosis	OVX + steroids + diet	Clinical examination, microCT, ZTE MRI	Tooth extraction to create osteonecrosis following administration of zoledronate; ZTE MRI offered as alternate imaging to microCT.
25843053	2016	Postmenopausal	OVX + steroids + diet	CT, microCT, osteolysis scoring, histomorph	Mandible tooth extraction study following administration of zoledronate.
27019848	2016	Postmenopausal	OVX + steroids + diet	MicroCT, pQCT, biomechanics	Anterior lumbar interbody fusion study for treatment of vertebral compression fractures w/ a scaffold following induction of osteoporosis.
25689083	2015	Postmenopausal/ Senile	Aged 8+ years + OVX + steroids	Bone biopsy, microCT, histology, serum biomarkers, IHC, histomorph	Model characterization.
25642445	2015	Metabolic acidosis	OVX + diet	Biomechanics, microCT	Samples collected from multiple different studies; Treatment with PTH, alendronate, or raloxifene administered via cannula to duodenum; Combination of diet alone and OVX + diet.
26618599	2015	Postmenopausal	OVX + steroids	Serum biomarkers, blood hormone levels, arthroscopy, DXA, microCT	Combination of OVX alone w/ OVX + steroids.
26082355	2015	Postmenopausal	OVX + steroids + diet	DXA, CT, microCT, FEA, histology, histomorph	Vertebral interbody drill hole defect and rhNELL-1 protein material implantation.

Table 1.1. Summary of Literature Review Publications

Publication PMID	Year	Osteoporosis Model	Induction Method	Outcomes	Comments
26542861	2015	Postmenopausal	OVX + steroids + diet	pQCT, microCT,	Model characterization; Vertebral compression fracture creation following induction of osteoporosis.
26365170	2015	Postmenopausal	OVX + steroids + diet	MicroCT, pQCT, biomechanics	Anterior lumbar interbody fusion study for treatment of vertebral compression fractures with eptotermin-alpha following induction of osteoporosis.
25050773	2014	Postmenopausal	OVX	Iliac biopsy, microCT, SEM imaging, histomorph, histology	Lumbar vertebral drill hole defect and implantation of bisphosphonate calcium phosphate bone cement following induction of osteoporosis.
24720887	2014	Postmenopausal	OVX	MicroCT, biomechanics	Model characterization.
24090875	2014	Postmenopausal	OVX	qBEI imaging	Administration of zoledronic acid.
24769217	2014	Postmenopausal	OVX	DEXA, microCT, histology, biomechanics	Model characterization.
23092698	2013	Metabolic acidosis	Diet	microCT, biomechanics, ashing, nanoindentation, Raman spectroscopy, SHG, FTIR,	Raloxifene and zoledronate administered through abomasa cannula.
23813786	2013	Postmenopausal	HPD	pQCT, microCT, histology	Distal femoral condyle metaphyseal fracture and treatment with hormone replacement therapy following induction of osteoporosis.
24102843	2013	Postmenopausal	HPD + OVX	Radiographs, histology, histomorph, pQCT	Model characterization; focused on mandible.
23440966	2013	Postmenopausal	HPD + OVX	Dynamic histomorph, pQCT, biomechanics, urinary biomarkers, serum biomarkers, radiographs, qBEI	Model characterization.

Table 1.1. Summary of Literature Review Publications

Publication PMID	Year	Osteoporosis Model	Induction Method	Outcomes	Comments
23634692	2013	Postmenopausal	OVX	DXA, microCT, dynamic histomorph, cartilage scoring, histology	Model characterization; Osteoarthritis and subchondral bone in an osteoporotic animal model.
23298803	2013	Postmenopausal	OVX	Biomechanics, histomorph, microCT	Expandable mandible implant study.
23027700	2013	Postmenopausal	OVX	AFM microscopy	Disease characterization.
24086381	2013	Postmenopausal	OVX + steroids	DXA, screw pullout, microCT, histomorph, histology	Vertebral posterior fusion with bone cement following induction of osteoporosis.
23079719	2013	Postmenopausal	OVX + steroids	MicroCT, histology, biomechanics	Bioactive glass pedicle screw implantation in the vertebrae.
23737220	2013	Postmenopausal	OVX + steroids + diet	DXA, microCT, histology	rhBMP-2 pellet implantation into vertebral vertebrae following induction of osteoporosis: monthly DXA scans.
22234948	2012	Postmenopausal	HPD + OVX	Dynamic histomorph, microCT, histology, urinary biomarkers, serum biomarkers, radiographs	Model characterization.
21430565	2012	Postmenopausal	OVX	Biomechanics, microCT, histology	Vertebral model to test L-EPS pedicle screw system in osteoporotic sheep.
22234960	2012	Postmenopausal	OVX + diet	DXA, biomechanics, microCT, histology	Lumbar spine pedicle screw study with calcium/phosphate treated pedicle screws following induction of osteoporosis.
23091772	2012	Postmenopausal	OVX + steroids + diet	DXA, microCT	Evaluated if there was a "bounce back" of BMD following cessation of steroids.
21626447	2012	Postmenopausal	OVX + steroids + diet	Dynamic histomorph, histology	Model characterization.
21087316	2011	Postmenopausal/ Senile	Aged 6+ years + OVX + diet + steroids	Histomorph	Model characterization; Assessment of the mandible following induction of osteoporosis.

Table 1.1. Summary of Literature Review Publications

Publication PMID	Year	Osteoporosis Model	Induction Method	Outcomes	Comments
21597262	2011	Metabolic acidosis	Diet	DEXA, iliac crest biopsies, FTIR	Administration of raloxifene or alendronate.
21293893	2011	Postmenopausal	OVX	DEXA, microCT, biomechanics	Vertebral defect model and implantation with rhBMP-2 and fibrin sealant following induction of osteoporosis.
21093863	2011	Postmenopausal	OVX	qBEI, nanoindentation	Treatment with zoledronic acid and animals sacrificed at 31 months total.
21544593	2011	Postmenopausal	OVX	Iliac biopsy, DXA, histomorph, histology	Dynesys pedicle screw placement in the lumbar vertebrae following induction of osteoporosis.
20844452	2011	Postmenopausal	OVX	Biomechanics, microCT, histology	Pedicle screw implantation with calcium sulfate cement in the vertebrae following induction of osteoporosis.
21477184	2011	Osteoporosis-induced Osteoarthritis	OVX	MicroCT	Model characterization; Looking specifically at the effect of OVX on subchondral bone structure in the tibia.
21574136	2011	Postmenopausal	OVX	SEM, qBEI	Model characterization.
21773815	2011	Postmenopausal	OVX + steroids + diet	Biomechanics, histology, histomorph, radiographs, CT, DXA	Bone cement kyphoplasty surgery in the lumbar vertebrae following induction of osteoporosis.
22115044	2011	Postmenopausal	Pinealectomy + OVX	MicroCT, histomorph, serum biomarkers, pQCT	Model characterization.
20643480	2010	Postmenopausal	OVX	MicroCT, histomorph, SEM, histology	Femoral defect and calcium deficient apatite and zoledronate material implantation following induction of osteoporosis.
20886644	2010	Postmenopausal	OVX	Histology (apoptosis staining, microdamage detection)	Administration of zoledronic acid.
19725098	2010	Postmenopausal	OVX	MicroCT, biomechanics, dynamic histomorph	Model characterization.

Table 1.1. Summary of Literature Review Publications

Publication PMID	Year	Osteoporosis Model	Induction Method	Outcomes	Comments
20577766	2010	Postmenopausal	OVX + diet	DXA, biomechanics, microCT, histology	Pedicle screw implantation in the vertebrae following induction of osteoporosis.
20503036	2010	Glucocorticoid-induced	OVX + steroids + diet	DXA, microCT	Model characterization; Focused on mandible and lumbar spine.
20110841	2010	Glucocorticoid-induced	Steroids + diet	MicroCT, biomechanics, serum biomarkers	Model characterization; Different levels and duration of corticosteroid administration to induce osteoporosis.
19932773	2009	Postmenopausal	OVX	AFM	Specifically looking at Type I collagen to provide early diagnostic technique.
18719215	2008	Postmenopausal/ Senile	Aged 6+ years, OVX + steroids + diet	QCT, microCT	Model characterization; Focused on dentition/teeth.
18376023	2008	Postmenopausal	OVX	Biomechanics, dynamic histomorph	Model characterization; Focused on microdamage to metatarsal; fluorochrome labeling.
18671203	2008	Postmenopausal	OVX	Iliac biopsy, microCT, SEM	Femoral defect and implantation of zoledronate coated implants.
18595763	2008	Postmenopausal	OVX	DXA, microCT, biomechanics	Model characterization; Compared bone properties 6 and 12 months post-OVX.
18978592	2008	Postmenopausal	OVX	DXA, dynamic histomorph, microCT, biomechanics	Model characterization; Assessment of bone turnover in the lumbar spine following OVX; lots of fluorochrome labeling.
18377708	2008	Postmenopausal	OVX + diet + movement restriction	MicroCT, histology	Femoral defect with pedicle screw implantation.
18782823	2008	Postmenopausal	OVX + steroids + diet	pQCT, radiographs, iliac biopsy, microCT, biomechanics	Model characterization; Five (5) total studies compiled into one paper. The novel study assessed different treatment regimens of steroids.

Table 1.1. Summary of Literature Review Publications

Publication PMID	Year	Osteoporosis Model	Induction Method	Outcomes	Comments
19015899	2008	Postmenopausal	OVX + steroids + diet	DXA, serum biomarkers, histology, histomorph, biomechanics, ashing	Model characterization; Looked at samples from iliac crest, femur, and lumbar spine.
17474132	2007	Postmenopausal/ Senile	Aged 9+ years + OVX	Iliac biopsy, histomorph, DXA, histology, biomechanics	Compared with young and aged sheep w/out OVX; Tibia defect and implantation of titanium implants following induction of osteoporosis.
17377911	2007	Postmenopausal/ Senile	Aged 9+ years + OVX	Iliac biopsy, histomorph, histology, biomechanics	Compared with young and aged sheep w/out OVX; Tibia defect and implantation of titanium implants following induction of osteoporosis.
17187191	2007	Postmenopausal	OVX	Iliac biopsy, pQCT, radiographs, microCT, serum biomarkers	Model characterization.
18090082	2007	Postmenopausal	OVX + diet	DXA, microCT, biomechanics	Vertebral body injection of BMP and fibrin sealant test material.
17364091	2007	Glucocorticoid-induced	OVX + steroids + diet	Iliac biopsy, vertebral biopsy, dynamic histomorph, microCT, radiographs, organ pathology	Model characterization; Compared 4 different steroid regimens to induce osteoporosis and minimize side effects; Discussed alopecia and health issues.
16934718	2006	Metabolic acidosis	OVX + diet	DXA, biomechanics, histology	Kyphoplasty and BMP-7 (OP-1) implantation/injection into vertebral body following induction of metabolic acidosis/decreased bone density.
16865404	2006	Postmenopausal	OVX + steroids + diet + movement restriction	Dynamic histomorph, radiographs, biomechanics, histology	Two level interbody fusion following induction of osteoporosis.
16139577	2005	Senile	Aged 8+ years	Radiographs, histology, biomechanics	Tibial defect and implantation of BMP-2 implants.
15619678	2005	Postmenopausal	OVX	MRI	Treatment with calcitonin; Focused on trabecular structure of femoral head.

Table 1.1. Summary of Literature Review Publications

Publication PMID	Year	Osteoporosis Model	Induction Method	Outcomes	Comments
15668580	2005	Glucocorticoid-induced	OVX + steroids + diet	pQCT, blood cortisone levels, iliac biopsy, umbar biopsy, microCT	Model characterization; Diet terminated after 18 weeks, steroids terminated after ~26 weeks; Study to determine potential rebound of BMD after cessation of steroids/special diet (slow rebound occurs, but still lost ~25% BMD by end of study); discusses alopecia and side effects.
15592799	2004	Metabolic acidosis	OVX + diet	DXA	Model characterization; Compared OVX alone vs. OVX + diet depletion.
15490266	2004	Metabolic acidosis	OVX + diet	DXA, serum chemistry, urine DPD, arterial blood pH	Model characterization; Effect of diet on bone loss on BMD.
12919871	2003	Postmenopausal	Aged 7+ years + OVX + steroids + diet	In-life biomechanics, pQCT, biomechanics	Model characterization; Tibial fracture model following induction of osteoporosis; Focused on callus healing.
12833444	2003	Postmenopausal	OVX	Iliac biopsy, histology, histomorph, indentation testing	Vertebral body HA coated pedicle screw implantation following induction of osteoporosis.
12906308	2003	Postmenopausal	OVX	Iliac biopsy, isolation and expansion of osteoblasts, immunoassay, MTT assay	Compared bone cells from human, sheep, and rat osteoblasts from osteopenic individuals.
14606514	2003	Glucocorticoid-induced	OVX + steroids	Tibia biopsy, microCT, biomechanics, histomorph,	Model characterization; Compared OVX + steroids vs. OVX w/out steroids; Steroids stopped after 6 months.
12086352	2002	Postmenopausal	Aged 7+ years + OVX + steroids + diet	pQCT, iliac biopsy, biomechanics, microCT	Model characterization.
12472232	2002	Postmenopausal	OVX	Biomechanics, histomorph	Vertebral body HA coated pedicle screw implantation following induction of osteoporosis.

Table 1.1. Summary of Literature Review Publications

Publication PMID	Year	Osteoporosis Model	Induction Method	Outcomes	Comments
11858572	2002	Postmenopausal	OVX	Histomorph	Implantation of Ti6AI4V implant in tibia following induction of osteoporosis.
11990439	2002	Postmenopausal	OVX	Gingival sulcular depth, blood/urine/saliva biomarkers, radiographs	Model characterization; Focused on mandible.
12107662	2002	Postmenopausal	OVX + steroids + diet	pQCT, microCT, biomechanics	Model characterization; Compared OVX + diet, OVX + steroids, and OVX + diet + steroids.
11797852	2001	Postmenopausal	OVX	Histomorph, biomechanics	Model characterization; Testing vertebral bodies following induction of osteoporosis.
11149494	2001	Postmenopausal	OVX + Lentaron	Blood and urine biomarkers, dynamic histomorph, iliac biopsy, DXA	Model characterization; Treatment with SERM modulator; Added aromatase inhibitor to OVX.
10906690	2000	Postmenopausal	OVX	Iliac biopsy, osteoblast culture and characterization, MTT assay	Osteoblast isolation and in vitro experimentation from osteoporotic sheep vs control sheep.
11110106	2000	Postmenopausal	OVX	Contrast coronary angiography, blood serum drug levels/hormones, histology	Determine estrogen role in prevention of coronary disease; Implantation with estradiol and raloxifene; No bone density/bone evaluation.
10832663	2000	Postmenopausal	OVX	Iliac biopsy, histomorph, SEM	Model characterization.
11149502	2000	Postmenopausal	OVX + steroids + diet	QCT, iliac biopsy, microCT, biomechanics	Model characterization; Compared OVX + diet, OVX + steroids, OVX + diet + steroids.
9916766	1999	Postmenopausal	OVX	Biomechanics	Model characterization.
9379331	1997	Postmenopausal	OVX	Serum and urine biomarkers, biomechanics, radiographs, periodontal probing depth, gingival histomorph, gingival biochemical analysis	Model characterization; Focused on mandible and gingiva.
8847302	1996	Disuse	External fixator	Dynamic histomorph, iliac biopsy	Model characterization; Metatarsal unloading.

Table 1.1. Summary of Literature Review Publications

Publication PMID	Year	Osteoporosis Model	Induction Method	Outcomes	Comments
8579942	1995	Postmenopausal	Aged 7+ years + OVX	DXA	Administration of 17-beta estradiol.
8574941	1995	Disuse	External fixator	Iliac biopsy, histomorph	Administration of calcitonin to prevent disuse osteoporosis.
7756057	1995	Disuse	External fixator	In-life biomechanics, dual photon absorptiometry, digital photographs (for trabecular area, etc.)	Test exercise as a treatment for osteoporosis.
8579947	1995	Postmenopausal	OVX	DXA, serum estrodiol	Administration of estradiol implant.
8453197	1993	Glucocorticoid-induced	Steroids	Serum biomarkers, histomorph	Model characterization; Compared different doses of steroid administration.
1237505	1975	Parasite-induced	*T. colubriformis* larvae	Serum chemistry, parasitic egg count, histology, ashing	Disease characterization; Long bone length stunted in lambs infected with parasites.
5956163	1966	Phosphorus depletion	Diet	Histology	Disease characterization; Low phosphorus with normal calcium in diet; osteoporosis observed

1.6 References

1. Vidal, M., et al., *Osteoporosis: a clinical and pharmacological update.* Clin Rheumatol, 2019. **38**(2): p. 385-395.
2. Burge, R., et al., *Incidence and economic burden of osteoporosis-related fractures in the United States, 2005-2025.* J Bone Miner Res, 2007. **22**(3): p. 465-75.
3. Chung, S.W., et al., *Factors affecting rotator cuff healing after arthroscopic repair: osteoporosis as one of the independent risk factors.* Am J Sports Med, 2011. **39**(10): p. 2099-107.
4. Lechtholz-Zey, E.A., et al., *Systematic Review and Meta-Analysis of the Effect of Osteoporosis on Fusion Rates and Complications Following Surgery for Degenerative Cervical Spine Pathology.* Int J Spine Surg, 2024.
5. Strømsøe, K., *Fracture fixation problems in osteoporosis.* Injury, 2004. **35**(2): p. 107-13.
6. Kenkre, J. and J. Bassett, *The bone remodelling cycle.* Annals of clinical biochemistry, 2018. **55**(3): p. 308-327.
7. Bhatnagar, A. and A.L. Kekatpure, *Postmenopausal osteoporosis: a literature review.* Cureus, 2022. **14**(9).
8. Fitzpatrick, L.A., *Secondary causes of osteoporosis.* Mayo Clin Proc, 2002. **77**(5): p. 453-68.
9. Rachner, T.D., S. Khosla, and L.C. Hofbauer, *Osteoporosis: now and the future.* The Lancet, 2011. **377**(9773): p. 1276-1287.
10. Feng, X. and J.M. McDonald, *Disorders of bone remodeling.* Annual Review of Pathology: Mechanisms of Disease, 2011. **6**: p. 121-145.

11. Ji, M. and Q. Yu, *Primary osteoporosis in postmenopausal women. Chronic Dis Transl Med 1: 9–13*. 2015.

12. Nagy, V. and J.M. Penninger, *The rankl-rank story.* Gerontology, 2015. **61**(6): p. 534-542.

13. Seibel, M.J., M.S. Cooper, and H. Zhou, *Glucocorticoid-induced osteoporosis: mechanisms, management, and future perspectives.* The lancet Diabetes & endocrinology, 2013. **1**(1): p. 59-70.

14. Adami, G. and K. Saag, *Glucocorticoid-induced osteoporosis: 2019 concise clinical review.* Osteoporosis International, 2019. **30**: p. 1145-1156.

15. Adinoff, A.D. and J.R. Hollister, *Steroid-induced fractures and bone loss in patients with asthma.* New England Journal of Medicine, 1983. **309**(5): p. 265-268.

16. Mazziotti, G., E. Canalis, and A. Giustina, *Drug-induced osteoporosis: mechanisms and clinical implications.* The American journal of medicine, 2010. **123**(10): p. 877-884.

17. Gado, M., et al., *Bad to the bone: the effects of therapeutic glucocorticoids on osteoblasts and osteocytes.* Frontiers in Endocrinology, 2022. **13**: p. 835720.

18. Canalis, E., et al., *Glucocorticoid-induced osteoporosis: pathophysiology and therapy.* Osteoporosis International, 2007. **18**(10): p. 1319-1328.

19. Camacho, P.M., et al., *American Association of Clinical Endocrinologists/American College of Endocrinology Clinical Practice Guidelines for the Diagnosis and Treatment of Postmenopausal Osteoporosis-2020 Update.* Endocr Pract, 2020. **26**(Suppl 1): p. 1-46.

20. Wright, N.C., et al., *The recent prevalence of osteoporosis and low bone mass in the United States based on bone mineral density at the femoral neck or lumbar spine.* J Bone Miner Res, 2014. **29**(11): p. 2520-6.

21. Long, G., et al., *Predictors of osteoporotic fracture in postmenopausal women: a meta-analysis.* Journal of Orthopaedic Surgery and Research, 2023. **18**(1): p. 574.

22. Black, D.M. and C.J. Rosen, *Postmenopausal osteoporosis.* New England journal of medicine, 2016. **374**(3): p. 254-262.

23. Szulc, P. and P. Delmas, *Biochemical markers of bone turnover: potential use in the investigation and management of postmenopausal osteoporosis.* Osteoporosis International, 2008. **19**: p. 1683-1704.

24. Tu, K.N., et al., *Osteoporosis: A Review of Treatment Options.* P t, 2018. **43**(2): p. 92-104.

25. Reid, I.R. and E.O. Billington, *Drug therapy for osteoporosis in older adults.* The Lancet, 2022. **399**(10329): p. 1080-1092.

26. Black, D.M., et al., *Atypical femur fracture risk versus fragility fracture prevention with bisphosphonates.* New England Journal of Medicine, 2020. **383**(8): p. 743-753.

27. Bonjour, J.-P., P. Ammann, and R. Rizzoli, *Importance of preclinical studies in the development of drugs for treatment of osteoporosis: a review related to the 1998 WHO guidelines.* Osteoporosis International, 1999. **9**: p. 379-393.

28. Thompson, D., et al., *FDA Guidelines and animal models for osteoporosis.* Bone, 1995. **17**(4): p. S125-S133.

29. Food and D. Administration, *Guidelines for preclinical and clinical evaluation of agents used in the prevention or treatment of postmenopausal osteoporosis.* Division of Metabolism and Endocrine Drug Products, Rockville, MD, 1994.

30. Organization, W.H., *Guidelines for preclinical evaluation and clinical trials in osteoporosis*. 1998: World Health Organization.

31. Komori, T., *Animal models for osteoporosis.* Eur J Pharmacol, 2015. **759**: p. 287-94.

32. Zhang, Z., et al., *Animal models for glucocorticoid-induced postmenopausal osteoporosis: An updated review.* Biomed Pharmacother, 2016. **84**: p. 438-446.

33. Lelovas, P.P., et al., *The laboratory rat as an animal model for osteoporosis research.* Comparative medicine, 2008. **58**(5): p. 424-430.

34. Smith, S.Y., A. Varela, and J. Jolette, *Nonhuman primate models of osteoporosis.* Osteoporosis Research: Animal Models, 2011: p. 135-157.

35. Turner, A.S., *Seasonal changes in bone metabolism in sheep: further characterization of an animal model for human osteoporosis.* Veterinary Journal (London, England: 1997), 2006. **174**(3): p. 460-461.

36. Arens, D., et al., *Seasonal changes in bone metabolism in sheep.* The Veterinary Journal, 2007. **174**(3): p. 585-591.

37. Nakamura, T., et al., *Estrogen prevents bone loss via estrogen receptor α and induction of Fas ligand in osteoclasts.* Cell, 2007. **130**(5): p. 811-823.

38. Turner, A.S., et al., *Dose-response effects of estradiol implants on bone mineral density in ovariectomized ewes.* Bone, 1995. **17**(4 Suppl): p. 421s-427s.

39. Hornby, S., et al., *Skeletal changes in the ovariectomised ewe and subsequent response to treatment with 17β oestradiol.* Bone, 1995. **17**(4): p. S389-S394.

40. Martini, L., et al., *Sheep model in orthopedic research: a literature review.* Comp Med, 2001. **51**(4): p. 292-9.

41. Newman, E., A. Turner, and J. Wark, *The potential of sheep for the study of osteopenia: current status and comparison with other animal models.* Bone, 1995. **16**(4): p. S277-S284.

42. Salamanna, F., et al., *Osteoporosis Preclinical Research: A Systematic Review on Comparative Studies Using Ovariectomized Sheep.* Int J Mol Sci, 2022. **23**(16).

43. Dias, I.R., et al., *Preclinical and translational studies in small ruminants (sheep and goat) as models for osteoporosis research.* Current Osteoporosis Reports, 2018. **16**: p. 182-197.

44. Lill, C.A., A.K. Fluegel, and E. Schneider, *Sheep model for fracture treatment in osteoporotic bone: a pilot study about different induction regimens.* J Orthop Trauma, 2000. **14**(8): p. 559-65; discussion 565-6.

45. Schorlemmer, S., et al., *Glucocorticoid treatment of ovariectomized sheep affects mineral density, structure, and mechanical properties of cancellous bone.* J Bone Miner Res, 2003. **18**(11): p. 2010-5.

46. MacLeay, J.M., et al., *Dietary-induced metabolic acidosis decreases bone mineral density in mature ovariectomized ewes.* Calcif Tissue Int, 2004. **75**(5): p. 431-7.

47. Macleay, J.M., J.D. Olson, and A.S. Turner, *Effect of dietary-induced metabolic acidosis and ovariectomy on bone mineral density and markers of bone turnover.* J Bone Miner Metab, 2004. **22**(6): p. 561-8.

48. Lill, C.A., et al., *Biomechanical evaluation of healing in a non-critical defect in a large animal model of osteoporosis.* J Orthop Res, 2003. **21**(5): p. 836-42.

49. Fini, M., et al., *Biological assessment of the bone-screw interface after insertion of uncoated and hydroxyapatite-coated pedicular screws in the osteopenic sheep.* J Biomed Mater Res A, 2003. **66**(1): p. 176-83.

50. Goldhahn, J., et al., *Osseointegration of hollow cylinder based spinal implants in normal and osteoporotic vertebrae: a sheep study.* Arch Orthop Trauma Surg, 2006. **126**(8): p. 554-61.

51. Phillips, F.M., et al., *In vivo BMP-7 (OP-1) enhancement of osteoporotic vertebral bodies in an ovine model.* Spine J, 2006. **6**(5): p. 500-6.

52. Wu, Z.X., et al., *Staged-injection procedure to prevent cement leakage during vertebroplasty: an in vitro study.* Spine (Phila Pa 1976), 2007. **32**(22): p. 2437-42.

53. Wan, S., et al., *Biomechanical and histological evaluation of an expandable pedicle screw in osteoporotic spine in sheep.* Eur Spine J, 2010. **19**(12): p. 2122-9.

54. Wan, S.Y., et al., *[Micro-CT evaluation and histological analysis of screw-bone interface of expansile pedicle screw in osteoporotic sheep].* Zhonghua Wai Ke Za Zhi, 2007. **45**(18): p. 1271-3.

55. Borsari, V., et al., *Sandblasted titanium osteointegration in young, aged and ovariectomized sheep.* Int J Artif Organs, 2007. **30**(2): p. 163-72.

56. Stadelmann, V.A., et al., *Implants delivering bisphosphonate locally increase periprosthetic bone density in an osteoporotic sheep model. A pilot study.* Eur Cell Mater, 2008. **16**: p. 10-6.

57. Rupp, M., et al., *Large Animal Model of Osteoporotic Defect Healing: An Alternative to Metaphyseal Defect Model.* Life (Basel), 2021. **11**(3).

58. Lill, C.A., A.K. Fluegel, and E. Schneider, *Effect of ovariectomy, malnutrition and glucocorticoid application on bone properties in sheep: a pilot study.* Osteoporos Int, 2002. **13**(6): p. 480-6.

59. Andreasen, C.M., et al., *A reversal phase arrest uncoupling the bone formation and resorption contributes to the bone loss in glucocorticoid treated ovariectomised aged sheep.* Bone, 2015. **75**: p. 32-9.

60. Dvorak, G., et al., *Cortical porosity of the mandible in an osteoporotic sheep model.* Clin Oral Implants Res, 2011. **22**(5): p. 500-5.

61. Dvorak, G., et al., *Trabecular bone structures in the edentulous diastema of osteoporotic sheep.* J Dent Res, 2008. **87**(9): p. 866-70.

62. Borsari, V., et al., *Osteointegration of titanium and hydroxyapatite rough surfaces in healthy and compromised cortical and trabecular bone: in vivo comparative study on young, aged, and estrogen-deficient sheep.* J Orthop Res, 2007. **25**(9): p. 1250-60.

63. Egermann, M., et al., *Pinealectomy affects bone mineral density and structure--an experimental study in sheep.* BMC Musculoskelet Disord, 2011. **12**: p. 271.

64. Oheim, R., et al., *Sheep model for osteoporosis: The effects of peripheral hormone therapy on centrally induced systemic bone loss in an osteoporotic sheep model.* Injury, 2017. **48**(4): p. 841-848.

65. Bindl, R., et al., *Metaphyseal fracture healing in a sheep model of low turnover osteoporosis induced by hypothalamic-pituitary disconnection (HPD).* J Orthop Res, 2013. **31**(11): p. 1851-7.

66. Oheim, R., et al., *Mandibular bone loss in ewe induced by hypothalamic-pituitary disconnection.* Clin Oral Implants Res, 2014. **25**(11): p. 1239-1244.

67. Oheim, R., et al., *Sheep model for osteoporosis: sustainability and biomechanical relevance of low turnover osteoporosis induced by hypothalamic-pituitary disconnection.* J Orthop Res, 2013. **31**(7): p. 1067-74.

68. Beil, F.T., et al., *Low turnover osteoporosis in sheep induced by hypothalamic-pituitary disconnection.* J Orthop Res, 2012. **30**(8): p. 1254-62.

69. Thomas, T., et al., *Architectural modifications and cellular response during disuse-related bone loss in calcaneus of the sheep.* J Appl Physiol (1985), 1996. **80**(1): p. 198-202.

70. Thomas, T., et al., *Ineffectiveness of calcitonin on a local-disuse osteoporosis in the sheep: a histomorphometric study.* Calcif Tissue Int, 1995. **57**(3): p. 224-8.

71. Skerry, T.M. and L.E. Lanyon, *Interruption of disuse by short duration walking exercise does not prevent bone loss in the sheep calcaneus.* Bone, 1995. **16**(2): p. 269-74.

72. Goldhahn, J., et al., *Slow rebound of cancellous bone after mainly steroid-induced osteoporosis in ovariectomized sheep.* J Orthop Trauma, 2005. **19**(1): p. 23-8.

73. Klopfenstein Bregger, M.D., et al., *Optimization of corticosteroid induced osteoporosis in ovariectomized sheep. A bone histomorphometric study.* Vet Comp Orthop Traumatol, 2007. **20**(1): p. 18-23.

74. Coelho, C.A., et al., *Evaluation of hematology, general serum biochemistry, bone turnover markers and bone marrow cytology in a glucocorticoid treated ovariectomized sheep model for osteoporosis research.* An Acad Bras Cienc, 2020. **92**(4): p. e20200435.

75. Cabrera, D., et al., *Effects of short-and long-term glucocorticoid-induced osteoporosis on plasma metabolome and lipidome of ovariectomized sheep.* BMC musculoskeletal disorders, 2020. **21**: p. 1-13.

76. El Khassawna, T., et al., *Osteocyte Regulation of Receptor Activator of NF-κB Ligand/Osteoprotegerin in a Sheep Model of Osteoporosis.* Am J Pathol, 2017. **187**(8): p. 1686-1699.

77. Dittmer, K.E., et al., *Expression of Renal Vitamin D and Phosphatonin-Related Genes in a Sheep Model of Osteoporosis.* Animals (Basel), 2021. **12**(1).

78. Egermann, M., et al., *A sheep model for fracture treatment in osteoporosis: benefits of the model versus animal welfare.* Lab Anim, 2008. **42**(4): p. 453-64.

79. Sigrist, I.M., et al., *The long-term effects of ovariectomy on bone metabolism in sheep.* J Bone Miner Metab, 2007. **25**(1): p. 28-35.

80. Maenz, S., et al., *The old sheep: a convenient and suitable model for senile osteopenia.* J Bone Miner Metab, 2020. **38**(5): p. 620-630.

81. Davison, M.R., et al., *Aminobisphosphonate-treated ewes as a model of osteonecrosis of the jaw and of dental implant failure.* J Periodontol, 2020. **91**(5): p. 628-637.

82. Casarrubios, L., et al., *Silicon substituted hydroxyapatite/VEGF scaffolds stimulate bone regeneration in osteoporotic sheep.* Acta Biomater, 2020. **101**: p. 544-553.

83. Petruczynik, P., et al., *Three-Component Reaction of Diamines with Triethyl Orthoformate and Diethyl Phosphite and Anti-Proliferative and Antiosteoporotic Activities of the Products.* Molecules, 2020. **25**(6).

84. Liu, F., et al., *Effects of micro/nano strontium-loaded surface implants on osseointegration in ovariectomized sheep.* Clin Implant Dent Relat Res, 2019. **21**(2): p. 377-385.

85. Izquierdo-Barba, I., et al., *Synergistic effect of Si-hydroxyapatite coating and VEGF adsorption on Ti6Al4V-ELI scaffolds for bone regeneration in an osteoporotic bone environment.* Acta Biomater, 2019. **83**: p. 456-466.

86. Gómez-Cerezo, N., et al., *Mesoporous bioactive glass/ε-polycaprolactone scaffolds promote bone regeneration in osteoporotic sheep.* Acta Biomater, 2019. **90**: p. 393-402.

87. Müller, R., et al., *Analysis of microscopic bone properties in an osteoporotic sheep model: a combined biomechanics, FE and ToF-SIMS study.* J R Soc Interface, 2019. **16**(151): p. 20180793.

88. Chandran, S., et al., *Strontium Hydroxyapatite scaffolds engineered with stem cells aid osteointegration and osteogenesis in osteoporotic sheep model.* Colloids Surf B Biointerfaces, 2018. **163**: p. 346-354.

89. Andreasen, C.M., et al., *Effects of substitute coated with hyaluronic acid or poly-lactic acid on implant fixation: Experimental study in ovariectomized and glucocorticoid-treated sheep.* J Tissue Eng Regen Med, 2018. **12**(2): p. e1122-e1130.

90. Cabrera, D., et al., *Glucocorticoids affect bone mineral density and bone remodelling in OVX sheep: A pilot study.* Bone Rep, 2018. **9**: p. 173-180.

91. Nachlinger, R.J., et al., *Application of donepezil increased collagen 1 expression in mesenchymal stroma cells of an ovine osteoporosis model.* J Musculoskelet Neuronal Interact, 2018. **18**(3): p. 354-365.

92. Heiss, C., et al., *A New Clinically Relevant T-Score Standard to Interpret Bone Status in a Sheep Model.* Med Sci Monit Basic Res, 2017. **23**: p. 326-335.

93. Kreipke, T.C., et al., *The roles of architecture and estrogen depletion in microdamage risk in trabecular bone.* J Biomech, 2016. **49**(14): p. 3223-3229.

94. Liu, D., et al., *Local Treatment of Osteoporotic Sheep Vertebral Body With Calcium Sulfate for Decreasing the Potential Fracture Risk: Microstructural and Biomechanical Evaluations.* Clin Spine Surg, 2016. **29**(7): p. E358-64.

95. Kiełbowicz, Z., et al., *Experimental osteoporosis in sheep--mechanical and histological approach.* Pol J Vet Sci, 2016. **19**(1): p. 109-18.

96. James, A.W., et al., *Vertebral implantation of NELL-1 enhances bone formation in an osteoporotic sheep model.* Tissue Engineering Part A, 2016. **22**(11-12): p. 840-849.

97. Voss, P., et al., *Evaluation of BP-ONJ in osteopenic and healthy sheep: comparing ZTE-MRI with μCT.* Dentomaxillofac Radiol, 2016. **45**(4): p. 20150250.

98. Voss, P.J., et al., *Zoledronate induces bisphosphonate-related osteonecrosis of the jaw in osteopenic sheep.* Clin Oral Investig, 2016. **20**(1): p. 31-8.

99. Eschler, A., et al., *Cementless Titanium Mesh Fixation of Osteoporotic Burst Fractures of the Lumbar Spine Leads to Bony Healing: Results of an Experimental Sheep Model.* Biomed Res Int, 2016. **2016**: p. 4094161.

100. Brock, G.R., et al., *The Effect of Osteoporosis Treatments on Fatigue Properties of Cortical Bone Tissue.* Bone Rep, 2015. **2**: p. 8-13.

101. Kiełbowicz, Z., et al., *The experimental osteoporosis in sheep--clinical approach.* Pol J Vet Sci, 2015. **18**(3): p. 645-54.

102. James, A.W., et al., *NELL-1 in the treatment of osteoporotic bone loss.* Nat Commun, 2015. **6**: p. 7362.

103. Eschler, A., et al., *The standardized creation of a lumbar spine vertebral compression fracture in a sheep osteoporosis model induced by ovariectomy, corticosteroid therapy and calcium/phosphorus/vitamin D-deficient diet.* Injury, 2015. **46 Suppl 4**: p. S17-23.

104. Eschler, A., et al., *Intrabody application of eptotermin alpha enhances bone formation in osteoporotic fractures of the lumbar spine; however, fails to increase biomechanical stability - results of an experimental sheep model.* Growth Factors, 2015. **33**(4): p. 290-7.

105. Verron, E., et al., *Vertebroplasty using bisphosphonate-loaded calcium phosphate cement in a standardized vertebral body bone defect in an osteoporotic sheep model.* Acta Biomater, 2014. **10**(11): p. 4887-4895.

106. Kreipke, T.C., et al., *Alterations in trabecular bone microarchitecture in the ovine spine and distal femur following ovariectomy.* J Biomech, 2014. **47**(8): p. 1918-21.

107. Brennan, M.A., et al., *Effects of ageing, prolonged estrogen deficiency and zoledronate on bone tissue mineral distribution.* J Mech Behav Biomed Mater, 2014. **29**: p. 161-70.

108. Zhang, Y., et al., *The variation of cancellous bones at lumbar vertebra, femoral neck, mandibular angle and rib in ovariectomized sheep.* Arch Oral Biol, 2014. **59**(7): p. 663-9.

109. Burket, J.C., et al., *Variations in nanomechanical properties and tissue composition within trabeculae from an ovine model of osteoporosis and treatment.* Bone, 2013. **52**(1): p. 326-36.

110. Holland, J.C., et al., *Examination of osteoarthritis and subchondral bone alterations within the stifle joint of an ovariectomised ovine model.* J Anat, 2013. **222**(6): p. 588-97.

111. Xiao, J.R., et al., *Evaluation of fixation of expandable implants in the mandibles of ovariectomized sheep.* J Oral Maxillofac Surg, 2013. **71**(4): p. 682-8.

112. Erickson, B., et al., *Nanoscale structure of type I collagen fibrils: quantitative measurement of D-spacing.* Biotechnol J, 2013. **8**(1): p. 117-26.

113. Liu, D., et al., *Comparison of expansive pedicle screw and polymethylmethacrylate-augmented pedicle screw in osteoporotic sheep lumbar vertebrae: biomechanical and interfacial evaluations.* PLoS One, 2013. **8**(9): p. e74827.

114. Li, Y., et al., *In vivo study of pedicle screw augmentation using bioactive glass in osteoporosis sheep.* J Spinal Disord Tech, 2013. **26**(4): p. E118-23.

115. Zarrinkalam, M.R., et al., *Recombinant human bone morphogenetic protein-type 2 (rhBMP-2) enhances local bone formation in the lumbar spine of osteoporotic sheep.* J Orthop Res, 2013. **31**(9): p. 1390-7.

116. Shi, L., et al., *A study of low elastic modulus expandable pedicle screws in osteoporotic sheep.* J Spinal Disord Tech, 2012. **25**(2): p. 123-8.

117. Shi, L., et al., *Improving fixation strength of pedicle screw by microarc oxidation treatment: an experimental study of osteoporotic spine in sheep.* J Orthop Res, 2012. **30**(8): p. 1296-303.

118. Zarrinkalam, M.R., et al., *Osteoporotic characteristics persist in the spine of ovariectomized sheep after withdrawal of corticosteroid administration.* J Osteoporos, 2012. **2012**: p. 182509.

119. Zarrinkalam, M.R., et al., *Changes in osteocyte density correspond with changes in osteoblast and osteoclast activity in an osteoporotic sheep model.* Osteoporos Int, 2012. **23**(4): p. 1329-36.

120. Calton, E.F., J. Macleay, and A.L. Boskey, *Fourier transform infrared imaging analysis of cancellous bone in alendronate- and raloxifene-treated osteopenic sheep.* Cells Tissues Organs, 2011. **194**(2-4): p. 302-6.

121. Wu, Z.X., et al., *Sustained-release rhBMP-2 increased bone mass and bone strength in an ovine model of postmenopausal osteoporosis.* J Orthop Sci, 2011. **16**(1): p. 99-104.

122. Brennan, O., et al., *The effects of estrogen deficiency and bisphosphonate treatment on tissue mineralisation and stiffness in an ovine model of osteoporosis.* J Biomech, 2011. **44**(3): p. 386-90.

123. Giavaresi, G., et al., *In vivo preclinical evaluation of the influence of osteoporosis on the anchorage of different pedicle screw designs.* Eur Spine J, 2011. **20**(8): p. 1289-96.

124. Liu, D., et al., *Augmentation of pedicle screw stability with calcium sulfate cement in osteoporotic sheep: biomechanical and screw-bone interfacial evaluation.* J Spinal Disord Tech, 2011. **24**(4): p. 235-41.

125. Holland, J.C., et al., *Subchondral trabecular structural changes in the proximal tibia in an ovine model of increased bone turnover.* J Anat, 2011. **218**(6): p. 619-24.

126. Brennan, M.A., et al., *Site specific increase in heterogeneity of trabecular bone tissue mineral during oestrogen deficiency.* Eur Cell Mater, 2011. **21**: p. 396-406.

127. Galovich, L.A., et al., *Biomechanical, histological and histomorphometric analyses of calcium phosphate cement compared to PMMA for vertebral augmentation in a validated animal model.* Eur Spine J, 2011. **20 Suppl 3**(Suppl 3): p. 376-82.

128. Verron, E., et al., *In vivo bone augmentation in an osteoporotic environment using bisphosphonate-loaded calcium deficient apatite.* Biomaterials, 2010. **31**(30): p. 7776-84.

129. Brennan, O., et al., *Effects of estrogen deficiency and bisphosphonate therapy on osteocyte viability and microdamage accumulation in an ovine model of osteoporosis.* J Orthop Res, 2011. **29**(3): p. 419-24.

130. Healy, C., et al., *Structural adaptation and intracortical bone turnover in an ovine model of osteoporosis.* J Orthop Res, 2010. **28**(2): p. 248-51.

131. Veigel, E., et al., *Osteopenia in the maxillofacial area: a study in sheep.* Osteoporos Int, 2011. **22**(4): p. 1115-21.

132. Ding, M., et al., *Glucocorticoid induced osteopenia in cancellous bone of sheep: validation of large animal model for spine fusion and biomaterial research.* Spine (Phila Pa 1976), 2010. **35**(4): p. 363-70.

133. Wallace, J.M., et al., *Distribution of type I collagen morphologies in bone: relation to estrogen depletion.* Bone, 2010. **46**(5): p. 1349-54.

134. Kennedy, O.D., et al., *The behaviour of fatigue-induced microdamage in compact bone samples from control and ovariectomised sheep.* Stud Health Technol Inform, 2008. **133**: p. 148-55.

135. Wu, Z.X., et al., *Effect of ovariectomy on BMD, micro-architecture and biomechanics of cortical and cancellous bones in a sheep model.* Med Eng Phys, 2008. **30**(9): p. 1112-8.

136. Kennedy, O.D., et al., *Effects of high bone turnover on the biomechanical properties of the L3 vertebra in an ovine model of early stage osteoporosis.* Spine (Phila Pa 1976), 2008. **33**(23): p. 2518-23.

137. Wan, S.Y., et al., *Micro-CT evaluation and histological analysis of screw-bone interface of expansive pedicle screw in osteoporotic sheep.* Chin J Traumatol, 2008. **11**(2): p. 72-7.

138. Zarrinkalam, M.R., et al., *Validation of the sheep as a large animal model for the study of vertebral osteoporosis.* Eur Spine J, 2009. **18**(2): p. 244-53.

139. Borsari, V., et al., *Osteointegration of titanium and hydroxyapatite rough surfaces in healthy and compromised cortical and trabecular bone: in vivo comparative study on young, aged, and estrogen-deficient sheep.* J Orthop Res, 2007. **25**(9): p. 1250-60.

140. Wu, Z.X., et al., *Staged-injection procedure to prevent cement leakage during vertebroplasty: an in vitro study.* Spine (Phila Pa 1976), 2007. **32**(22): p. 2437-42.

141. Sachse, A., et al., *Osteointegration of hydroxyapatite-titanium implants coated with nonglycosylated recombinant human bone morphogenetic protein-2 (BMP-2) in aged sheep.* Bone, 2005. **37**(5): p. 699-710.

142. Jiang, Y., et al., *Femoral neck trabecular microstructure in ovariectomized ewes treated with calcitonin: MRI microscopic evaluation.* J Bone Miner Res, 2005. **20**(1): p. 125-30.

143. Torricelli, P., et al., *Osteoblasts cultured from osteoporotic bone: a comparative investigation on human and animal-derived cells.* Artif Cells Blood Substit Immobil Biotechnol, 2003. **31**(3): p. 263-77.

144. Lill, C.A., et al., *Bone changes due to glucocorticoid application in an ovariectomized animal model for fracture treatment in osteoporosis.* Osteoporos Int, 2002. **13**(5): p. 407-14.

145. Aldini, N.N., et al., *Pedicular fixation in the osteoporotic spine: a pilot in vivo study on long-term ovariectomized sheep.* J Orthop Res, 2002. **20**(6): p. 1217-24.

146. Fini, M., et al., *Titanium alloy osseointegration in cancellous and cortical bone of ovariectomized animals: histomorphometric and bone hardness measurements.* Int J Oral Maxillofac Implants, 2002. **17**(1): p. 28-37.

147. Johnson, R.B., et al., *Effect of estrogen deficiency on skeletal and alveolar bone density in sheep.* J Periodontol, 2002. **73**(4): p. 383-91.

148. Giavaresi, G., et al., *The ovariectomized ewe model in the evaluation of biomaterials for prosthetic devices in spinal fixation.* Int J Artif Organs, 2001. **24**(11): p. 814-20.

149. Chavassieux, P., et al., *Effects of a new selective estrogen receptor modulator (MDL 103,323) on cancellous and cortical bone in ovariectomized ewes: a biochemical, histomorphometric, and densitometric study.* J Bone Miner Res, 2001. **16**(1): p. 89-96.

150. Torricelli, P., et al., *Isolation and characterization of osteoblast cultures from normal and osteopenic sheep for biomaterials evaluation.* J Biomed Mater Res, 2000. **52**(1): p. 177-82.

151. Gaynor, J.S., et al., *The effect of raloxifene on coronary arteries in aged ovariectomized ewes.* J Vet Pharmacol Ther, 2000. **23**(3): p. 175-9.

152. Fini, M., et al., *The ovariectomised sheep as a model for testing biomaterials and prosthetic devices in osteopenic bone: a preliminary study on iliac crest biopsies.* Int J Artif Organs, 2000. **23**(4): p. 275-81.

153. Weinhold, P.S., et al., *Assessment of the directional elastic moduli of ewe vertebral cancellous bone by vibrational testing.* Ann Biomed Eng, 1999. **27**(1): p. 103-10.

154. Johnson, R.B., et al., *Alveolar bone loss one year following ovariectomy in sheep.* J Periodontol, 1997. **68**(9): p. 864-71.

155. Chavassieux, P., et al., *Glucocorticoid-induced inhibition of osteoblastic bone formation in ewes: a biochemical and histomorphometric study.* Osteoporos Int, 1993. **3**(2): p. 97-102.

156. Sykes, A.R., R.L. Coop, and K.W. Angus, *Experimental production of osteoporosis in growing lambs by continuous dosing with Trichostrongylus colubriformis larvae.* J Comp Pathol, 1975. **85**(4): p. 549-59.

157. Young, V.R., et al., *Phosphorus depletion in sheep and the ratio of calcium to phosphorus in the diet with reference to calcium and phosphorus absorption.* Br J Nutr, 1966. **20**(4): p. 783-94.

CHAPTER 2:
COMPARISON OF ADVANCED IMAGING TECHNIQUES TO DETERMINE BONE DENSITY IN AN OVINE MODEL OF OSTEOPOROSIS[1]

2.1 Introduction

Clinical diagnosis of osteoporosis relies heavily on the bone mineral density (BMD) quantification of an individual patient, as fracture risk increases significantly as BMD decreases [1]. BMD is most commonly measured at the femoral head or lumbar spine [2, 3] using dual-X-ray absorptiometry (DXA). Patient BMD values are compared to those of the average healthy population using a T-score to determine osteoporotic or osteopenic status [4, 5], wherein if the patient's T-score is less than 2.5, they are diagnosed as having osteoporotic bone [6]. DXA is considered as the "gold standard" for clinical measurement of BMD because of its low radiation exposure and simplicity of use [7]. However, because DXA quantifies bone density based on a two-dimensional region of interest, there are limitations with its preclinical and clinical applications. Specifically, precise patient positioning and the inability to differentiate cortical and trabecular bone can lead to overestimation of BMD [8, 9], thus risking underdiagnosis. Furthermore, trabecular bone is more susceptible to morphological changes during the early stages of osteoporotic bone loss in perimenopausal and aging patients [10-14]. Other clinical factors such as obesity [15], degenerative spinal disease [16], aortic calcification [17], and osteoarthritic osteophytes [18] can also result in artificially high BMD measurements with DXA. Because of these limitations, auxiliary imaging and diagnostic strategies that provide more detailed assessments relative to DXA are needed.

[1] This chapter includes the published manuscript: Bisazza, K.T., et al., *Computed Tomography Provides Improved Quantification of Trabecular Lumbar Spine Bone Loss Compared to Dual-Energy X-Ray Absorptiometry in Ovariectomized Sheep.* JBMR plus, 2023. **7**(12): p. e10807.

Quantitative computed tomography (QCT) is emerging as an alternative screening modality to DXA by providing a volumetric quantification of BMD [19-23]. QCT has the ability to distinguish between trabecular and cortical bone, resulting in earlier detection of low trabecular BMD and reduced overestimation issues noted with DXA [24, 25]. Considering the superior sensitivity of QCT for early and subtle detection of trabecular BMD changes in clinical patients [19], we sought to understand if QCT provided improved quantification of bone loss relative to DXA.

Large animal preclinical models offer researchers the ability to test multiple imaging modalities and compare bone changes in the same animals over time, allowing for a more comprehensive insight into the progression of postmenopausal and age-related bone loss. Similar to humans, DXA has historically been the most common imaging tool used to observe changes in lumbar spine BMD over time in the sheep osteoporosis model [26, 27] and the use of QCT in longitudinal research studies has been limited to high resolution peripheral QCT (HR-pQCT) in the radius or tibia [28-30]. Few sheep osteoporosis studies have employed sequential *in vivo* imaging with age-matched seasonal controls in conjunction with micro-computed tomography (microCT) outcomes using serial bone biopsies [30, 31], which emphasize bone microarchitectural characteristics of the bone rather than just density. To our knowledge, QCT was not previously evaluated in direct comparison with DXA to quantify BMD in the lumbar spine of sheep. Additionally, no studies have directly compared QCT, DXA, and microCT changes via serial sampling over time in the same subjects – preclinically or clinically.

The objectives of this study were: 1) to compare BMD and trabecular microCT outcomes between control and experimental animals over the course of a year, and 2) to compare BMD measurements of the lumbar vertebrae over time in a sheep model of osteoporosis using both DXA, QCT, and compare to microCT outcomes from iliac crest biopsies. We first hypothesized that there would be a significant decrease in BMD and change in microCT outcomes in the osteoporotic group as compared to the control group animals following OVX and steroid administration. Secondly, we hypothesized that QCT would be more sensitive to changes in trabecular bone density as compared to DXA, and that QCT trabecular outcomes would more closely correlate with microCT outcomes for the same animals.

2.2 Materials and Methods

2.2.1 Animals and In Vivo Study Design

All procedures were approved by the Colorado State University Institutional Animal Care and Use Committee (Protocol #2060) and were performed in an AAALAC accredited facility. Sixteen (N=16) healthy skeletally mature conventionally-raised Rambouillet-cross ewes, aged 4-6 years, were enrolled in this study based on incisor presentation [32]. Any animals without full incisor eruption or animals with "broken-mouth" or heavily worn-down teeth were excluded from enrollment. Ten (N=10) sheep were randomly assigned to the osteoporotic group (OP) and six (N=6) sheep were assigned to the control group. The proposed OP group sample size (10 sheep) was calculated using an a-priori power analysis using longitudinal DXA BMD data from a previous study [33] (GPower Version 3.1.1). This power analysis resulted in an effect size of 1.2 and a power of 90%, using a standard deviation of 0.05 for all groups. All animals were enrolled at the same time of year to avoid seasonal impacts of bone loss and fed a standard diet of alfalfa and grass hay mix with grain supplementation, as needed. Animals were cohoused in

standard indoor box pen for the first two weeks following surgical procedures, followed by turnout to pasture for the remainder of the study. Animals were fed a standard diet of alfalfa-mix hay, except for 12-24 hours prior to scanning or surgical procedures when the animals were held off from feed for prevention of bloat while under anesthesia.

2.2.2 Osteoporosis Induction

Osteoporosis was induced in the sheep assigned to OP group (N=10) via laparoscopic bilateral ovariectomy (OVX) [34] and administration of corticosteroids. Two weeks following OVX, methylprednisolone acetate (Depo-Medrol®, Zoetis) was administered to all animals at a dose of 500 mg intramuscularly (IM) (5-7 mg/kg) every three weeks for a total of five doses and then reduced to half dose for three additional doses, as performed previously [33, 35] (**Fig. 2.1**). *In-vivo* imaging and bone biopsy collections were performed under general anesthesia at five time points for all animals: Baseline (prior to OVX), 3-months, 6-months, 9-months, and 12-months after OVX (**Fig. 2.1**).

For surgical and imaging/biopsy procedures, general anesthesia was induced by injecting a combination of midazolam (0.1 mg/kg) and ketamine (3.3-5 mg/kg) intravenously (IV) into a peripheral ear venous catheter. Anesthesia was maintained using isofluorane (1.5-3%) in 100% oxygen through an endotracheal tube. Blood pressure was monitored continuously throughout the procedures either through a peripheral arterial catheter or blood pressure cuff. One day prior to OVX surgery and each biopsy collection procedure, transdermal fentanyl patches (150 mcg) were adhered to the forelimb for sustained release over five days and phenylbutazone (1 g) was administered once per day orally for seven days for analgesic effect. Additionally, penicillin

procaine G (3 million units) was administered subcutaneously once per day for five days for prevention of infection starting the day prior to each procedure.

2.2.3 Quantitative Computed Tomography (QCT)

OP animals underwent a lumbar CT scan in a Siemens Somatom Definition AS 64-slice scanner (SIEMENS Healthineers, Munich, Germany) at each of the described five time points. Control animals did not undergo QCT scanning and analysis. OP animals were placed in the scanner in dorsal recumbency under general anesthesia and a Siemens Osteo phantom (Siemens Healthcare, Erlangen, Germany) was placed along the dorsal aspect of the animal's lumbar region to ensure inclusion of bone-like and water-like phase reference values in each scan. A single 10 mm thickness slice with a voxel size of 0.32 x 0.32 mm (voltage 80 kVp, current 300 mA) was acquired in the transverse plane of the midsection of three individual lumbar vertebrae, L3 through L5. Scans were analyzed using the syngo Osteo software (Siemens AG, version VA48A, Munich, Germany). Automatic contour tracing of each vertebral body and the phantom was performed, allowing for automatic separation between trabecular and cortical bone (**Fig. 2.2A**). The automated segmentation was visually verified and manual adjustments were performed if the cortical and trabecular bone were mis-registered. Mean trabecular volumetric BMD (Tb. vBMD) and mean cortical BMD (Ct. vBMD) were reported for each scanned vertebrae in mgCa-HA/cm^3.

2.2.4 Dual-Energy X-Ray Absorptiometry (DXA)

All animals underwent a DXA scan with a pixel size of 0.90 x 0.90 mm using a Hologic Discovery A scanner (Hologic, Inc., version 13.3.0.1, Marlborough, MA). Animals were

positioned in dorsal recumbency on the DXA table under anesthesia and a scan of the lumbar spine region (L3-L5) was performed. Scans were performed in triplicate for each animal to ensure minimal disruption of BMD measurements due to positioning and averaged together for a final reported value. DXA device calibration was carried out using a Hologic spine phantom (Hologic, Inc., Marlborough, MA) prior to each scanning time point according to the manufacturer's protocol. Areal BMD (aBMD) of the lumbar vertebrae was determined by manually defining the area between the caudal intervertebral disk to the cranial facets of the vertebral body and calculating the aBMD using the Hologic software (**Fig. 2.2B)**. aBMD was reported in g/cm^2 for each vertebra.

2.2.5 Bone Biopsy Collection

A 10 mm diameter biopsy was collected from the iliac crest of each animal at each of the previously described time points (**Fig. 2.1**) using a 10mm OATS® autograft system (Arthrex). Iliac crest laterality was alternated at each subsequent biopsy time point. At the 6, 9, and 12-month time points, the incision was placed a few centimeters away from the previous incision site and the bone was palpated for defects prior to collection prevent harvesting from a previous biopsy site. Samples were immediately submerged in 10% neutral buffered formalin (NBF) for fixation and transferred into phosphate-buffered saline (PBS) after 3-4 days.

2.2.6 Micro-Computed Tomography (MicroCT)

The formalin fixed iliac crest biopsy collected from each animal at each time point was used for microCT analysis to quantify the trabecular microarchitecture changes over time. Samples were scanned at a resolution of 10 μm^3 at 70 kVp, 113 µA, and 500 ms integration time

(Scanco μCT 80, version 1.1.15.0, Scanco USA, Inc., Wayne, PA). One region of interest (ROI) (5 mm diameter, 400 slices) was drawn per sample to include only trabecular bone and reconstructed using fixed optimal threshold values (upper bound = 2760.5 HU, lower bound = 456.7 HU). Threshold bounding was confirmed by visual inspection. The following output measures of trabecular microarchitecture were quantified from the three-dimensional reconstruction of each ROI cylinder: bone volume fraction (BV/TV), trabecular thickness (Tb.Th), trabecular number (Tb.N), trabecular spacing (Tb.Sp), connectivity density (Conn.D), and structural model index (SMI).

2.2.7 Statistics

Continuous data were compared to baseline values within groups using a one-way analysis of variance (ANOVA) with Tukey multiple comparisons and between groups across time points using a mixed model ANOVA with Šidák multiple comparisons. Comparisons between DXA, QCT, and microCT outcomes were made using a Pearson correlation, and a correlation coefficient (R^2) and 95% confidence interval (CI) was reported for each relationship. An R^2 value of 0.0-0.19 indicated a very weak correlation, 0.20-0.39 a weak correlation, 0.40-0.59 a moderate correlation, 0.60-0.79 a strong correlation, and 0.80-1.0 a very strong correlation [36, 37]. Correlation coefficients for aBMD versus combined vBMD (average of Ct. vBMD and Tb. vBMD) were calculated separately for each time point and include values for each lumbar vertebra (L3, L4, L5). When comparing to the iliac crest microCT outcomes, vBMD and aBMD values were averaged across the whole measured lumbar spine (L3-L5). The best-fit line of the relationship was determined by simple linear regression. For all statistical analyses, an alpha

value of 0.05 or less ($p \leq 0.05$) was considered significant (GraphPad Prism 9.5.0, San Diego, CA).

2.3 Results

2.3.1 DXA Measurements Between Groups

aBMD at L3 in the OP group was significantly lower than the control group at 3, 6, and 9-months. OP group BMD was significantly decreased from baseline at 6-months. There were no significant differences in L3 aBMD at any of the time points compared to baseline for the control group and at time points 3, 8, and 12-months for the OP group (**Fig. 2.3A**). L4 aBMD was significantly lower in OP group animals compared to the control group at 3, 6, 9, and 12-months. There were no significant differences in L4 aBMD at any of the time points compared to baseline for both the OP and control groups (**Fig. 2.3B**). OP group L5 aBMD was significantly lower than the control group at 3, 6, and 12-months. The control group L5 aBMD was significantly greater at 12-months compared to baseline. The OP group L5 aBMD was significantly lower at 6-months compared to baseline. All other time point comparisons were not found to be statistically significant for both groups (**Fig. 2.3C**). OP group proximal tibia aBMD was significantly lower than that of the control group at 9 and 12-months. Proximal tibia aBMD was significantly lower in the OP group animals at 6 and 9-months compared to baseline values. All other time point comparisons were not found to be statistically significant for both groups (**Fig. 2.3D**).

2.3.2 OP Sheep Lumbar Spine QCT Measurements

OP group Tb. vBMD measurements ranged from 309.9 mgCa-HA/cm^3 to 494.2 mgCa-HA/cm^3 at baseline, whereas Ct. vBMD ranged from 478.6 mgCa-HA/cm^3 to 802.7 mgCa-

HA/cm^3. Similar to DXA, average Tb. vBMD significantly decreased when compared to baseline values across L3, L4, and L5 at 3-months ($p = 0.004$, $p = 0.002$, $p = 0.006$, respectively) and 6-months ($p = 0.002$, $p = 0.009$, $p = 0.007$, respectively) (**Fig. 2.4B**). However, L5 Tb. vBMD was also noted to be significantly decreased from baseline at the 9-month ($p = 0.04$) and 12-month ($p = 0.02$) time points (**Fig. 2.4B**). There was no change compared to baseline L3 and L4 Tb. vBMD values at 9 and 12-months. Average Ct. vBMD did not significantly change between any time points at any of the measured vertebrae (**Fig. 2.4C**) when compared to baseline values. QCT Tb. vBMD measurements decreased, on average, by 12.47% (± 7.61%) at 3-months, 12.90% (± 8.76%) at 6-months, 9.93% (± 9.55%) at 9-months, and 8.08% (± 7.88%) at 12-months (**Fig. 2.4D**) post-OVX across the whole measured lumbar spine (L3-L5). Average Ct. vBMD decreased by 1.34% (± 10.08%) at 3-months, 2.15% (± 8.56%) at 6-months, and increased by 1.68% (± 10.02%) at 9-months and 3.35% (± 13.23%) at 12-months compared to baseline (**Fig. 2.4D**).

2.3.3 Iliac Crest MicroCT Trabecular Microarchitecture

Iliac crest biopsy bone volume fraction (BV/TV) was significantly lower in OP group animals at 6-months as compared to the control group. OP group BV/TV was also significantly lower at 6 and 9-months compared to baseline values. All other time point and group comparisons were not significantly different (**Fig. 2.5E**). OP group iliac crest biopsy Tb.N was significantly lower at 6 and 9-months compared to baseline values. No differences were observed between control and OP group values (**Fig. 2.5F**). OP group iliac crest Tb.Sp was significantly greater than control group values at 6-months. OP group Tb.Sp was also significantly greater than baseline values at 6-months. All other time point and group comparisons were not

significantly different (**Fig. 2.5G**). OP group iliac crest biopsy Tb.Th was significantly lower at 9-months than Control group. OP group Tb.Th was significantly lower at 9-months compared to baseline values. All other time point and group comparisons were not significantly different (**Fig. 2.5H**).

2.3.4 Comparison of Imaging Modalities in OP Animals

Tb. vBMD (QCT) bone loss was significantly greater than both aBMD (DXA) and Ct. vBMD (QCT) at 3-months ($p = 0.003$, $p < 0.0001$, respectively), 6-months ($p = 0.03$, $p < 0.0001$, respectively), 9-months ($p < 0.0001$, $p < 0.0001$, respectively), and 12-months ($p < 0.0001$, $p < 0.0001$, respectively) (**Fig.2.4D**). While aBMD bone loss was also significantly greater than Ct. vBMD at 3-months ($p = 0.003$) and 6-months ($p = 0.0004$), there were no significant differences observed at 9-months ($p = 0.16$) and 12-months ($p = 0.60$) (**Fig. 2.4D**). When comparing DXA aBMD and combined QCT vBMD (average of Tb. and Ct. vBMD measurements) of L3, L4, and L5 at each of the time points (baseline, 3, 6, 9, and 12-months), the correlation coefficients (R^2) were 0.46 (moderate, $p < 0.0001$), 0.58 (moderate, $p < 0.0001$), 0.60 (moderate, $p < 0.0001$), 0.62 (strong, $p < 0.0001$), and 0.19 (very weak, $p = 0.02$), respectively (**Fig. 2.6A-E**). Significant moderate correlations were found between lumbar spine Tb. vBMD (QCT) and iliac crest BV/TV (microCT) at baseline ($R^2 = 0.54$, $p = 0.02$), 3-months ($R^2 = 0.57$, $p = 0.01$), 9-months ($R^2 = 0.56$, $p = 0.01$), and 12-months ($R^2 = 0.48$, $p = 0.03$), and a significant strong correlation was found at 6-months ($R^2 = 0.66$, $p = 0.004$) (**Table 2.1**). When comparing lumbar spine aBMD (DXA) and iliac crest BV/TV, significant correlations were only found at 3-months ($R^2 = 0.55$, $p = 0.01$), and 6-months ($R^2 = 0.41$, $p = 0.05$) (**Table 2.1**). Correlations between lumbar spine Tb. vBMD (QCT) and iliac crest Tb.N (micoCT) were significant at baseline ($R^2 = 0.47$, $p = 0.03$),

3-months ($R^2 = 0.57$, $p = 0.01$), 9-months ($R^2 = 0.46$, $p = 0.03$), and 12-months ($R^2 = 0.62$, $p = 0.007$) (**Table 2.1**), whereas a significant correlation was only found at 3-months ($R^2 = 0.52$, $p = 0.02$) when comparing lumbar spine aBMD and iliac crest Tb.N (**Table. 2.1**).

2.4 Discussion

This study measured BMD values utilizing DXA, QCT, and microCT across a 12-month period in a sheep model of osteoporosis. We demonstrate significant bone density loss in the lumbar spine and tibia, as well as microarchitectural changes, in our OP group compared to controls throughout model progression. Results also showed QCT measurements and BMD losses more closely matching that of the microCT values as compared to DXA in osteoporotic animals, supporting our original hypothesis. The lumbar spine, rich in trabecular bone, offers a key insight into early bone loss and accurate screening can be indicative of an individual's risk for vertebral fracture. While microCT is not an option in a clinical setting without the use of bone biopsy, QCT and DXA can be utilized to measure changes in BMD in patients noninvasively. Limitations in current bone scanning modalities, primarily the use of DXA, have implored the search for more precise screening tools in the clinical and preclinical spaces. Although there are advantages to the use of DXA, advances in QCT software present a superior alternative to quantifying trabecular and cortical bone densities and early identification of individuals at high risk for fracture. While radiation exposure is increased in comparison to DXA, the opportunistic use of CT scans [38-42] and low-dose protocols [7, 43] can reduce the need for additional scanning time and patient exposure.

Previous clinical studies have shown correlative relationships between DXA and QCT BMD values in the lumbar spine [20, 37, 44], but there have been no clinical and limited preclinical studies looking at the same subjects over time. While CT Hounsfield Units (HU) and DXA aBMD have been compared in dogs [45, 46], ours is the first study to directly compare QCT and DXA in the sheep lumbar spine and to correlate those values to microCT outcomes in the same animals over a long-term study using a preclinical model of osteoporosis. We show moderate to strong correlations (R^2 ranging from 0.4-0.6) between QCT vBMD and DXA aBMD values at each time point, indicating that changes in BMD observed in an animal on DXA is reflected by similar trending changes in BMD on QCT when cortical and trabecular bone are analyzed together. This correlation is expected, as both cortical and trabecular bone contribute to DXA aBMD. However, when observing the trabecular bone changes alone using QCT, a higher percentage of bone loss is observed at 9-months and 12-months compared to DXA. We suspect this is due to trabecular regions being more susceptible to rapid BMD and microarchitectural changes than cortical bone, which is a key feature of early-stage bone loss in peri- and postmenopausal osteoporosis [13]. It is not unusual to observe a "bounce-back" of BMD values in sheep following osteoporosis induction [47, 48], which we indeed observed in this study when we looked at values determined by DXA alone. However, QCT has contrarily shown sustained trabecular BMD loss in the sheep lumbar spine throughout the duration of the one-year study. While we were unable to harvest serial bone biopsies of the lumbar spine trabecular bone as a direct comparison to DXA and QCT measurements, we were able to obtain iliac crest bone biopsies to compare potentially similar trabecular bone changes in the body at a higher resolution using microCT. We observed a continued decrease in iliac crest trabecular bone microCT values BV/TV and Tb.N at 9-months and 12-months when compared to baseline, demonstrating

sustained microarchitectural changes to the trabecular bone of the iliac crest following osteoporosis induction. Thus, we suspect that DXA potentially underestimates the actual change in BMD over time in our preclinical models and may inaccurately represent the amount of sustained loss of trabecular bone.

Differences in scanning resolution also played a key role in the outcomes of this study. MicroCT is one of the highest resolution scanning tools available to researchers to investigate changes in bone structure. Unfortunately, microCT is an *ex vivo* method and cannot be utilized in-life for humans or large animals. Although microCT can be utilized on bone biopsies from patients, a non-invasive scanning technique more indicative of trabecular bone changes is preferable to understand patient risk for osteoporotic fractures. HR-pQCT offers a way to look at bone microarchitecture at a higher resolution than standard in-life imaging modalities while maintaining relatively low radiation exposure to the patient [49, 50], however, its application is limited to the distal tibia and radius due to scanner size limitations. Since trabecular bone microarchitecture heavily factors into the overall bone strength and a disruption to microarchitecture increases fracture risk [11, 12, 51, 52], it is probably more useful to screen an anatomical location with a larger trabecular bone area, such as the lumbar spine. We show stronger and more significant correlations at all time points between microCT BV/TV and QCT Tb. vBMD than with DXA aBMD, as well as significant correlations with Tb.N at a greater number of time points than DXA. Higher imaging resolution of QCT versus DXA likely allowed for more precise segmentation of bone, and thus a stronger correlation with high-resolution iliac crest microCT outcomes. This is in agreement with a previous study conducted by Bodic *et al.*, wherein they observed significant correlative relationships between microCT values (BV/TV and

Tb.N) and CT HU measurements in the iliac crest of humans, but observed no significant relationship when compared to DXA BMD measurements in the same samples [53]. In this way, we demonstrate that lumbar spine QCT more strongly correlates to iliac crest trabecular bone microarchitectural changes than DXA in our sheep model, thus demonstrating higher sensitivity to multiple properties of osteoporotic bone loss.

This study is not without its limitations. Primarily, we acknowledge that the bone biopsies utilized for microCT and the area used for *in vivo* scanning are different anatomical locations (iliac crest for microCT vs. lumbar spine for DXA and QCT). Although we expect that we would observe similar changes in BMD and trabecular microarchitecture at both anatomical locations, we are unable to confirm that the QCT and DXA findings directly apply to the lumbar spine trabecular microarchitecture. While some previous studies have shown that there are differences in trabecular bone mass and connectivity [54] properties across various anatomical sites of the body, significant correlations in mechanical [55] and microarchitectural [56] properties between the iliac crest and lumbar spine have been demonstrated. Although this has not been verified directly in sheep, similar trends in bone density loss have been observed over time in previous sheep osteoporosis studies between the lumbar spine and iliac crest [57]. Future research would be required to directly compare microarchitectural changes between the iliac crest and lumbar vertebrae trabecular bone in the sheep model of osteoporosis. Additionally, we acknowledge that there is subtle variability in bone microarchitecture across the iliac crest that could have impacted our microCT results, as we were not consistent between animals with respect to exact location of iliac crest biopsy collection site at each time point [54]. There are inherent limitations with using conventionally-raised sheep in research studies, primarily aging

of animals. While we do our best control for age based on eruption of incisors, it is difficult to exactly determine age in sheep after reaching skeletal maturity. Therefore, we excluded any animals with not yet erupted or worn-down incisors that would indicate young or old age, estimating an age between 4-6 years and control for age effects [32]. A limitation to the use of QCT in preclinical research is the use of multiple lumbar CT scans over a longitudinal study, which could add up to high radiation exposure and cost. This is an important factor when considering the use of QCT in human subjects or long-term animal studies. For reference, animals in our study received an approximate effective radiation dose of 0.06 mSv per single QCT lumbar vertebra scan, whereas DXA radiation exposure typically ranges between 0.022-0.047 mSv for a full lumbar spine scan [58]. There is typically higher cost of scanning using CT as compared to DXA. Additionally, a trained radiology technician is required to operate a CT scanner, whereas less extensive training is required for DXA operation. However, CT may be more readily available to researchers in a preclinical or veterinary setting than DXA. While anesthesia is required for use of both DXA and CT in a preclinical setting, no differences in time required for scanning and animal positioning were observed between modalities. Lastly, the lack of reference data available for QCT leaves researchers and clinicians alike unable to calculate T-scores, as is available with DXA. Further clinical and preclinical studies using QCT in human patients and animal models with osteoporotic, osteopenic, and normal bone are required to build reference datasets for future use in low bone density screening. While limitations exist with both methods, the available instrumentation ultimately dictates which scanning modality is to be used in a longitudinal preclinical study.

In conclusion, the results of this study indicate that bone loss is observed in osteoporotic sheep compared to controls over the course of one year following OVX and steroid administration. QCT offers a more precise tool to measure lumbar spine trabecular BMD in a large animal osteoporosis model as compared to DXA. Accurate *in vivo* bone imaging modalities can reduce the number of animals needed for preclinical studies and provide more detailed insight into the progression of hormone or age-related bone loss that can be translated to humans. This preclinical data adds to the growing body of clinical literature on the use of QCT in lieu of DXA to quantify bone density for early and accurate diagnosis of osteoporosis.

2.5 Figures / Tables

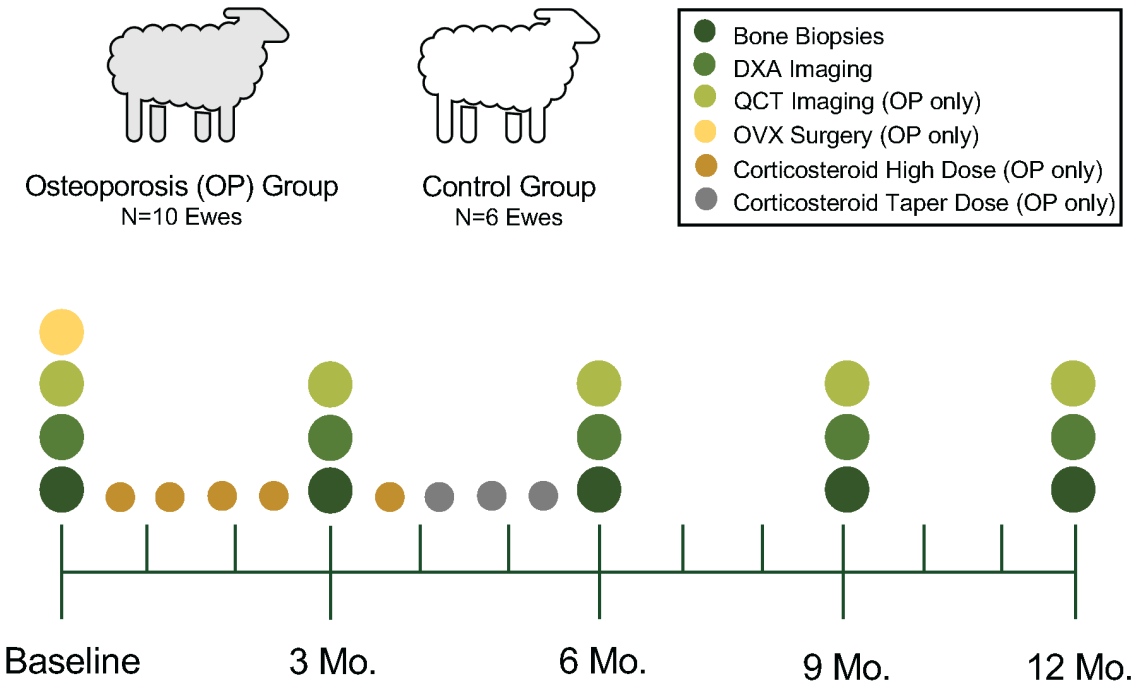

Figure 2.1. Aim 1 *in vivo* study design and sample collection time points.

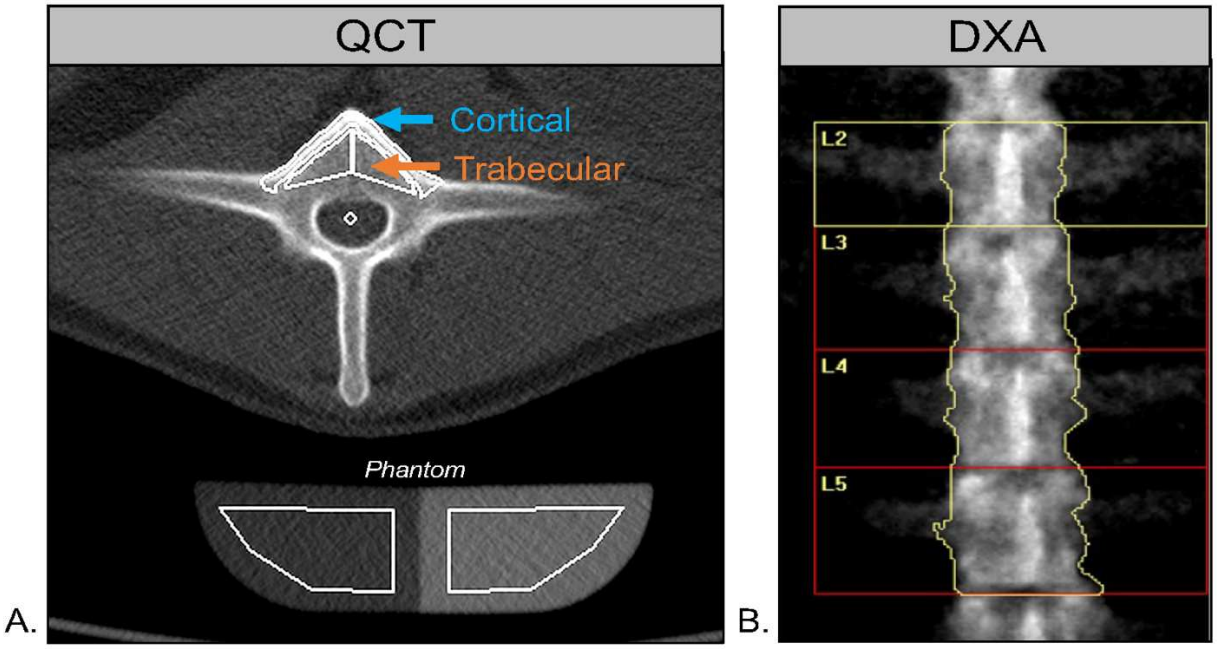

Figure 2.2. Imaging segmentation and measurement of bone mineral density (BMD) in the sheep lumbar spine. A) Quantitative computed tomography (QCT) semi-automated analysis using the syngo Osteo software. Trabecular volumetric BMD (Tb. vBMD) was determined from the inner vertebral body cancellous bone region (orange arrow) and the cortical volumetric BMD (Ct. vBMD) from the anterior cortical shell of the same vertebrae (blue arrow). Hounsfield units (HU) were converted to mg Ca-HA/cm^3 using the water (0 mg/cm^3, left side) and bone-phase (200 mg/cm^3, right side) phantom. B) Dual-energy X-ray absorptiometry (DXA) semi-automated analysis using the Hologic scanner software. Each vertebra was manually defined as extending from the intervertebral disk to the facets. Phantom calibration of the DXA scanner was performed daily prior to imaging animals.

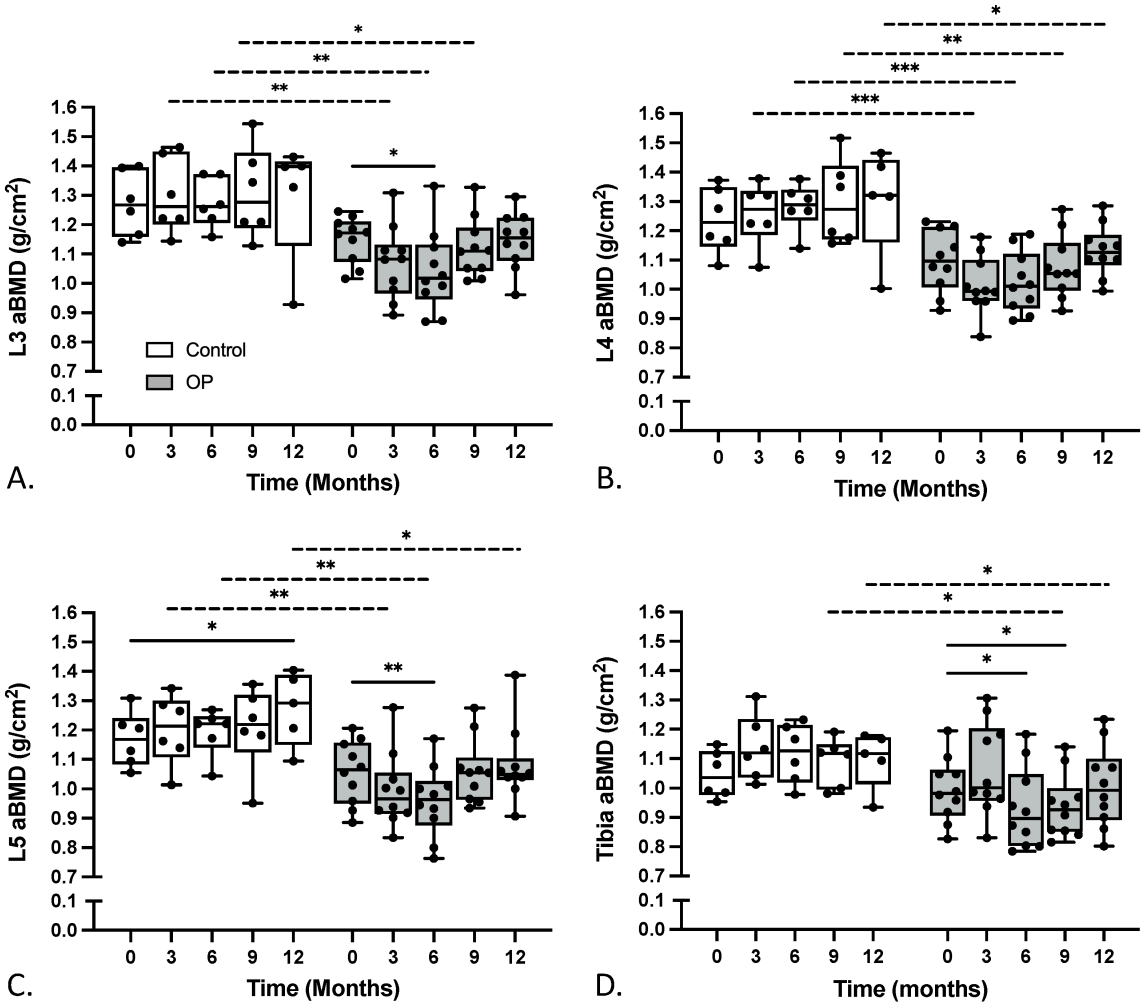

Figure 2.3. Comparisons of areal BMD (aBMD) measurements between OP (N=10) and control (N=6) sheep acquired through *in vivo* dual X-ray absorptiometry (DXA) imaging across study time points (baseline (0), 3, 6, 9, and 12 months). A) Lumbar vertebra L3 aBMD measurements. B) Lumbar vertebra L4 aBMD measurements. C) Lumbar vertebra L5 aBMD measurements. D) Proximal tibia aBMD measurements. Significance indicators: *p<0.05, **p<0.01, ***p<0.001, ****p<0.0001.

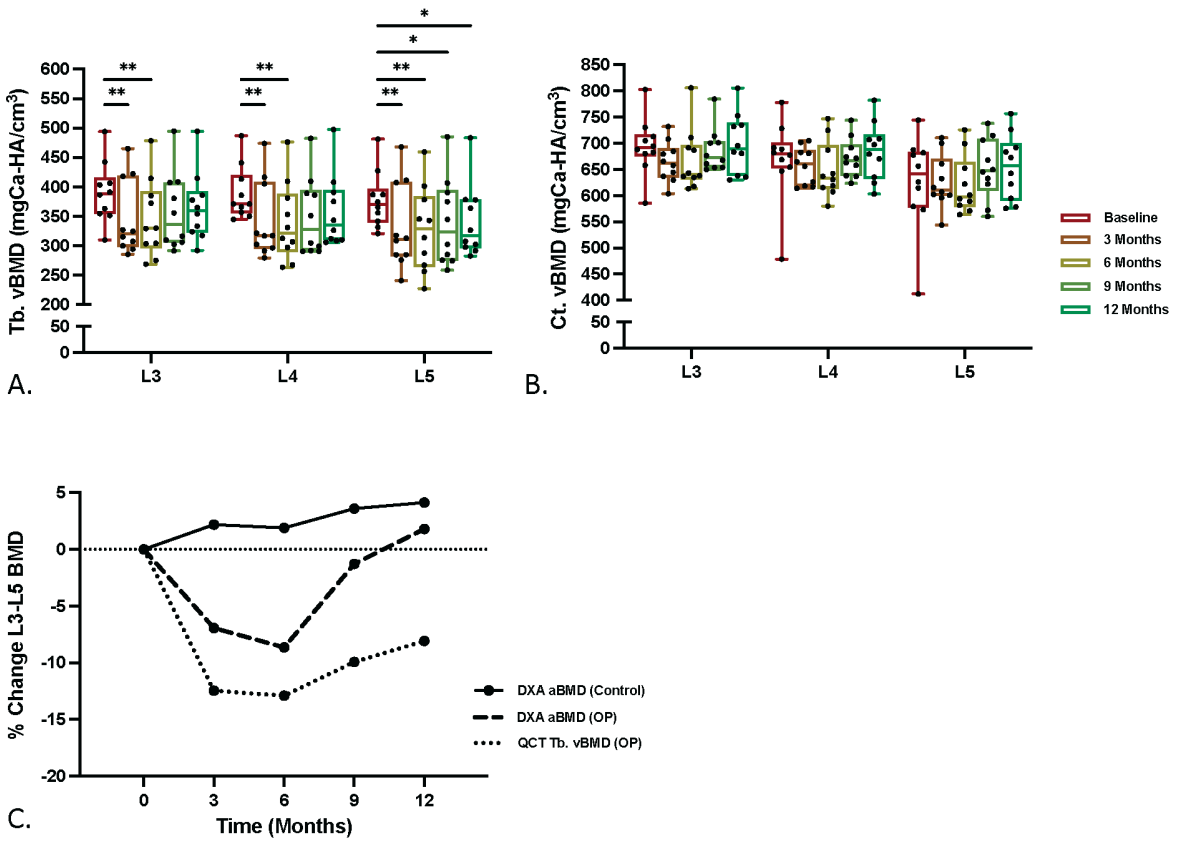

Figure 2.4. A) Volumetric trabecular bone density (Tb.vBMD) and cortical bone density (Ct.vBMD) measurements using quantitative computed tomography (QCT) in lumbar vertebrae (L3, L4, L5) of OP sheep over time. B) Tb.vBMD and Ct.vBMD measurements using QCT in lumbar vertebrae (L3, L4, L5) of OP sheep over time. C) Mean percentage change of L3-L5 BMD as compared to baseline values across time using two imaging modalities (QCT and DXA). Note: QCT was only performed for OP group. Data is represented as mean ± SD with individual animals marked. Significance indicators: *p<0.05, **p<0.01.

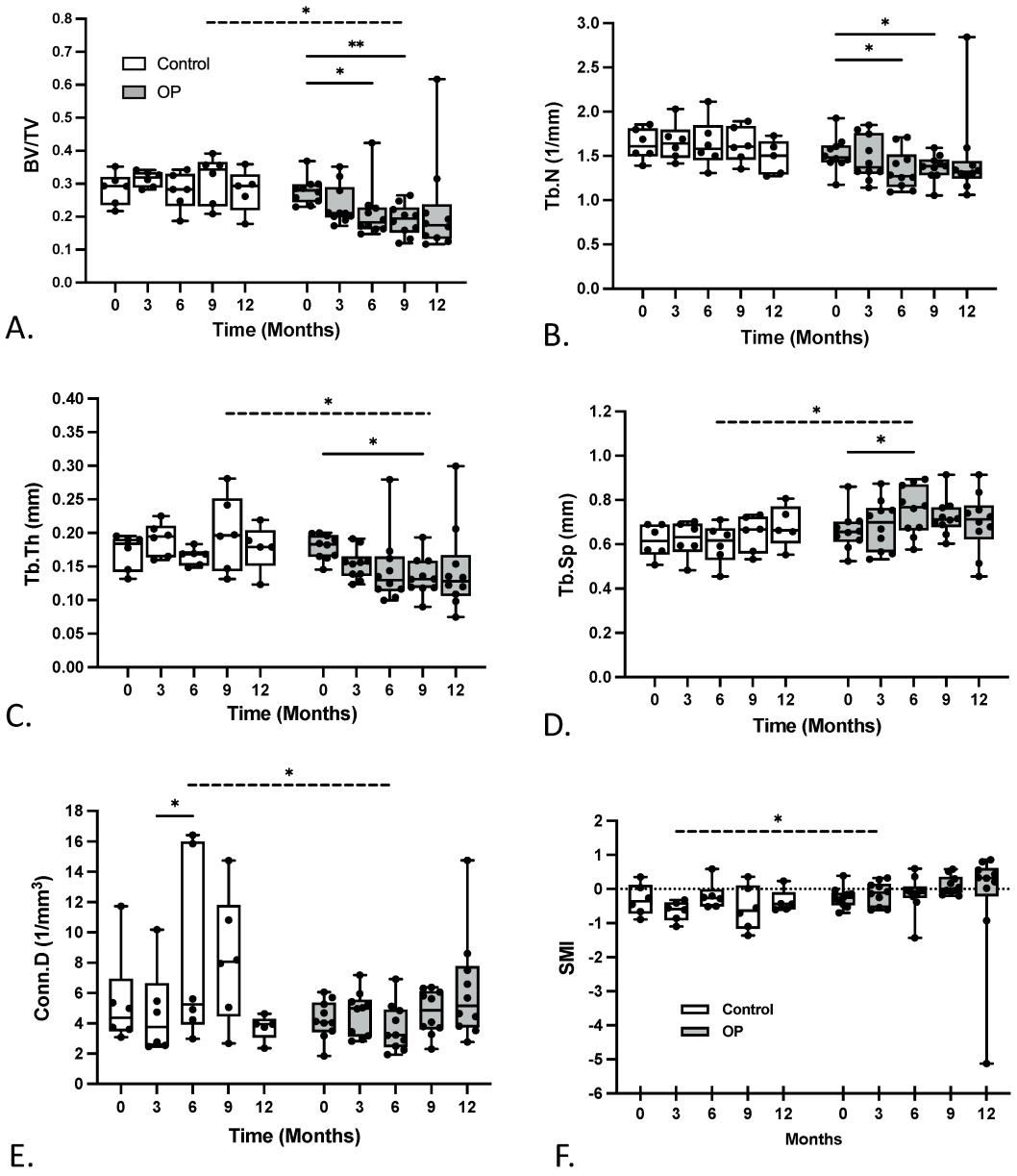

Figure 2.5. Bone microarchitectural changes measured using microCT in the sheep iliac crest biopsies across study time points (baseline (0), 3, 6, 9, and 12 months). A) Bone volume fraction (BV/TV) at each time point compared to baseline values. B) Trabecular number (Tb.N) values at each time point compared to baseline values. C) Trabecular thickness (Tb.Th) values at each time point compared to baseline values. D) Trabecular spacing (Tb.Sp) values at each time point compared to baseline values. Data is represented as mean $\pm$ SD with individual animals marked. Significance indicator: *$p<0.05$.

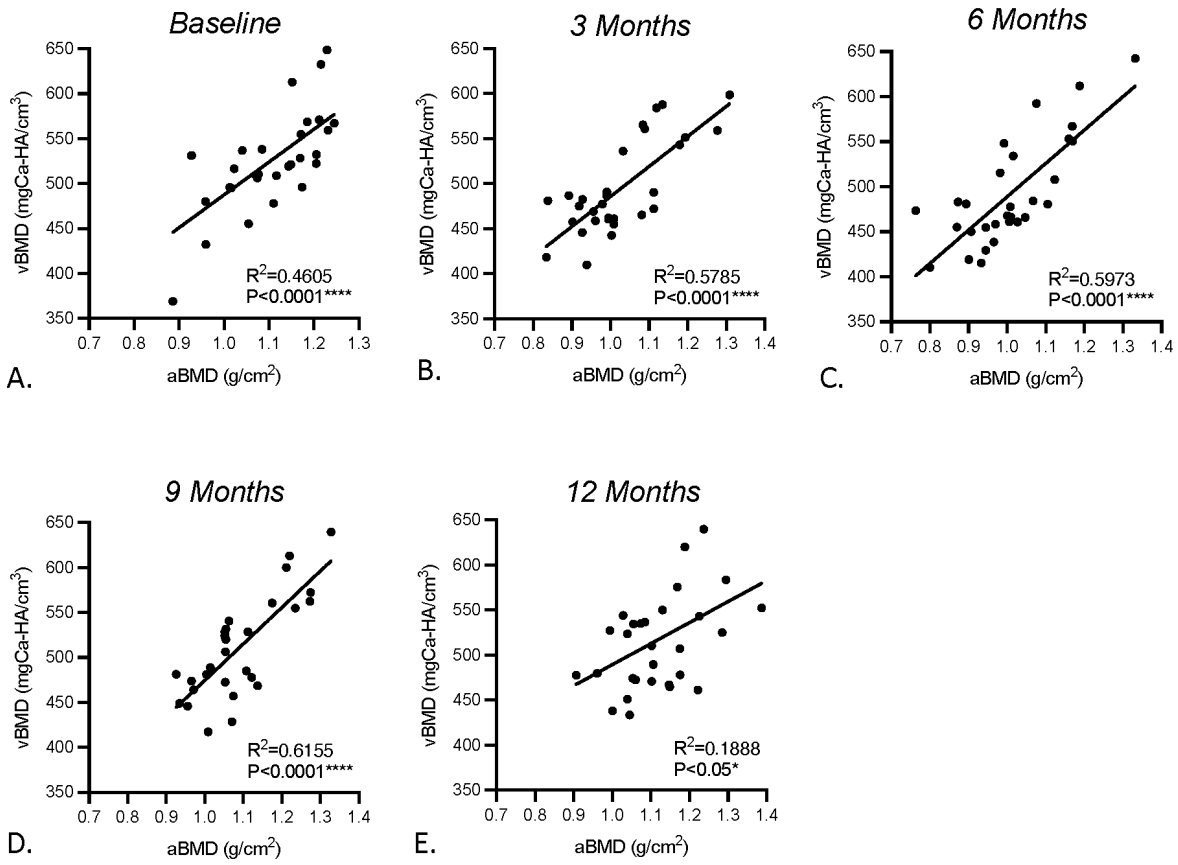

Figure 2.6. Relationship between dual-energy X-ray absorptiometry (DXA) areal bone mineral density (aBMD) and combined quantitative computed tomography (QCT) volumetric BMD (vBMD) (trabecular and cortical vBMD average) of OP group lumbar vertebrae (L3, L4, L5) (N=10 subjects). A) Correlation between aBMD and vBMD at baseline, before ovariectomy (OVX). B) Correlation between aBMD and vBMD at 3-months after OVX. C) Correlation between aBMD and vBMD at 6-months after OVX. D) Correlation between aBMD and vBMD at 9-months after OVX. E) Correlation between aBMD and vBMD at 12-months after OVX. Statistical comparisons made using a Pearson's correlation and simple linear regression. Significance indicators: *p<0.05, ****p<0.0001.

Table 2.1

Pearson correlations for relationships between iliac crest trabecular bone microCT volume and microarchitecture parameters and bone mineral density acquired by DXA and QCT for n=10 osteoporotic sheep.

MicroCT Outcome		DXA aBMD (g/cm^2)		QCT Tb. vBMD ($mgCa\text{-}HA/cm^3$)	
	Time Point	Correlation coefficient (R^2)	95% Confidence Interval	Correlation coefficient (R^2)	95% Confidence Interval
BV/TV	Baseline	0.2281	-0.22 to 0.85	0.5364[a]	0.19 to 0.93
	3 Months	0.5530[a]	0.21 to 0.94	0.5661[a]	0.23 to 0.94
	6 Months	0.4057[a]	0.01 to 0.90	0.6576[b]	0.37 to 0.95
	9 Months	0.2027	-0.25 to 0.84	0.5600[a]	0.22 to 0.94
	12 Months	0.1894	-0.27 to 0.84	0.4826[a]	0.12 to 0.92
Tb.N (1/mm)	Baseline	0.1378	-0.34 to 0.81	0.4665[a]	0.09 to 0.92
	3 Months	0.5196[a]	0.17 to 0.93	0.5748[a]	0.25 to 0.94
	6 Months	0.2487	-0.07 to 0.89	0.3403	-0.19 to 0.86
	9 Months	0.2068	-0.25 to 0.84	0.4605[a]	0.09 to 0.92
	12 Months	0.1849	-0.27 to 0.83	0.6155[b]	0.31 to 0.95
Tb.Th (mm)	Baseline	0.0372	-0.50 to 0.73	0.0806	-0.42 to 0.78
	3 Months	0.3738	-0.03 to 0.90	0.3088	-0.11 to 0.88
	6 Months	0.2081	-0.24 to 0.84	0.5055[a]	0.15 to 0.93
	9 Months	0.0582	-0.46 to 0.76	0.2374	-0.21 to 0.85
	12 Months	0.1572	-0.31 to 0.82	0.3460	-0.07 to 0.89
Tb.Sp (mm)	Baseline	0.0404	-0.74 to 0.49	0.2859	-0.87 to 0.14
	3 Months	0.5053[a]	-0.93 to -0.15	0.5557[a]	-0.94 to -0.22
	6 Months	0.2815	-0.87 to 0.15	0.1401	-0.82 to 0.33
	9 Months	0.1453	-0.82 to 0.33	0.3461	-0.89 to 0.07
	12 Months	0.1049	-0.79 to 0.38	0.2587	-0.86 to 0.18

MicroCT = micro-computed tomography; DXA = dual-energy X-ray absorptiometry; aBMD = areal bone mineral density; QCT = quantitative computed tomography; Tb. vBMD = trabecular volumetric bone mineral density; Ct. vBMD = cortical volumetric bone mineral density; BV/TV = bone volume over total volume; Tb.N = trabecular number; Tb.Th = trabecular thickness; Tb.Sp = trabecular spacing; [a] = $P < 0.05$; [b] = $P < 0.01$.

2.6 References

1. Unnanuntana, A., et al., *The assessment of fracture risk.* J Bone Joint Surg Am, 2010. **92**(3): p. 743-53.
2. Chou, S.H. and M.S. LeBoff, *Vertebral Imaging in the Diagnosis of Osteoporosis: a Clinician's Perspective.* Curr Osteoporos Rep, 2017. **15**(6): p. 509-520.
3. Xue, S., et al., *An Updated Reference for Calculating Bone Mineral Density T-Scores.* J Clin Endocrinol Metab, 2021. **106**(7): p. e2613-e2621.
4. Camacho, P.M., et al., *American Association of Clinical Endocrinologists/American College of Endocrinology Clinical Practice Guidelines for the Diagnosis and Treatment of Postmenopausal Osteoporosis-2020 Update.* Endocr Pract, 2020. **26**(Suppl 1): p. 1-46.
5. Wright, N.C., et al., *The recent prevalence of osteoporosis and low bone mass in the United States based on bone mineral density at the femoral neck or lumbar spine.* J Bone Miner Res, 2014. **29**(11): p. 2520-6.
6. Kanis, J.A., et al., *A reference standard for the description of osteoporosis.* Bone, 2008. **42**(3): p. 467-75.
7. Damilakis, J., et al., *Radiation exposure in X-ray-based imaging techniques used in osteoporosis.* Eur Radiol, 2010. **20**(11): p. 2707-14.
8. Sebro, R. and S.S. Ashok, *A Statistical Approach Regarding the Diagnosis of Osteoporosis and Osteopenia From DXA: Are We Underdiagnosing Osteoporosis?* JBMR Plus, 2021. **5**(2): p. e10444.
9. Bolotin, H.H., *Inaccuracies inherent in dual-energy X-ray absorptiometry in vivo bone mineral densitometry may flaw osteopenic/osteoporotic interpretations and mislead assessment of antiresorptive therapy effectiveness.* Bone, 2001. **28**(5): p. 548-55.

10. Whitmarsh, T., et al., *A cross-sectional study on the age-related cortical and trabecular bone changes at the femoral head in elderly female hip fracture patients.* Sci Rep, 2019. **9**(1): p. 305.

11. Chen, H., et al., *Age-related changes in trabecular and cortical bone microstructure.* Int J Endocrinol, 2013. **2013**: p. 213234.

12. Osterhoff, G., et al., *Bone mechanical properties and changes with osteoporosis.* Injury, 2016. **47 Suppl 2**(Suppl 2): p. S11-20.

13. Finkelstein, J.S., et al., *Bone mineral density changes during the menopause transition in a multiethnic cohort of women.* J Clin Endocrinol Metab, 2008. **93**(3): p. 861-8.

14. Riggs, B.L. and L.J. Melton, 3rd, *The prevention and treatment of osteoporosis.* N Engl J Med, 1992. **327**(9): p. 620-7.

15. Yu, E.W., et al., *Simulated increases in body fat and errors in bone mineral density measurements by DXA and QCT.* J Bone Miner Res, 2012. **27**(1): p. 119-24.

16. Guglielmi, G., et al., *Effect of spinal degenerative changes on volumetric bone mineral density of the central skeleton as measured by quantitative computed tomography.* Acta Radiol, 2005. **46**(3): p. 269-75.

17. Smith, J.A., et al., *Aortic calcification contributing to bone densitometry measurement.* J Clin Densitom, 1999. **2**(2): p. 181-3.

18. Liu, G., et al., *Effect of osteoarthritis in the lumbar spine and hip on bone mineral density and diagnosis of osteoporosis in elderly men and women.* Osteoporos Int, 1997. **7**(6): p. 564-9.

19. Adams, J.E., *Quantitative computed tomography.* Eur J Radiol, 2009. **71**(3): p. 415-24.

20. Pinto, E.M., et al., *Efficacy of Hounsfield Units Measured by Lumbar Computer Tomography on Bone Density Assessment: A Systematic Review.* Spine (Phila Pa 1976), 2022. **47**(9): p. 702-710.

21. Oei, L., et al., *Quantitative imaging methods in osteoporosis.* Quant Imaging Med Surg, 2016. **6**(6): p. 680-698.

22. Link, T.M., *Osteoporosis imaging: state of the art and advanced imaging.* Radiology, 2012. **263**(1): p. 3-17.

23. Genant, H.K., K. Engelke, and S. Prevrhal, *Advanced CT bone imaging in osteoporosis.* Rheumatology (Oxford), 2008. **47 Suppl 4**(Suppl 4): p. iv9-16.

24. Li, N., et al., *Comparison of QCT and DXA: Osteoporosis Detection Rates in Postmenopausal Women.* Int J Endocrinol, 2013. **2013**: p. 895474.

25. Choksi, P., K.J. Jepsen, and G.A. Clines, *The challenges of diagnosing osteoporosis and the limitations of currently available tools.* Clin Diabetes Endocrinol, 2018. **4**: p. 12.

26. Biehl, C., et al., *DXA reference values of the humanoid sheep model in preclinical studies.* PeerJ, 2021. **9**: p. e11183.

27. Turner, A.S., et al., *Dual-energy X-ray absorptiometry in sheep: experiences with in vivo and ex vivo studies.* Bone, 1995. **17**(4 Suppl): p. 381S-387S.

28. Egermann, M., et al., *Pinealectomy affects bone mineral density and structure--an experimental study in sheep.* BMC Musculoskelet Disord, 2011. **12**: p. 271.

29. Egermann, M., et al., *A sheep model for fracture treatment in osteoporosis: benefits of the model versus animal welfare.* Lab Anim, 2008. **42**(4): p. 453-64.

30. Sigrist, I.M., et al., *The long-term effects of ovariectomy on bone metabolism in sheep.* J Bone Miner Metab, 2007. **25**(1): p. 28-35.

31. Fini, M., et al., *The ovariectomised sheep as a model for testing biomaterials and prosthetic devices in osteopenic bone: a preliminary study on iliac crest biopsies.* Int J Artif Organs, 2000. **23**(4): p. 275-81.

32. Cocquyt, G., B. Driessen, and P. Simoens, *Variability in the eruption of the permanent incisor teeth in sheep.* Veterinary record, 2005. **157**(20): p. 619-623.

33. James, A.W., et al., *NELL-1 in the treatment of osteoporotic bone loss.* Nat Commun, 2015. **6**: p. 7362.

34. Easley, J.T., et al., *A 3-portal laparoscopic ovariectomy technique in ewes.* Small Ruminant Research, 2014. **121**(2): p. 336-339.

35. Klopfenstein Bregger, M.D., et al., *Optimization of corticosteroid induced osteoporosis in ovariectomized sheep. A bone histomorphometric study.* Vet Comp Orthop Traumatol, 2007. **20**(1): p. 18-23.

36. Lucas, K., et al., *Comparative investigation of bone mineral density using CT and DEXA in a canine femoral model.* J Orthop Res, 2017. **35**(12): p. 2667-2672.

37. Alawi, M., et al., *Dual-Energy X-Ray Absorptiometry (DEXA) Scan Versus Computed Tomography for Bone Density Assessment.* Cureus, 2021. **13**(2): p. e13261.

38. Lenchik, L., et al., *Opportunistic Screening for Osteoporosis Using Computed Tomography: State of the Art and Argument for Paradigm Shift.* Curr Rheumatol Rep, 2018. **20**(12): p. 74.

39. Gausden, E.B., et al., *Opportunistic Use of CT Imaging for Osteoporosis Screening and Bone Density Assessment: A Qualitative Systematic Review.* J Bone Joint Surg Am, 2017. **99**(18): p. 1580-1590.

40. Berger-Groch, J., et al., *Assessment of bone quality at the lumbar and sacral spine using CT scans: a retrospective feasibility study in 50 comparing CT and DXA data.* Eur Spine J, 2020. **29**(5): p. 1098-1104.

41. Leonhardt, Y., et al., *Opportunistic QCT Bone Mineral Density Measurements Predicting Osteoporotic Fractures: A Use Case in a Prospective Clinical Cohort.* Front Endocrinol (Lausanne), 2020. **11**: p. 586352.

42. Kim, K.J., et al., *Hounsfield Units on Lumbar Computed Tomography for Predicting Regional Bone Mineral Density.* Open Med (Wars), 2019. **14**: p. 545-551.

43. Goo, H.W., *CT radiation dose optimization and estimation: an update for radiologists.* Korean J Radiol, 2012. **13**(1): p. 1-11.

44. Schreiber, J.J., et al., *Hounsfield units for assessing bone mineral density and strength: a tool for osteoporosis management.* J Bone Joint Surg Am, 2011. **93**(11): p. 1057-63.

45. Kwon, D., et al., *Quantitative computed tomographic evaluation of bone mineral density in beagle dogs: comparison with dual-energy x-ray absorptiometry as a gold standard.* J Vet Med Sci, 2018. **80**(4): p. 620-628.

46. Lee, D., et al., *Quantitative CT assessment of bone mineral density in dogs with hyperadrenocorticism.* J Vet Sci, 2015. **16**(4): p. 531-42.

47. Goldhahn, J., et al., *Slow rebound of cancellous bone after mainly steroid-induced osteoporosis in ovariectomized sheep.* J Orthop Trauma, 2005. **19**(1): p. 23-8.

48. Zarrinkalam, M.R., et al., *Osteoporotic characteristics persist in the spine of ovariectomized sheep after withdrawal of corticosteroid administration.* J Osteoporos, 2012. **2012**: p. 182509.

49. Doi, M., et al., *Bone microstructure in healthy men measured by HR-pQCT: Age-related changes and their relationships with DXA parameters and biochemical markers.* Bone, 2022. **154**: p. 116252.

50. Macdonald, H.M., et al., *Age-related patterns of trabecular and cortical bone loss differ between sexes and skeletal sites: a population-based HR-pQCT study.* J Bone Miner Res, 2011. **26**(1): p. 50-62.

51. Xie, F., et al., *Microstructural properties of trabecular bone autografts: comparison of men and women with and without osteoporosis.* Arch Osteoporos, 2018. **13**(1): p. 18.

52. Parfitt, A.M., et al., *Relationships between surface, volume, and thickness of iliac trabecular bone in aging and in osteoporosis. Implications for the microanatomic and cellular mechanisms of bone loss.* J Clin Invest, 1983. **72**(4): p. 1396-409.

53. Bodic, F., et al., *Relationships between bone mass and micro-architecture at the mandible and iliac bone in edentulous subjects: a dual X-ray absorptiometry, computerised tomography and microcomputed tomography study.* Gerodontology, 2012. **29**(2): p. e585-94.

54. Amling, M., et al., *Heterogeneity of the skeleton: comparison of the trabecular microarchitecture of the spine, the iliac crest, the femur, and the calcaneus.* J Bone Miner Res, 1996. **11**(1): p. 36-45.

55. Britton, J.M. and M.W. Davie, *Mechanical properties of bone from iliac crest and relationship to L5 vertebral bone.* Bone, 1990. **11**(1): p. 21-8.

56. Dempster, D.W., et al., *Relationships between bone structure in the iliac crest and bone structure and strength in the lumbar spine.* Osteoporos Int, 1993. **3**(2): p. 90-6.

57. Zarrinkalam, M.R., et al., *Validation of the sheep as a large animal model for the study of vertebral osteoporosis.* Eur Spine J, 2009. **18**(2): p. 244-53.

58. Shi, J., et al., *Guidelines for Dual Energy X-Ray Absorptiometry Analysis of Trabecular Bone-Rich Regions in Mice: Improved Precision, Accuracy, and Sensitivity for Assessing Longitudinal Bone Changes.* Tissue Eng Part C Methods, 2016. **22**(5): p. 451-63.

CHAPTER 3:
CHARACTERIZATION OF THE CLINICAL AND SYSTEMIC EFFECTS OF HIGH-DOSE STEROIDS AND ESTROGEN DEPLETION IN AN OVINE MODEL OF OSTEOPOROSIS

3.1 Introduction

The sheep model of osteoporosis has historically been widely used to study the effects of estrogen deficiency on bone loss, much like postmenopausal osteoporosis in women. Menopause is defined as the period of time following the cessation of the final menstruation cycle. Prior to menopause, production of estradiol by the ovary, the body's primary source of estradiol synthesis, is due to follicular activity [1, 2]. Loss of estradiol synthesis during menopause results in an increased rate of bone resorption by direct and indirect mechanisms. Estrogen is an important steroid hormone with multiple important functions, including regulation of bone homeostasis. The period of time between the 1.5 years before menopause to 1.5 years after menopause (also known as perimenopause), lumbar spine bone mineral density decreases by approximately 2.56% per year, compared with a pre-menopausal loss rate of 0.13% per year [1]. Estradiol, the active form of estrogen primarily involved in direct and indirect regulation of bone cells, is derived from cholesterol and acts primarily as a genomic transcription regulator. The hormone circulates the blood serum in protein-bound form, passively translocates to the nucleus, and binds to estrogen receptor to activate the receptor complex and alter the pattern of gene expression in a cell [3]. In adults, estradiol increases bone formation and mineralization and reduces bone resorption, thus reducing risk of osteoporosis [2].

In addition to estrogen loss following menopause, glucocorticoid administration also has a significant negative impact on bone. It has been estimated that up to 4.6% of postmenopausal women are prescribed glucocorticoids for other pathologies [4]. While glucocorticoids are

successful at treating various chronic inflammatory diseases, they have the ability to cause significant side effects when prescribed at high doses.

In recent years, the sheep model of osteoporosis has been successfully used for testing the efficacy and safety of orthopaedic implants in low quality bone. One of the adaptations to the model was the introduction of corticosteroid administration to the animals, as this proved even more successful in driving down bone loss percentages in order to mimic a clinically relevant low-quality, low-turnover bone scenario [5-7]. However, one of the drawbacks to corticosteroid administration is the implications for drastic systemic health changes in the animals. Animal loss has also been reported in previous studies where this model was employed, bringing up concerns surrounding animal welfare [8]. While it is well understood that bone loss can be successfully achieved in a sheep model of osteoporosis, it is not well described how this model development impacts the animal just beyond bone parameters.

The aim of this study was to report on the sheep clinical pathologies throughout osteoporosis model development (i.e., administration of steroids) and any potential impact on the model over 12-months. To our knowledge, no studies have comprehensively characterized clinical parameters in the sheep model of osteoporosis via serial sampling in a long-term study. We hypothesized that systemic impacts would be observed during the process of model development in our study animals compared to age-matched controls, and that any acute changes observed would be primarily due to glucocorticoid administration.

3.2 Materials and Methods

3.2.1 Animals and Osteoporosis Induction

All animal procedures were approved by the Colorado State University Institutional Animal Care and Use Committee (Protocol #2060). Animal selection, experimental grouping, and osteoporosis induction methods are previously outlined in Chapter 2. Briefly, sixteen (N=16) healthy skeletally mature conventionally-raised Rambouillet-cross ewes aged 4-6 years were enrolled in this study based on incisor presentation [9]. Ten (N=10) sheep were randomly assigned to the osteoporotic group (OP) and underwent osteoporosis induction by OVX and corticosteroid administration. Blood for clinical pathology and bone marrow sample collections were performed under general anesthesia at five time points for all animals: Baseline (prior to OVX), 3-months, 6-months, 9-months, and 12-months after OVX (**Fig. 3.1**). Body weights and blood serum for hormone analysis were performed monthly, including at baseline (**Fig. 3.1**).

3.2.2 Bone Marrow Aspirate Nucleated Cell Counts

Bone marrow aspirate (BMA) samples were collected from all animals every 3-months and a total nucleated cell count was performed to assess bone marrow cellularity. To harvest BMA, sheep were placed in sternal recumbency on the surgical table and the iliac crest was prepped for aseptic sample collection using alternating scrubs of chlorhexidine and alcohol. A Monoject ™ 11 G Jamshidi needle (Covidien, Medtronic, Dublin, Ireland) was placed percutaneously through the skin into the iliac crest. A heparin flushed syringe (2,500IU/mL, ~1mL heparin retained in the syringe) was attached to the needle and approximately 4-7mL of BMA was aspirated. The aspirate was immediately placed on ice until further processing. BMA samples were assessed for quality and cellularity by total nucleated cell counts (TNC) the same day as collection. In a biosafety hood, BMA samples were transferred into 15 mL conical tube

and mixed thoroughly. Cell counts were performed by adding 90 µL 0.8% ammonium chloride (Sigma) to a 10 µL aliquot from each BMA sample to obtain a 1:10 sample dilution. Diluted samples were loaded onto a Bright-Line™ hemocytometer (Hausser Scientific, Horsham, PA) and bright nucleated cells were visualized and manually counted using an inverted microscope. If cell density was too high to count, samples were diluted 1:100. Cell concentration per mL was determined using the following equation:

Total number of nucleated cells/mL of BMA = Avg. cell count per square x Dilution factor x 10^4

3.2.3 Estradiol Radioimmunoassay

Blood serum was collected from all animals at baseline and monthly throughout the study and were stored frozen in Eppendorf tubes at -80ºC until ready for analysis. Frozen sheep serum samples were then transferred to the Nett Endocrinology Laboratory at Colorado State University for evaluation of circulating estradiol. One day prior to assay, 500 µl of serum sample was extracted twice by vortexing for 2 minutes with 5 ml of Diethyl Ether. The extracted serum was then frozen in a dry ice/methanol bath and the organic phase poured off and taken to dryness. Finally, 500 µl of PBS-Gel was added to the dried extract and the sample extract allowed to reconstitute overnight. The E2 assay utilized an antibody-E2 serum (A737 Dr. Mason, Eli Lilly & CO. Lot #0205041673) diluted with 1:400 normal rabbit serum in PBS-EDTA buffer (pH 7) to a working dilution of 1:400,000. The standard curve for E2 was made by diluting purified E2 standard (A890; USP Cat. # E8875, Lot # 026K1806) to a concentration of 0.2ng/ml in PBS-GEL (Standard 1), and serial diluting Standard 1 to create a six-point standard curve using a dilution factor of 0.4 (0.2 ng/ml, 0.08, 0.032, 0.0128, 0.005, 0.002). The second antibody was

Goat anti-Rabbit serum (GAR; A968, from Dr. Richard Maulding/Doug Eckery, National Wildlife Research Center) diluted to a working dilution of 1:100 in PBS-EDTA. The ^{125}I-Estradiol tracer used was (MP Biomedicals Cat# 07-138124) and the QCs (A890) were prepared with PBS-Gel: high QC 240 pg/ml, Medium QC 60 pg/ml and Low QC 15 pg/ml. Sample extracts (200 µl), Quality Control (QCs) (80 µl) and standard (200 µl) were first incubated in 500 µl PBS-Gel buffer with 200 µl antibody and 100 µl of ^{125}I-Estradiol tracer, prepared with PBS-Gel, for 24 hours at 4°C. Then 200 µl GAR was added and the incubation continued for 72 hours at 4°C. The tubes were then centrifuged at 1700xg for 30 minutes and the supernatant decanted. Finally, the radioactivity associated with each pellet were counted in a gamma counter for one minute. Calibration curves were determined by computer analysis using the computer program RIANAL. Once the calibration curve was established, it was then used to calculate the concentration of E2 in each sample from individual runs.

3.2.4 Cortisol Radioimmunoassay

Aliquots of frozen sheep serum from all animals at baseline and monthly time points were also transferred to the Nett Endocrinology Laboratory at Colorado State University for evaluation of endogenous circulating cortisol. Serum cortisol values were determined by radioimmunoassay according to the manufacturer's instructions (Cortisol RIA Kit, MP Biomedicals, Solon, OH). Briefly, samples and standards were added to the anti-cortisol coated tubes. Cortisol-^{125}I was then added to each tube, vortexed, and incubated for 45-minutes at 37ºC. The tubes were then counted in a gamma counter calibrated for ^{125}I.

3.2.5 Blood Hematology and Chemistry Analyses

Blood samples were collected at baseline and every 3-months for hematology and serum serology outcomes. Blood samples were submitted to the Clinical Pathology Laboratory at the CSU Veterinary Teaching Hospital the same day as collection. A hemogram was performed on whole blood using an Advia® 120 Hematology System (SIEMENS Healthineers, Munich, Germany) the same day as collection. Hematology parameters were automated using flow cytometry: hemoglobin (HGB), hematocrit (HCT), red blood cell count (RBC), mean corpuscular volume (MCV), red blood cell distribution width (RDW), mean corpuscular hemoglobin concentration (MCHC), cellular hemoglobin concentration mean (CHCM), platelets, mean platelet volume (MPV), nucleated cells, and white blood cell differentials (lymphocytes, monocytes, eosinophils, basophils, leukocytes (LUC)). Blood in non-additive tubes were centrifuged and the serum analyzed for chemistry panel values using a Cobas® c501 analyzer (Roche Diagnostics Corporation, Indianapolis, IN). Chemistry parameters were automated using photometry and ion selective electrode (ISE) determinations: glucose, blood urea nitrogen (BUN), creatinine (CRE), phosphorus, magnesium, total protein, albumin, globulin, albumin/globulin ratio (A/G), creatinine kinase (CK), T-bilirubin, aspartate transferase (AST), gamma-glutamyl transferase (GGT), sorbitol dehydrogenase (SDH), iron, sodium, potassium, chloride, bicarbonate (HCO_3^-), and anion gap.

3.2.6 Statistics

Continuous data were compared between groups over time using a two-way mixed-model ANOVA with Šidák multiple comparisons with group and time as variables. For all statistical analyses, an alpha value of 0.05 or less ($p \leq 0.05$) was considered significant (GraphPad Prism 9.2.0, San Diego, CA).

3.3 Results

3.3.1 Clinical Observations

One control animal (BOV12) was euthanized at 11-months post-OVX due to acute respiratory distress resulting from pulmonary caseous lymphadenitis. Wool-break, a condition where wool is shed spontaneously resulting in alopecia, was noted in 8/10 OP animals by 3-months and in 9/10 OP animals by 6-months post-OVX (**Fig. 3.2A-B**). Wool had resumed normal growth by 12-months in all OP animals. No wool-break or alopecia was observed in any control animals throughout the study. Animal weights did not differ between groups at baseline. OP animal weights were lower than the control animals after 2-months post-OVX, although only statistically significant at 7 and 12-months ($p=0.015$, $p=0.036$ respectively) (**Fig. 3.2C**).

3.3.2 Steroid Hormones

Serum cortisol was statistically lower in OP animals than controls at 3-months and higher than control values at 9 and 10-months post-OVX (**Fig. 3.3A-B**). Although not significant, average OP serum cortisol values were notably closer to zero than control animals between 1 and 5-months post-OVX, consistent with the corticosteroid administration time frame. Surprisingly, estradiol levels of OP animals were not significantly lower from those of control animals except at 8 and 10-months post-OVX (**Fig. 3.3C-D**). Interestingly, fasting seemed to impact both estradiol and cortisol levels, resulting in a decrease in estradiol concentrations and increased cortisol levels at fasting time points (baseline, 3, 6, and 9-months). The fasting effect noted in the assessment of steroid hormones, primarily the serum estradiol, to our knowledge has not been previously reported in sheep.

3.3.3 Bone Marrow Cellularity and Hematology Analysis

No significant differences were noted in bone marrow aspirate total nucleated cell counts (TNC) between groups at 3, 6, 9, or 12-months (**Table 3.1**). No significant differences in whole blood hematology values observed between groups at baseline. At 3-months, OP group platelet counts and MPV were significantly greater than control animals (**Table 3.2**). White blood cell (WBC) percentages appeared to also be impacted at 3-months, with increased neutrophil percentage observed in the OP group, as well as decreased monocytes, lymphocytes, and eosinophils when compared to the control group (**Table 3.2**). At 6-months, red blood cell (RBC) counts were lower in OP animals along with an increase in MCV (**Table 3.2**). No significant hematological differences were observed at 9 and 12-months between groups.

3.3.4 Serum Chemistry Analysis

No serological values were significantly different between groups at baseline (**Table 3.3**). At 3-months, serum phosphorus and GGT levels were elevated in OP animals compared to control animals, while total protein, select electrolytes (sodium, bicarbonate), BUN, and CRE were all statistically decreased in OP animals compared to controls at the same time point (**Table 3.3**). At 6-months, OP animals showed significant increases of serum iron and sustained increases of GGT levels, along with sustained decreases in BUN, CRE, and total protein levels when compared to control animals (**Table 3.3**). At 12-months, OP group animals showed lower albumin levels compared to controls (**Table 3.3**). No other significant differences were observed at any other time point between groups. See **Appendix 1** for full hematology values and **Appendix 2** for full serology values.

3.4 Discussion

The sheep has been a useful large animal model to study osteoporosis and perform long-term preclinical studies on bone quality. It has become industry standard to induce osteoporotic bone loss in these animals via both ovariectomy (OVX) and corticosteroid administration, thereby significantly decreasing the bone density and disrupting trabecular microarchitecture over a relatively short period of time. While many studies have focused primarily on boney changes, few have explored the systemic changes in these animals. Given that osteoporosis is a complex metabolic condition, it is important that we map out the wholistic changes occurring in our animal models of osteoporosis – not just the impact on the bone. Additionally, previous studies have noted side effects in the animals as a result of high-dose corticosteroid administration [10, 11] but have not explored the clinical impact of model development in these animals in great detail. While one study reported on hematology, serology, and steroid hormone levels in a sheep model of osteoporosis [12], only two time points were reported for these animals and a control group was not utilized for comparison of clinical pathology parameters at the same time points.

In this present study, we compared systemic values of steroid hormones, hematological, and serological parameters in an ovine model of osteoporosis over a time frame of 12-months. Unsurprisingly, we note the greatest number of significant differences in hematological and serological parameters between control and OP group animals at 3 and 6-months following OVX. We attribute many of these changes to the administration of corticosteroids based on timing, as we completed administration of the final high dose of steroids at 15-weeks

(approximately 3-months) and the final taper dose at 24-weeks (approximately 6-months). We observed significant hematological impacts to white blood cell differentials, platelet parameters, and red blood cell values. Notably, the increase in neutrophils and subsequent decrease in lymphocytes, monocytes, and eosinophils is consistent with what has been historically reported in the clinical literature for human patients undergoing treatment with high-dose corticosteroids [13-15], where neutrophilia accompanied by decreases in monocytes and eosinophils are common outcomes. Our findings are also aligned with reported clinical pathology values by Coelho *et al.* [12], which compared between osteoporotic-induced sheep at baseline and 6-months following osteoporosis induction, including decreased RBC counts with increased MCV at 6-months, as well as increased platelet counts and decreased red blood cell counts. Observations of an increase of serum phosphorus in our OP animals is contradictory to the results authored by Ardissone *et al*, where a decrease in serum phosphorus levels were observed following administration of high-dose methylprednisolone and prednisone in human patients [16]. However, some values do not align with the literature and require further investigation, such as increases in serum iron levels at 6-months, decreases in total protein and CRE, and increases in GGT. While it was important that we compare values within the animals over time, it was even more significant that we highlight differences between a control group undergoing the same biopsy procedures and anesthesia events. Clinical blood values are wide ranging in sheep, making it difficult to ascertain meaning of results without a control group.

At 3-months into the study, serum cortisol levels were significantly diminished in the OP group compared to control animals but returned to normal levels following the cessation of steroid administration. Similar trends in endogenous serum cortisone have also been reported

previously in osteoporotic sheep [11], hinting that adrenal insufficiency may be induced in these animals early in the model development requiring the implementation of taper doses to prevent widespread infection resulting from immunosuppression. Previous studies have reported alopecia, or "wool-break", in sheep which were administered high-dose or long-acting glucocorticoids [10, 11, 17, 18]. This phenomenon was also notable side effect also observed in the majority of our study animals, with 9/10 osteoporotic group animals showing some form of wool shedding by 6-months. Given the timing of alopecia and corresponding low endogenous cortisol levels in our osteoporotic group, we can potentially infer that there is a correlation between the two events. High levels of stress and endogenous cortisol can lead to "wool break" or decreased wool fiber length in sheep [19-21]. Since administration of high dose glucocorticoids can flood the body with synthetic cortisol, one possible explanation for the observation of alopecia in our osteoporotic animals may be that the glucocorticoids are generating a physiologic high stress state for the body and resulting in loss of wool.

Although performing OVX removes the ovarian production of estradiol, we only noted a significant decrease in serum estradiol levels between 3 and 4-months following OVX in OP animals compared to controls, with levels returning to normal at 5-months. This observed bounce-back of serum estradiol, although not commonly reported, has been observed in previous sheep osteoporosis studies [22-24]. While the ovaries are the primary source of endogenous 17beta-estradiol, the most potent form of estrogen in mammals, estradiol is also produced in multiple other extragonadal organs such as the adrenal glands, skin, and adipose tissue [2]. In humans, for example, adipose tissue is considered to be the major secondary source of circulating estrogen by converting estrone to estradiol [25, 26]. It has been suggested that these

extragonadal sources of estradiol synthesis may compensate well for the loss of the ovaries in our OVX sheep and contribute to minimal changes in circulating levels of estradiol [22]. This could also contribute to the low percentage bone loss that is observed when historically OVX alone has been used to model osteoporosis in sheep. Further investigation into extragonadal sources of estradiol synthesis in sheep is required to understand the impact on circulating estradiol levels and, thus, on bone homeostasis following OVX.

We acknowledge that there were several limitations in this study. Primarily, there is great variability in standard reference ranges for sheep clinical pathology values. While we tried our best to control for this by enrollment of a control group, we remain unable to determine what is within normal clinical limits. Additionally, there may have been other underlying medical conditions that could have impacted the results. For example, the animal that was euthanized early was due to a case of caseous lymphadenitis that did not present until immediately prior to euthanasia. While all other animals did not clinically present with any interfering pathologies, it is possible that other animals could also have had something similar. Since sheep are prey animals, they are notorious for hiding any symptoms of pain, making it difficult to rule out animals that may have had any underlying medical conditions prior to assignment onto the study. And finally, while we do our best to age the animals based on incisor presentation, we cannot verify the actual ages of these animals. Since age has been reported to impact bone density in sheep [27], it is possible that the difference in age in animals could have impacted the hematology, serology, and potentially the estradiol levels, as well. However, further investigation into whether age of sheep impacts clinical pathology parameters is needed.

In conclusion, we successfully report on systemic parameters in an established sheep model of osteoporosis via OVX and corticosteroid administration. We demonstrate the effect of model development on steroid hormone levels, hematology, and serology in the same animals over the course of 12-months via serial sampling. Comprehensive characterization of the clinical manifestations of the sheep model is necessary to appropriately use in preclinical studies of osteoporosis.

3.5 Figures / Tables

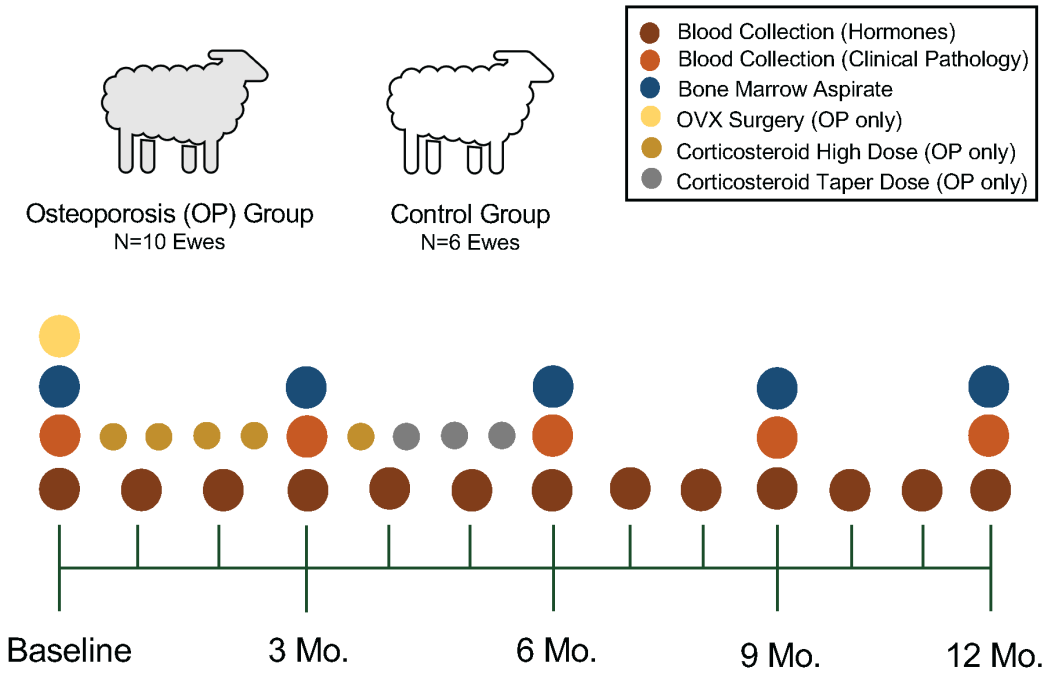

Figure 3.1. Aim 2 *in vivo* study design and sample collection time points.

A.

B.

	Animal ID	3-Months	6-Months
Experimental	BOV01	Minor	Significant
	BOV02	None	None
	BOV03	Significant	Significant
	BOV04	Significant	Significant
	BOV05	None	Minor
	BOV06	Minor	Significant
	BOV07	Significant	Significant
	BOV08	Significant	Significant
	BOV09	Minor	Significant
	BOV10	Minor	Significant
Control	BOV11	None	None
	BOV12	None	None
	BOV13	None	None
	BOV14	None	None
	BOV15	None	None
	BOV16	None	None

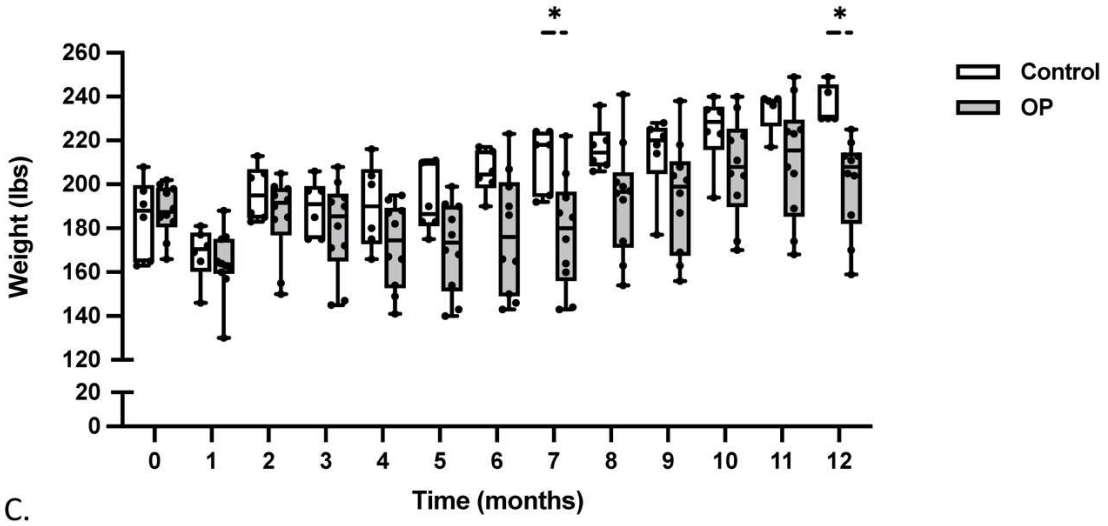

C.

Figure 3.2. Clinical results. A) Representative image of wool-break and alopecia in OP sheep. B) Observations of wool-break in study animals at 3 and 6-months. Wool-break was subjectively assessed as either minor if only affecting a small portion of the animals' fleece or significant when affecting the majority of the fleece. C) Monthly body weights of all study animals starting at baseline (0). Significance indicators: *$p<0.05$.

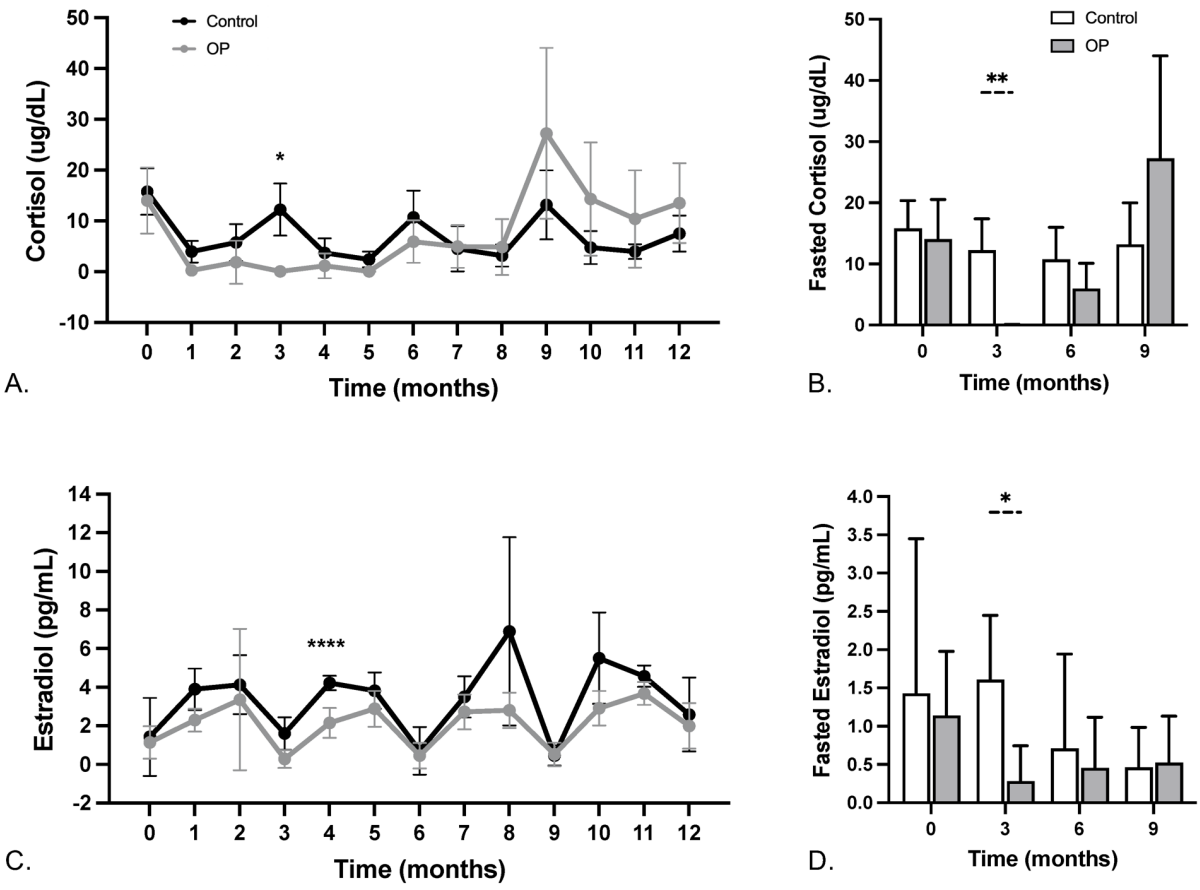

Figure 3.3. Steroid hormone levels. A) Monthly serum cortisol levels of all study animals. B) Serum cortisol levels at fasted time points only (baseline (0), 3, 6, and 9 months). C) Monthly serum estradiol levels of all study animals. D) Serum estradiol levels at fasted time points only ((baseline (0), 3, 6, and 9 months). Significance indicators: *p<0.05, **p<0.01, ****p<0.0001.

Table 3.1. Bone Marrow Aspirate Cellularity

	Control Group			OP Group		
Time Point	Avg. TNC (10^6/mL)	SD	Sample Size	Avg. TNC (10^6/mL)	SD	Sample Size
3 Months	6.68	2.55	6	7.14	7.87	10
6 Months	12.17	9.23	6	5.55	3.54	10
9 Months	5.59	2.05	6	6.16	4.72	10
12 Months	8.42	3.46	5	6.72	2.63	10

TNC = total nucleated cell count; SD = standard deviation; OP = Osteoporotic

Table 3.2. Relative whole blood hematological values of osteoporotic sheep compared to age and seasonal-matched controls.

Hematology Parameter	Baseline	3-Months	6-Months	9-Months	12 Months
HGB	-	-	-	-	-
HCT	-	-	-	-	-
RBCs	-	-	↓ [b]	-	-
MCV	-	-	↑ [a]	-	-
MCHC	-	-	-	-	-
Platelets	-	↑ [c]	-	-	-
MPV	-	↑ [a]	-	-	-
Neutrophils (%)	-	↑ [a]	-	-	-
Lymphocytes (%)	-	↓ [a]	-	-	-
Monocytes (%)	-	↓ [c]	-	-	-
Eosinophils (%)	-	↓ [b]	-	-	-

HGB = hemaglobin; HCT = hematocrit; RBC = red blood cells; MCV = mean corpuscular volume; MCHC = mean corpuscular hemoglobin concentration; MPV = mean platelet volume; a = $p<0.05$; b = $p<0.01$; c = $p<0.0001$.

Table 3.3. Relative blood serum serological values of osteoporotic sheep compared to age and seasonal-matched controls.

Serological Parameter	Baseline	3-Months	6-Months	9-Months	12 Months
Phosphorus	-	↑ [d]	↑ [a]	-	-
Calcium	-	-	-	-	-
Magnesium	-	-	-	-	-
Iron	-	-	↑ [c]	-	-
Total Protein	-	↓ [b]	↓ [a]	-	-
Albumin	-	-	-	-	↓ [a]
Globulin	-	-	-	-	-
A/G Ratio	-	-	-	-	-
Potassium	-	-	-	-	-
Chloride	-	-	-	-	-
Bicarbonate	-	↑ [a]	-	-	-
Sodium	-	↑ [c]	-	-	-
AST	-	-	-	-	-
GGT	-	↑ [d]	↑ [b]	-	-
SDH	-	-	-	-	-
CK	-	-	-	-	-
Glucose	-	-	-	-	-
BUN	-	↓ [c]	↓ [a]	-	-
CRE	-	↓ [b]	↓ [a]	-	-
T-Bilirubin	-	-	-	-	-

A/G = albumin globulin ratio; AST = aspartate transaminase; GGT = gamma glutamyltransferase; SDH = sorbitol dehydrogenase; CK = creatinine kinase; BUN = blood urea nitrogen; CRE = creatinine; T-Bilirubin = total bilirubin
a = $p<0.05$; b = $p<0.01$; c = $p<0.001$; d = $p<0.0001$.

3.6 References

1. Lobo, R., *The postmenopausal state and estrogen deficiency.* Estrogens and Antiestrogen. Philadelphia: Lippincott-Raven, 1997.
2. Barakat, R., et al., *Extra-gonadal sites of estrogen biosynthesis and function.* BMB reports, 2016. **49**(9): p. 488.
3. Turner, R., *Effects on bone and mineral metabolism: basic aspects.* Estrogens and antiestrogens. Lippcott-Raven, Philadelphia, 1997: p. 129-150.
4. Seibel, M.J., M.S. Cooper, and H. Zhou, *Glucocorticoid-induced osteoporosis: mechanisms, management, and future perspectives.* The lancet Diabetes & endocrinology, 2013. **1**(1): p. 59-70.
5. Chavassieux, P., et al., *Glucocorticoid-induced inhibition of osteoblastic bone formation in ewes: a biochemical and histomorphometric study.* Osteoporos Int, 1993. **3**(2): p. 97-102.
6. Rupp, M., et al., *Large Animal Model of Osteoporotic Defect Healing: An Alternative to Metaphyseal Defect Model.* Life (Basel), 2021. **11**(3).
7. Schorlemmer, S., et al., *Glucocorticoid treatment of ovariectomized sheep affects mineral density, structure, and mechanical properties of cancellous bone.* J Bone Miner Res, 2003. **18**(11): p. 2010-5.
8. Egermann, M., et al., *A sheep model for fracture treatment in osteoporosis: benefits of the model versus animal welfare.* Lab Anim, 2008. **42**(4): p. 453-64.
9. Cocquyt, G., B. Driessen, and P. Simoens, *Variability in the eruption of the permanent incisor teeth in sheep.* Veterinary record, 2005. **157**(20): p. 619-623.

10. Klopfenstein Bregger, M.D., et al., *Optimization of corticosteroid induced osteoporosis in ovariectomized sheep. A bone histomorphometric study.* Vet Comp Orthop Traumatol, 2007. **20**(1): p. 18-23.

11. Goldhahn, J., et al., *Slow rebound of cancellous bone after mainly steroid-induced osteoporosis in ovariectomized sheep.* J Orthop Trauma, 2005. **19**(1): p. 23-8.

12. Coelho, C.A., et al., *Evaluation of hematology, general serum biochemistry, bone turnover markers and bone marrow cytology in a glucocorticoid treated ovariectomized sheep model for osteoporosis research.* An Acad Bras Cienc, 2020. **92**(4): p. e20200435.

13. Frenkel, A., et al., *The association of glucocorticosteroid treatment with WBC count in patients with COPD exacerbation.* Journal of Clinical Medicine, 2019. **8**(10): p. 1697.

14. McKay, L. and J. Cidlowski, *Physiologic and pharmacologic effects of corticosteroids.* Holland-Frei cancer medicine, 2003. **6**.

15. Rinehart, J.J., et al., *Effects of corticosteroid therapy on human monocyte function.* New England Journal of Medicine, 1975. **292**(5): p. 236-241.

16. Ardissone, P., et al., *Effects of high doses of corticosteroids on bone metabolism.* Journal of endocrinological investigation, 2002. **25**: p. 129-133.

17. Andreasen, C.M., et al., *A reversal phase arrest uncoupling the bone formation and resorption contributes to the bone loss in glucocorticoid treated ovariectomised aged sheep.* Bone, 2015. **75**: p. 32-9.

18. McDonald, B., G. Suter, and P. Hopkins, *Defleecing Effect of Betamethasone and other Long-acting Corticosteroids, their Influence on Wool Growth and some Physiological Processes in Sheep.* Australian Journal of Biological Sciences, 1982. **35**(1): p. 33-48.

19. Sawyer, G., D.R. Fox, and E. Narayan, *Pre-and post-partum variation in wool cortisol and wool micron in Australian Merino ewe sheep (Ovis aries).* PeerJ, 2021. **9**: p. e11288.

20. Colditz, I., et al., *Some physiological responses associated with reduced wool growth during blowfly strike in Merino sheep.* Australian veterinary journal, 2005. **83**(11): p. 695-699.

21. Ansari-Renani, H. and P. Hynd, *Cortisol-induced follicle shutdown is related to staple strength in Merino sheep.* Livestock Production Science, 2001. **69**(3): p. 279-289.

22. Sigrist, I.M., et al., *The long-term effects of ovariectomy on bone metabolism in sheep.* J Bone Miner Metab, 2007. **25**(1): p. 28-35.

23. Kiełbowicz, Z., et al., *The experimental osteoporosis in sheep--clinical approach.* Pol J Vet Sci, 2015. **18**(3): p. 645-54.

24. Turner, A.S., et al., *Dual-energy X-ray absorptiometry in sheep: experiences with in vivo and ex vivo studies.* Bone, 1995. **17**(4 Suppl): p. 381S-387S.

25. Simpson, E.R., *Sources of estrogen and their importance.* The Journal of steroid biochemistry and molecular biology, 2003. **86**(3-5): p. 225-230.

26. Hetemäki, N., et al., *Adipose tissue estrogen production and metabolism in premenopausal women.* The Journal of steroid biochemistry and molecular biology, 2021. **209**: p. 105849.

27. Maenz, S., et al., *The old sheep: a convenient and suitable model for senile osteopenia.* J Bone Miner Metab, 2020. **38**(5): p. 620-630.

CHAPTER 4:
CHARACTERIZATION OF BONE PROTEIN AND CELLULAR COMPOSITION IN AN OVINE MODEL OF OSTEOPOROSIS

4.1 Introduction

Bone is comprised of three main constituents: inorganic material (~ 60% of bone weight), organic material (~ 30%), and water (~10%) [1]. The organic matrix is formed by primarily type I collagen and other non-collagenous proteins, while the inorganic matrix is composed of mineralized hydroxyapatite crystals [2, 3]. Bone is mineralized following deposition of calcium phosphate crystals in the structural matrix by osteoblasts. Disruptions to bone integrity and strength can arise either from excessive bone turnover mechanisms thereby decreasing bone mineralization rates, or by low turnover mechanisms, which does not allow for the turnover of old mineral material, resulting in brittle bones [4]. While the majority of the extracellular matrix is composed of type I collagens, other non-collagenous proteins have been shown to play just as important a role in the turnover of bone, especially in terms of initiating and participating in cell signaling cascades [4, 5]. For example, transforming growth factor beta (TGF-beta) signaling has been shown to play a crucial role in bone metabolism, involving non-collagenous proteins such as bone morphogenic proteins (BMP), growth factors, and an abundance of cytokines to induce progenitor cell differentiation to osteoblasts [4, 6]. TGF-beta also works in conjunction with another key pathway, the wingless-type mouse mammary tumor virus integration site family (Wnt). The Wnt pathway is also noted to be essential in bone formation by way of suppressing adipogenesis of the same progenitor cells [4, 7].

Although great strides have been made to uncover the cellular mechanisms of osteoporosis associated with clinical bone loss, clear understandings of molecular pathways impacting bone loss remain elusive. The emergence of the study of -omics (metabolomics, transcriptomics, proteomics, etc.) has allowed researchers to infer molecular pathways of diseases or conditions by quantifying certain biomolecules present in a tissue or cell using mass spectrometry. Proteomics helps promote insight into the functional production of an organism's genes and has been utilized to determine a substantial number of proteins involved in the structure and function of bone tissue [8]. A combination of mass spectrometry and liquid chromatography separation (LC/MS/MS) is used to describe the proteome, or all of the proteins present in a tissue, whereby whole proteins are digested into peptide fragments followed by separation by liquid chromatography (LC). Finally, the mass of each peptide is quantified using mass spectrometry (MS) and matched to a protein using a protein database [8]. Use of -omics has allowed researchers to generate potential underlying molecular explanations for the clinical manifestations of osteoporosis.

The final phase of experimentation in this overall study aimed to further elucidate the molecular pathways by which bone loss occurs in the sheep model of osteoporosis. To date, few studies have utilized proteomics in clinical human patients [9, 10]. The objectives of this aim were to 1) characterize the histomorphometrical changes and 2) the protein changes in osteoporotic ewes over 12 months. To the best of our knowledge, the bone proteome has not been explored in sheep with either healthy bone or following osteoporosis induction. We hypothesized that global untargeted proteomics would reveal molecular changes in our ovariectomized and steroid administered ewes compared with age-matched controls.

4.2 Materials and Methods

4.2.1 Animals and Experimental Design

As previously described in Chapter 2, sixteen (16) skeletally mature Rambouillet-cross ewes between 4-6 years of age were enrolled onto study. Briefly, osteoporosis was induced in N=10 osteoporotic (OP) animals via ovariectomy (OVX) and corticosteroid administration. High-dose corticosteroids were administered for 16-weeks and then tapered for an additional 3 doses (24-weeks total time of corticosteroid administration) (**Fig. 4.1**). The remaining N=6 animals were allocated to the healthy control group. No OVX or corticosteroids were administered to the control group animals. Bone biopsies for histomorphometry and proteomic analysis were collected from the iliac crest of each animal at five study time points under anesthesia: baseline, 3, 6, 9, and 12-months (**Fig. 4.1**).

4.2.2 Iliac Crest Biopsies

Two bone biopsies were harvested from the iliac crest of each animal at the five study time points. A large (10 mm diameter) biopsy was first harvested using a 10 mm Arthrex OATS™ autograft system (ABS-8981-10S, Arthrex, Naples, FL) and fixed in 10% neutral buffered formalin for a minimum of 72-hours prior to transfer to phosphate buffered saline (PBS). A second small (4.5 mm diameter) biopsy was then collected from the same iliac crest directly adjacent to the 10 mm biopsy site using a 4.5 mm mosaicplasty set (L50343786, Smith & Nephew Inc., Fort Worth, TX), flash frozen in liquid nitrogen, and stored at -80°C until further processing. Laterality for biopsy collection was alternated between collection time points.

4.2.3 Histology and Histomorphometry

Large (10 mm) formalin-fixed bone biopsies were placed in a 10% ethylenediaminetetraacetic acid (EDTA) solution for one week, followed by placement in a 5% EDTA solution until adequately decalcified, with solution replacement occurring weekly. Samples were routinely processed for paraffin embedding (30 minutes/step). It was noted that not all samples were fully decalcified during initial slide cutting. Therefore, the previously prepared paraffin blocks were reprocessed by heating at 60°C to remove excess paraffin and samples placed in new cassettes. Samples were placed in xylene for three changes at 3-hours each. Samples were then placed into 100% reagent alcohol for 3-hours, re-processed in a tissue processor, re-embedded, and then sectioned at 5 microns and stained with Goldner's Trichrome. Slides were imaged at 10x magnification using an Olympus vs200 research slide scanner (Evident, Tokyo, Japan). The slide images were then semi-automatically quantified in Image Pro-Premier (version 9.3, Media Cybernetics, Rockville, MD, USA) for mean trabecular bone area (Tb.B.Ar), trabecular bone area ratio (Tb.B.Ar./Tt.Ar), percentage change in Tb.B.Ar/Tt.Ar, number of cortical holes, mean cortical bone area (Ct.B.Ar), and mean cortical width (Ct.Wi). Ct.Wi was determined by averaging 50 perpendicular length measurements along the cortical layer.

4.2.4 Bone Proteomics Sample Preparation and Extraction

Small (4.5 mm) bone biopsies were transferred on dry ice to the University of Colorado Mass Spectrometry Proteomics Shared Resource Facility and lyophilized overnight. Dried samples were then milled to a fine powder using a Cell Crusher (CellCrusher) the following day. Milled samples were delipidated with 3 washes of ice-cold acetone and 3 mg of material was

measured out from each sample to be extracted and analyzed. Samples were extracted using a two-step extracellular matrix (ECM)-optimized extraction method. All buffers were applied at 200 µL buffer per mg of tissue. After each extraction step, samples were spun for 20 mins at 18,000xg and the supernatant was reserved. Samples were first decellularized using 3 consecutive washes with HS/CHAPS buffer (50mM Tris-HCl (pH 7.4), .25% CHAPS, 25mM EDTA, 3M NaCl). Next, ECM proteins were extracted using hydroxylamine digest buffer (1M $NH_2OH{-}HCl$, 4.5 M Gnd−HCl, 0.2 M K_2CO_3, pH adjusted to 9.0 with NaOH). All fractions were flash frozen at -80C until digestion.

4.2.5 Sample Digestion

Small bone biopsy sample extracts were subjected to trypsin digestion via the filter-aided sample preparation (FASP) protocol [11] using a 10 kDa cutoff filter. Samples were reduced using Tris (2-carboxyethly) phosphine (TCEP), alkylated with 2-chloroacetimide (ClAA), and digested with trypsin (1:100 enzyme:substrate ratio) for approximately 15 hours at 37 degrees Celsius. The digest was eluted and acidified with 150 uL of 0.2% formic acid.

4.2.6 Mass Spectrometry Acquisition

Digested peptides were loaded onto individual Evotips following the manufacturers protocol and separated on an Evosep One chromatography system (Evosep, Odense, Denmark) using a Pepsep column, (150 um inter diameter, 15 cm) packed with ReproSil C18 1.9 um, 120A resin. Samples were analyzed using the instrument default “30 samples per day” LC gradient. The system was coupled to the timsTOF Pro mass spectrometer (Bruker Daltonics, Bremen, Germany) via the nano-electrospray ion source (Captive Spray, Bruker Daltonics). The mass

spectrometer was operated in PASEF mode. The ramp time was set to 100 ms and 10 PASEF MS/MS scans per topN acquisition cycle were acquired. MS and MS/MS spectra were recorded from m/z 100 to 1700. The ion mobility was scanned from 0.7 to 1.50 Vs/cm2. Precursors for data-dependent acquisition were isolated within ± 1 Th and fragmented with an ion mobility-dependent collision energy, which was linearly increased from 20 to 59 eV in positive mode. Low-abundance precursor ions with an intensity above a threshold of 500 counts but below a target value of 20000 counts were repeatedly scheduled and otherwise dynamically excluded for 0.4 min.

4.2.7 Proteomic Data Processing and Annotation

Data was searched using MSFragger version 3.8 through the FragPipe version 19.0 pipeline. Precursor tolerance was set to ±12 ppm and fragment tolerance was set to ±20 ppm. Data was searched against UniProt restricted to *Ovies aries* with common contaminants derived from version 1.1 of the CRAPome [11]. Each fraction was searched independently using a semi-specific trypsin cleavage definition. Fixed modifications were set as carbamidomethyl (C). Variable modifications were set as oxidation (M), oxidation (P) (hydroxyproline), Gln->pyro-Glu (N-term Q), and acetyl (Peptide N-term). Results were filtered to 1% FDR at the peptide and protein level. ECM-associated proteins were annotated using MatrisomeDB database [12]. Prior to filtering, data were log(2) transformed using NormalyzerDE version 1.14.0 [13]. Data filtering, imputation of missing values, and normalization was carried out in MetaboAnalyst version 6.0 [14]. Proteins were filtered out of the dataset if not present in at least 67% (or 2/3) of samples. Any remaining intensity values listed as zero or below detectable levels were imputed

with 1/5 of the lowest intensity value for the corresponding protein. Data was then scaled by mean-centering and dividing by the standard deviation of each variable.

4.2.8 Statistical Comparisons and Data Presentation

Histomorphometry data was assessed for statistical significance using a mixed model ANOVA with Šidák post-hoc multiple comparisons in GraphPad version 10.2.0 (Prism, San Diego, CA). Proteomic data global comparisons were assessed for statistical significance in MetaboAnalyst version 6.0 [14] using a two-way ANOVA and paired time point comparisons were made using a one-way ANOVA, with significance set at $p<0.05$ and fold change threshold at >2 for each comparison. Differentially expressed proteins (DEPs) were reported using the false discovery rate (FDR) adjusted p-value. Venn diagrams of DEPs between comparisons were generated using the Bioinformatics & Evolutionary Genomics Venn diagram tool (https://bioinformatics.psb.ugent.be/webtools/Venn/). KEGG pathway analysis of DEPs was performed in ShinyGO v.0.80 [15] using the Ensembl assembly "sheep genes Oar_rambouillet_v1.0".

4.3 Results

4.3.1 Bone Histomorphometry

Representative histology images of iliac crest bone biopsies qualitatively show thinning and disconnected trabecular bone in OP sheep over time (**Fig. 4.2A-E**), while minimal disruptions to trabecular connectivity and thickness are shown in control sheep bone throughout the study (**Fig. 4.2F-J**). No differences were observed in control animals at any of the time points compared to baseline values for any histomorphometry parameter. OP group iliac crest

mean Tb.B.Ar decreased significantly at 3 and 6-months when compared to baseline values. However, there was no difference in Tb.B.Ar values between control and OP animals at any time point (**Fig. 4.3A**). The trabecular bone ratio (Tb.B.Ar/Tt.Ar), or the percentage of trabecular bone area over total tissue area (cortical bone excluded), of OP animal bone biopsies was significantly lower than control animals at 9-months. (**Fig. 4.3B**). While not significant, percentage change in a trending decrease in % Tb.B.Ar/Tt.Ar is observed in the OP group compared to controls between 3 and 9-months (**Fig. 4.3C**). No differences in number of cortical holes (**Fig. 4.3D**), Ct.B.Ar (**Fig. 4.3E**), or Ct.Wi (**Fig. 4.3F**) were noted between or within groups at any time point.

4.3.2 Initial Proteomic Output

A total number of 4,765 proteins were identified in 79 samples. Extracellular Matrix-associated proteins were annotated using MatrisomeDB [12], revealing 245 ECM-associated proteins and 4,520 non-ECM-associated proteins. Following data filtering and imputation, a total of 186 ECM-associated and 2,488 non-ECM-associated proteins were used for further analysis.

4.3.3 Differentially Expressed Proteins

A total of 1,610 DEPs were compiled following comparisons between Control and OP groups at all time points. Global differences were observed between control ECM-associated (**Fig. 4.4A**) and non-ECM proteins (**Fig. 4.4B**). When looking at the OP group alone, a total of 909 DEPs were identified between all time points and baseline (i.e., baseline vs 3-months, baseline vs. 6-months, etc.). No proteins were significantly different between OP and control groups at baseline.

4.3.4 Proteomic Profiling and Functional Gene Enrichment at 3-Months

A total of 14 DEPs were identified at 3-months as compared to baseline values in the OP group. Thirteen (13) proteins were significantly downregulated and 1 protein was significantly upregulated (**Fig. 4.5A-B**). KEGG pathway analysis revealed two enriched pathways of DEPs (**Fig. 4.5C**): Sphingolipid signaling pathway and Influenza A-associated pathway. The top biological processes of DEPs were negative regulation of monocyte differentiation, followed by monocyte differentiation, and negative regulation of myeloid leukocyte differentiation (**Fig. 4.5D**). No DEPs were identified in control samples at 3-months compared to baseline.

4.3.5 Proteomic Profiling and Functional Gene Enrichment at 6-Months

A total of 834 DEPs were identified at 6-months as compared to baseline values in the OP group, with 828 significantly downregulated proteins and 6 significantly upregulated proteins (**Fig. 4.6A-B**). KEGG pathway analysis revealed enrichment of the DNA replication, Aminoacyl-tRNA biosynthesis, and cysteine and methionine metabolism pathways at 6-months in OP samples (**Fig. 4.6C**). A high number of metabolic pathway genes were also noted to be impacted at this time point (**Fig. 4.6C**). The top enriched biological processes of 6-month OP group DEPs included nucleoside phosphate metabolic processes, oxoacid metabolic processes, and carboxylic acid metabolic processes (**Fig. 4.6D**). High numbers of genes involved in phosphate-containing compound metabolic processes and phosphorus metabolic processes were also noted at 6-months (**Fig. 4.6D**). No DEPs were identified in control samples at 6-months compared to baseline.

4.3.6 Proteomic Profiling and Functional Gene Enrichment at 9-Months

A total of 323 DEPs were identified at 9-months as compared to baseline values in the OP group, with 322 proteins significantly downregulated and 1 protein significantly upregulated (**Fig. 4.7A-B**). KEGG pathway analysis revealed enrichment of DNA replication, aminoacyl-tRNA biosynthesis, and nucleotide metabolism pathways at 9-months in OP samples (**Fig. 4.7C**). A high number of metabolic pathway genes were also noted to be impacted at this time point (**Fig. 4.7C**). Top enriched biological processes of 9-month OP group DEPs included positive regulation of chromosome condensation, DNA unwinding involved in DNA replication, and post-transcriptional regulation of gene expression (**Fig. 4.7D**). No DEPs were identified in control samples at 9-months compared to baseline.

4.3.7 Proteomic Profiling and Functional Gene Enrichment at 12-Months

A total of 401 DEPs were identified at 12-months as compared to baseline values in the OP group, 388 of which were non-ECM associated and 13 of which were ECM-associated. Of the identified DEPs, 379 proteins were significantly downregulated and 22 proteins were significantly upregulated at 12-months (**Fig. 4.8A-B**). KEGG pathway analysis revealed enrichment of DNA replication, mismatch repair, and ferroptosis pathways at 9-months in OP samples (**Fig. 4.8C**). A high number of cell cycle, purine metabolism, mRNA surveillance, and nucleocytoplasmic transport pathways were also noted to impacted at this time point (**Fig. 4.8C**). Top enriched biological processes of 12-month OP group DEPs included myeloid cell activation involved in immune response, phagocytosis, and regulation of phagocytosis (**Fig. 4.8D**). A high number of genes involved in other biological processes, including immune system processes, regulation of protein metabolic processes, and cellular localization were also noted at this time

point (**Fig. 4.8D**). A total of 440 DEPs were also identified in the control group samples at 12-months as compared to baseline values, with 438 of which were non-ECM associated and 2 ECM-associated. Of the identified control group DEPs at 12-months, 439 proteins were significantly downregulated and 1 protein was significantly upregulated (**Fig. 4.9A-B**). KEGG pathway analysis revealed enrichment of mismatch repair, protein export, and DNA replication pathways in 12-month control samples (**Fig. 4.9C**). A high number of genes involved in metabolic and spliceosome pathways are also noted at this time point (**Fig. 4.9C**). Top enriched biological processes of 12-month control group DEPs included RNA splicing via transesterification reactions, RNA splicing via transesterification reactions with bulged adenosine, and mRNA splicing via spliceosome (**Fig. 4.9D**). High number of genes involved in cellular localization processes are also noted in 12-month control samples (**Fig. 4.9D**).

4.3.8 Functional Enrichment of Shared DEPs

In order to identify proteins that remained consistently affected throughout the study following osteoporosis induction, we compared DEPs identified at each time point as compared with baseline values in our OP group. We identify 467 proteins that were unique to a single time point, 297 proteins shared between only two time points, 161 proteins shared between three time points, and 7 total DEPs shared between all time points (**Fig. 4.10A**). To identify throughline processes that may be impacted due to osteoporosis development in the sheep, we identified and performed functional gene analysis on the 7 DEPs that were present in all time point comparisons (**Fig. 4.10B**). KEGG pathway analysis of the 7 shared proteins reveal enrichment of p53 signaling, mRNA surveillance, sphingolipid signaling, and oocyte meiosis pathways (**Fig. 4.10C**). Top biological processes impacted between all time points include monocyte

differentiation, myeloid cell differentiation, and hemopoiesis (**Fig. 4.10D**). Since we identified a number of DEPs at 12-months in our control group samples, we aimed to identify which DEPs were unique to OP group bone samples. Following comparison of the 401 OP 12-month DEPs and 440 control group 12-month DEPs, a total of 108 DEPs were determined to be shared between the two groups at 12-months (**Fig. 4.11A**). KEGG analysis of shared DEPs revealed enrichment of mismatch repair pathways, DNA replication, and nucleotide excision repair (**Fig. 4.11B**). Top biological processes impacted by shared DEPs included monocyte differentiation regulation, regulation of substrate adhesion-dependent cell spreading, immune response myeloid cell activation, and leukocyte degranulation (**Fig. 4.11C**).

4.4 Discussion

In this aim, we evaluated both the morphometry and proteomic changes of iliac crest bone biopsy samples to help elucidate the mechanisms driving bone loss in our preclinical sheep model of osteoporosis over 12-months. Histomorphometrically, we observed significant decreases in trabecular bone area in our OP animals compared to baseline values at 3 and 6-months, with no changes observed in our control group between time points. We can also qualitatively observe changes to the trabecular bone quality in our OP animals compared to the controls. Importantly, we show visible thinning and disconnection of the trabeculae following osteoporotic induction. This trend in histological trabecular bone loss of our osteoporotic group is in alignment with previous studies [16, 17], where the most significant bone loss manifested by 3-6 months following OVX and steroid administration. While minimal significance between groups was observed in the analysis of cortical bone parameters (width, porosity, area), this finding is also in alignment to previous observations in the sheep OVX model. Given that

trabecular bone loss is the primary source of bone loss in the early phases of osteoporosis, it makes sense that we would observe significant changes to the trabecular bone and minimal to the cortical surfaces [18, 19] during our study duration. However, further assessments are needed to assess microscopic changes in cortical osteons and bone cellular activity in the sheep osteoporosis model.

This is the first study to assess protein changes to bone tissue in the same subjects over time using proteomic analysis in a longitudinal sheep model of osteoporosis. A previous study from Cabrera et al explored the impact to the metabolome and lipidome through use of metabolomics in a sheep model of osteoporosis [20], but direct assessment of the bone tissue was not performed. Our initial exploration of the sheep bone proteome resulted in the identification of a vast number of proteins, both ECM-associated and non-ECM associated. Seven proteins were shared between each time point (CTR9, INPP5D, CDK6, PPP2R5C, NUP133, ITPRIPL1, W5PH60_SHEEP) and are therefore speculated to be key in osteoporosis progression in the sheep. Of note, cyclin-dependent kinase 6 (CDK6) is a key regulator of the p53 pathway, which is most commonly associated with select cancer mechanisms. Elevated levels of p53 have also been associated with decreases in bone mass [21]. It has been shown through *in vitro* experimentation that CDK6 may play a role in osteoblast differentiation, as it regulates activity of BMP proteins [22]. Serine/threonine-protein phosphatase 2A 56 kDa regulatory subunit protein (PPP2R5C) is a subunit of PP2A, a key regulator in the AMP-K and P13K-AKT signaling pathways. PP2A has been discussed as a potential target in the downregulation of osteoclastogenesis, as its downregulation significantly decreases osteoclast numbers and RANKL expression *in vitro* [23]. Both CDK6 and PP2A also play a role in the P13-Akt

signaling pathway, which is hypothesized to be involved in the promotion of osteoblast proliferation and differentiation and therefore the inhibition of osteoporosis [24]. PPP2R5C and NUP133 have been identified as potential biomarkers associated with menopausal status in women [25] and CDK6 was also identified as a key candidate in a micro-array study intended to identify genes distinguishing osteoporosis from osteoarthritis in humans [26].

Pathway enrichment was utilized to help understand which molecular processes contain high levels of our differentially expressed proteins. For example, proteins enriched at 3-months were associated the sphingolipid lipid signaling pathway. Interestingly, another study performing proteomics using femoral bone tissue harvested from osteoporotic and healthy aged humans undergoing hip surgery demonstrated significant changes to levels of apolipoprotein A-I in the bone of osteoporotic patients compared to controls [10]. At the same time point, we observe enrichment of immune-related biological processes, including dysregulation to monocyte differentiation and regulation, myeloid leukocyte differentiation and regulation, hemopoiesis, and erythrocyte differentiation. It is well established that therapy with corticosteroids is intended to suppress inflammatory processes, particularly in examples of organ transplantation and chronic inflammatory disorders [27]. Similarly, proteomic analysis of blood serum from human patients with osteoporosis demonstrate dysregulation of immune proteins and Ig protein levels, indicating a potential action of osteoporosis development on mature B cell action [9]. We observed overlapping enrichment of pathways and biological processes between various time points during osteoporosis development in our animals. Across 6, 9, and 12-months, we see high enrichment of DNA replication, cell cycle, and purine metabolism pathways. At 6 and 9-months, we also see enrichment of pathways associated with aminoacyl-tRNA biosynthesis and

metabolic pathways. Of note, purine metabolism has been noted to play an important role in the process of bone remodeling, as alterations in purine metabolism have been associated with osteoporosis through metabolic analysis [28, 29]. Disruptions to DNA replication and cell cycles are indications of possible cellular senescence, commonly associated with aging [30]. Further investigation is required to understand the connection between cellular senescence and osteoporosis in the sheep model.

There are several limitations that must be mentioned in this study aim. Primarily, as this is the first study to truly assess the proteomics of sheep bone in the context of bone loss, there were inherent limitations in the derivation of biological relevance from the differentially expressed proteins described in our results. The sheep proteome has not been significantly annotated for association between disease states relating to bone, as few studies have been previously published on this subject [31, 32]. Therefore, many of the significant proteins could not be included in KEGG pathway analysis due to limited published data on the sheep proteome. Additional work will be required to link sheep proteins with biological processes. While collecting whole bone biopsies for proteomic analysis, it is possible that samples contained additional non-bone materials, including blood, adipose tissue, periosteum, and other connective tissues. The potential inclusion of these tissues may have impacted our proteomic results and could potentially account for certain hemopoietic protein expressions between sample comparisons. However, all these tissues are important factors in the bone tissue and may still render meaningful results when comparing between time points and groups. While we did the best to utilize our control animals to eliminate DEPs that were both expressed in our osteoporotic and control animals at each time point, there are several DEPs that were noted to be expressed in

our control animals but not in our OP animals. While we would expect there to be no significant proteomic differences observed in our control animals over time that were not also expressed in our OP sheep at the same time points, there were indeed several DEPs that were only expressed in our control animals that were not observed in our osteoporotic animals, bringing up questions of the significance of these proteins to the experiment. Further experimentation into the proteomic changes that occur over the course of a year in sheep are required to determine if these observed DEPs are part of natural aging or seasonality in sheep.

In summary, we have conducted the first study to evaluate the proteomic impacts of ovariectomy and glucocorticoid administration in the bone of sheep. We identified significant protein dysregulation in our osteoporotic group, in conjunction with changing bone morphometry, compared to baseline values in the same animals. This exploratory study adds to the growing field of tissue-specific -omics research. In particular, this study has identified potential mechanisms by which bone loss occurs in a widely accepted large animal model of osteoporosis.

4.5 **Figures / Table**

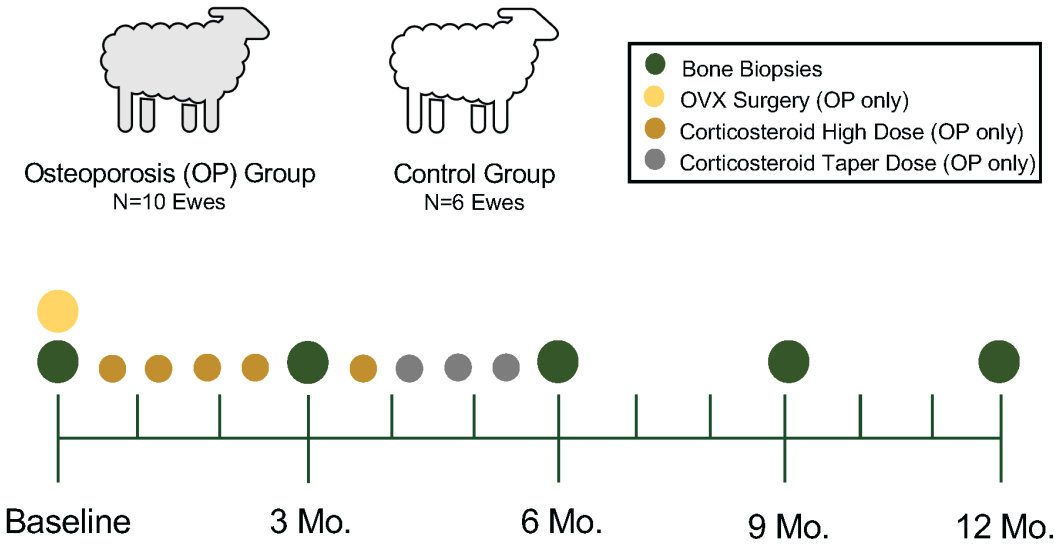

Figure 4.1. Aim 3 *in vivo* study design.

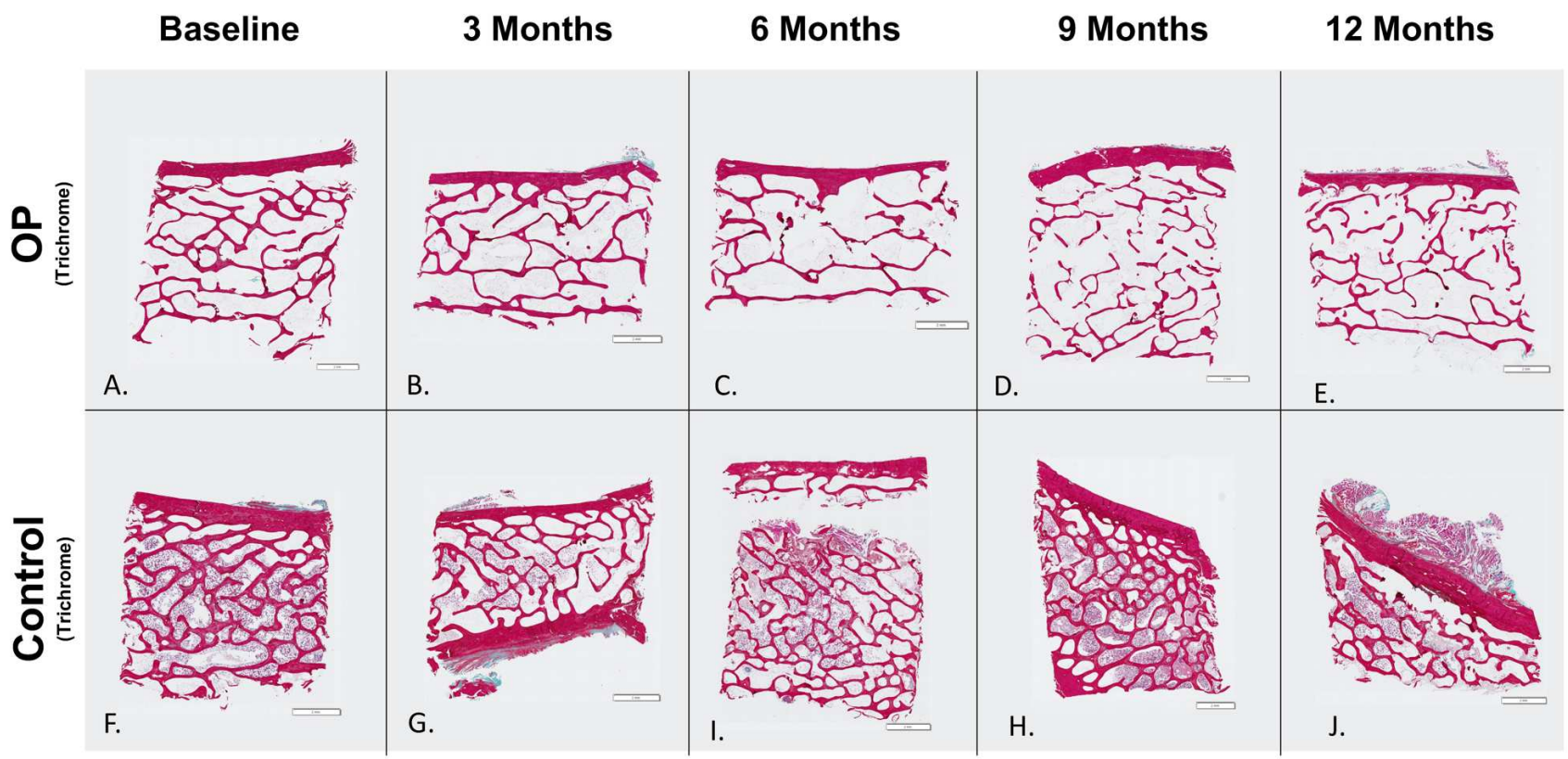

Figure 4.2. Representative histology images of sheep iliac crest bone biopsies stained with Goldner's Trichrome. (A-E) Representative images of bone biopsies from animal BOV02 (OP group) across study time points: A) baseline, B) 3-months, C) 6-months, D) 9-months, and E) 12-months. (F-J) Representative images of bone biopsies from animal BOV11 (control group) across study time points: A) baseline, B) 3-months, C) 6-months, D) 9-months, and E) 12-months.

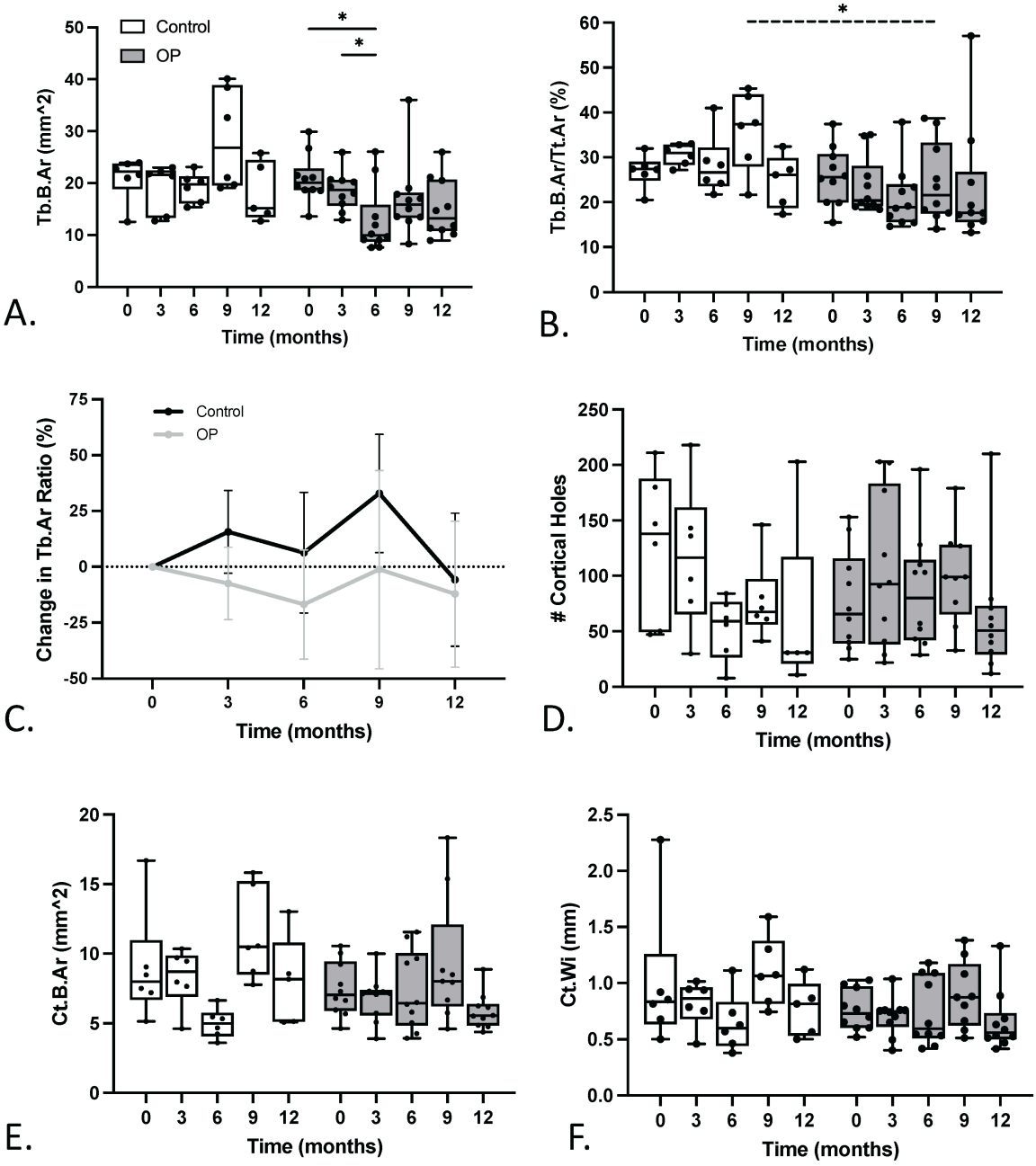

Figure 4.3. Histomorphometry results of OP and control iliac crest bone biopsies across all study time points (baseline (0), 3, 6, 9, and 12-months). A) Trabecular bone area (Tb.B.Ar). B) Trabecular bone area over total tissue area (Tb.B.Ar/Tt.Ar). C) Percentage change in Tb.B.Ar/Tt.Ar as compared to baseline. D) Number of holes in cortical bone. E) Cortical bone area (Ct.B.Ar). F) Cortical width (Ct.Wi). All data are represented as mean $\pm$ standard deviation. Significance indicator: *$p \leq 0.05$.

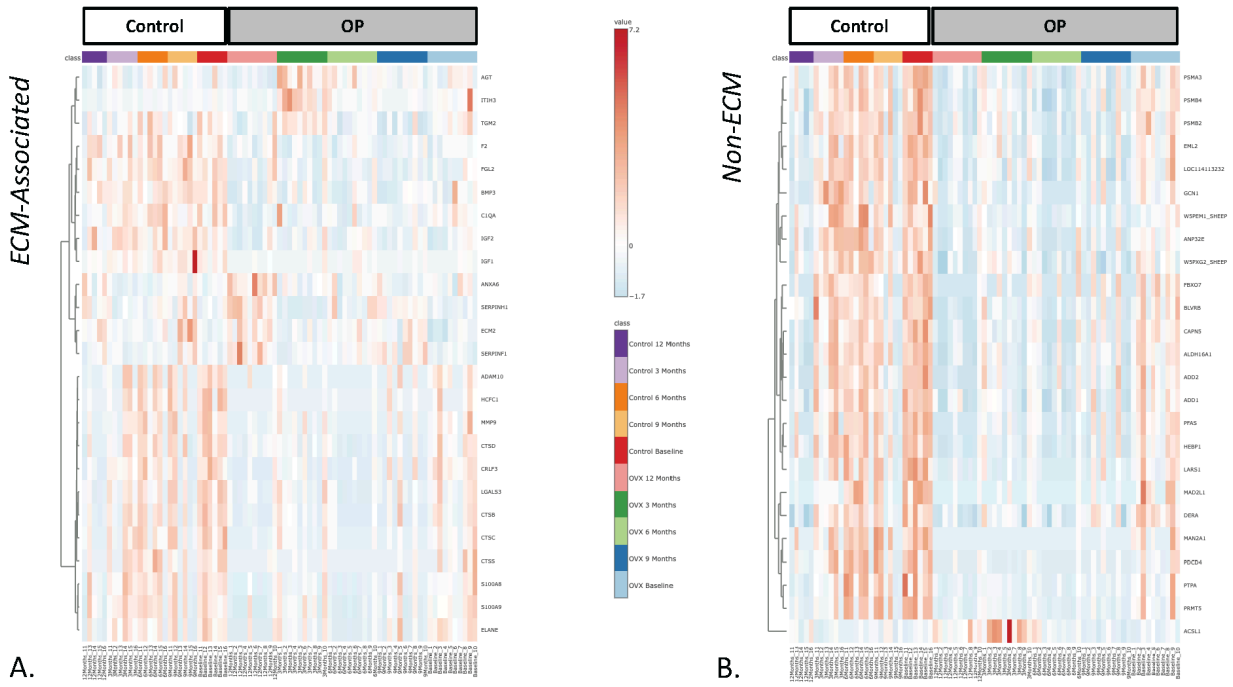

Figure 4.4. Heatmaps of top 25 proteins with the greatest fold change between groups at each time point. A) A total of 186 ECM-associated proteins were compared and B) a total of 2,488 non-ECM proteins were compared. Heatmaps produced in MetaboAnalyst.

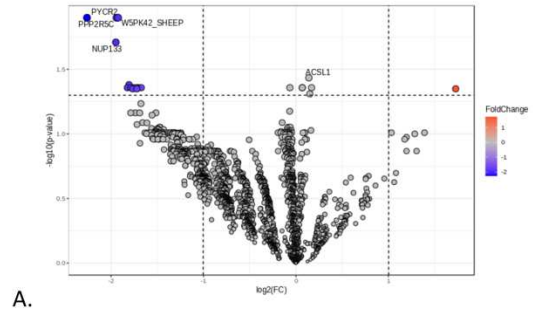

A.

Downregulated Gene	Association	Log(2) FC
PPP2R5C	non-ECM	-2.2599
NUP133	non-ECM	-1.948
PYCR2	non-ECM	-1.9404
W5PK42_SHEEP	non-ECM	-1.9239
ITPRIPL1	non-ECM	-1.8236
INPP5D	non-ECM	-1.8058
NUP210	non-ECM	-1.7872
LOC101116816	non-ECM	-1.7658
CDK6	non-ECM	-1.7566
W5PH60_SHEEP	non-ECM	-1.7244

Upregulated Gene	Association	Log(2) FC
W5P633_SHEEP	non-ECM	1.7279

B.

Total number of DEPs = 14

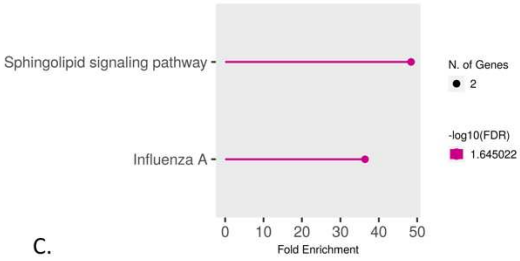

C.

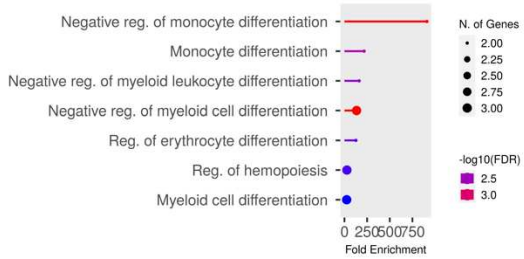

D.

Figure 4.5. OP group baseline vs. 3-months non-ECM associated protein analysis. A total of 14 DEPs were identified (13 downregulated, 1 upregulated). No ECM DEPs were identified. A) Volcano plot using a paired one-way ANOVA in MetaboAnalyst. B) Top 10 significant downregulated and all upregulated in MetaboAnalyst with log(2) fold change. C) Top enriched KEGG pathways. D) Top 10 GO Biological Processes.

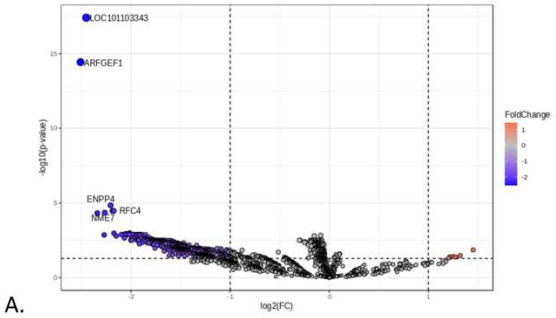

A.

Downregulated Gene	Association	Log(2) FC
ARFGEF1	non-ECM	-2.5089
LOC101103343	non-ECM	-2.4518
TNPO2	non-ECM	-2.3404
LOC101104114	non-ECM	-2.2644
ENPP4	non-ECM	-2.2061
NME7	non-ECM	-2.1858
RFC4	non-ECM	-2.175
DOCK2	non-ECM	-2.1723
BPI	non-ECM	-2.0535
ALOX5	non-ECM	-2.013

Upregulated Gene	Association	Log(2) FC
W5PJ13_SHEEP	non-ECM	1.4517
KRT79	non-ECM	1.3209
W5Q831_SHEEP	non-ECM	1.2751
PLTP	non-ECM	1.2489
AOC2	non-ECM	1.2152
W5PA20_SHEEP	non-ECM	1.2048

B.

Total number of DEPs = 834

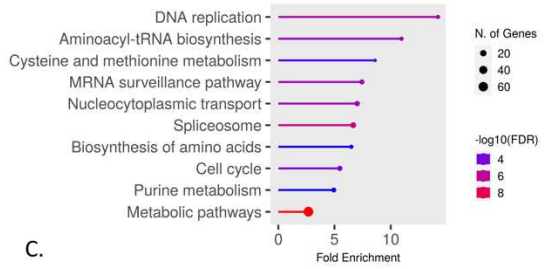

C.

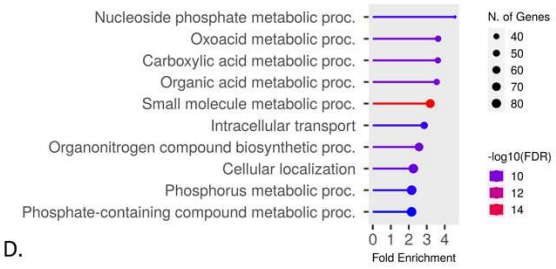

D.

Figure 4.6. OP group baseline vs. 6-months non-ECM associated protein analysis. A total of 834 DEPs were identified (828 downregulated, 6 upregulated). No ECM DEPs were identified. A) Volcano plot using a paired one-way ANOVA in MetaboAnalyst. B) Top 10 downregulated and all upregulated proteins in MetaboAnalyst with log(2) fold change. C) Top 10 enriched KEGG pathways. D) Top 10 GO Biological Processes.

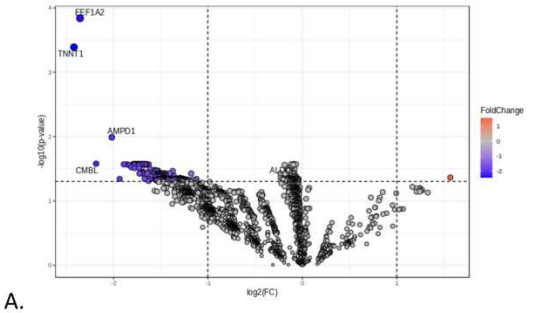

A.

Downregulated Gene	Association	Log(2) FC
TNNT1	non-ECM	-2.4185
EEF1A2	non-ECM	-2.3542
CMBL	non-ECM	-2.1835
AMPD1	non-ECM	-2.0175
MYBPC2	non-ECM	-1.9348
PGAM2	non-ECM	-1.89
LOC101107541	non-ECM	-1.857
PTPN6	non-ECM	-1.8311
SMC1A	non-ECM	-1.8104
KLHL41	non-ECM	-1.7947

Upregulated Gene	Association	Log(2) FC
PLTP	non-ECM	1.5672

B.

Total number of DEPs = 323

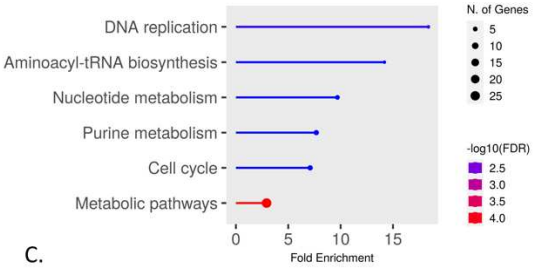

C.

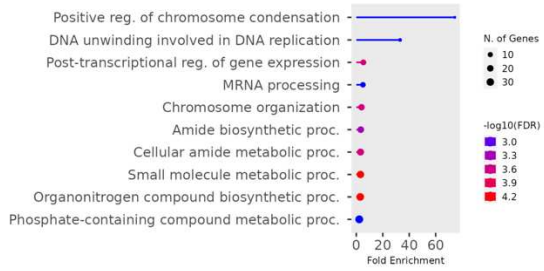

D.

Figure 4.7. OP group baseline vs. 9-month protein analysis. A total of 323 DEPs were identified (322 downregulated, 1 upregulated). No ECM DEPs were identified. A) Volcano plot of non-ECM associated proteins using a paired one-way ANOVA in MetaboAnalyst (no significant ECM-associated proteins). B) Top 10 downregulated and all upregulated proteins in MetaboAnalyst with log(2) fold change. C) Top enriched KEGG pathways. D) Top 10 GO Biological Processes.

A.

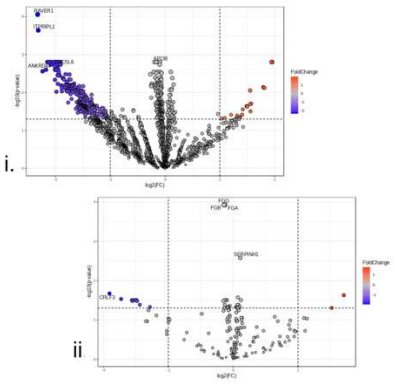

B.

Downregulated Gene	Association	Log(2) FC
RAVER1	non-ECM	-2.3277
ITPRIPL1	non-ECM	-2.3165
PPP2R5C	non-ECM	-2.2387
NCAPD2	non-ECM	-2.1744
DOCK2	non-ECM	-2.1501
PLA2G4A	non-ECM	-2.1228
ANKRD44	non-ECM	-2.0876
SMC2	non-ECM	-2.0868
BPI	non-ECM	-2.0325
W5PMY9_SHEEP	non-ECM	-2.0323

Upregulated Gene	Association	Log(2) FC
NPR3	non-ECM	1.9512
RCN3	non-ECM	1.9435
W5PJ13_SHEEP	non-ECM	1.8104
PLS1	non-ECM	1.7926
MYH15	ECM	1.7075
RYR1	non-ECM	1.5707
ACSM1	non-ECM	1.5588
CAMK2A	non-ECM	1.5519
P4HA1	non-ECM	1.5482
GOLGB1	ECM	1.5200

Total number of DEPs = 401

C.

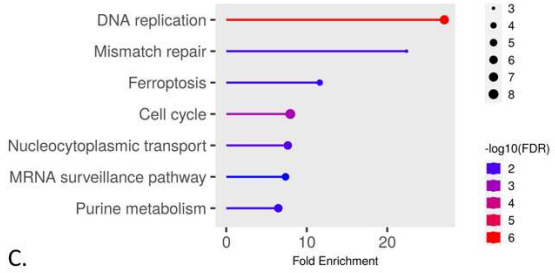

D.

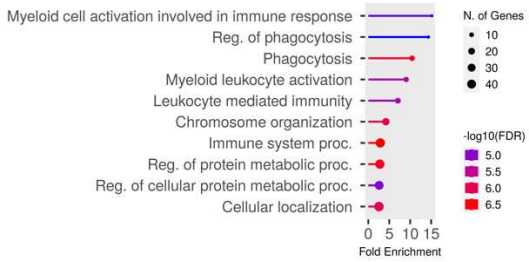

Figure 4.8. OP group baseline vs. 12-months protein analysis. A total of 388 non-ECM associated DEPs were identified (367 downregulated, 21 upregulated), and 13 ECM DEPs were identified (12 downregulated, 1 upregulated). A) Volcano plots of (i) non-ECM associated proteins and (ii) ECM proteins using a paired one-way ANOVA in MetaboAnalyst. B) Top 10 downregulated and upregulated proteins in MetaboAnalyst with log(2) fold change. C) Top enriched KEGG pathways. D) Top 10 GO Biological Processes.

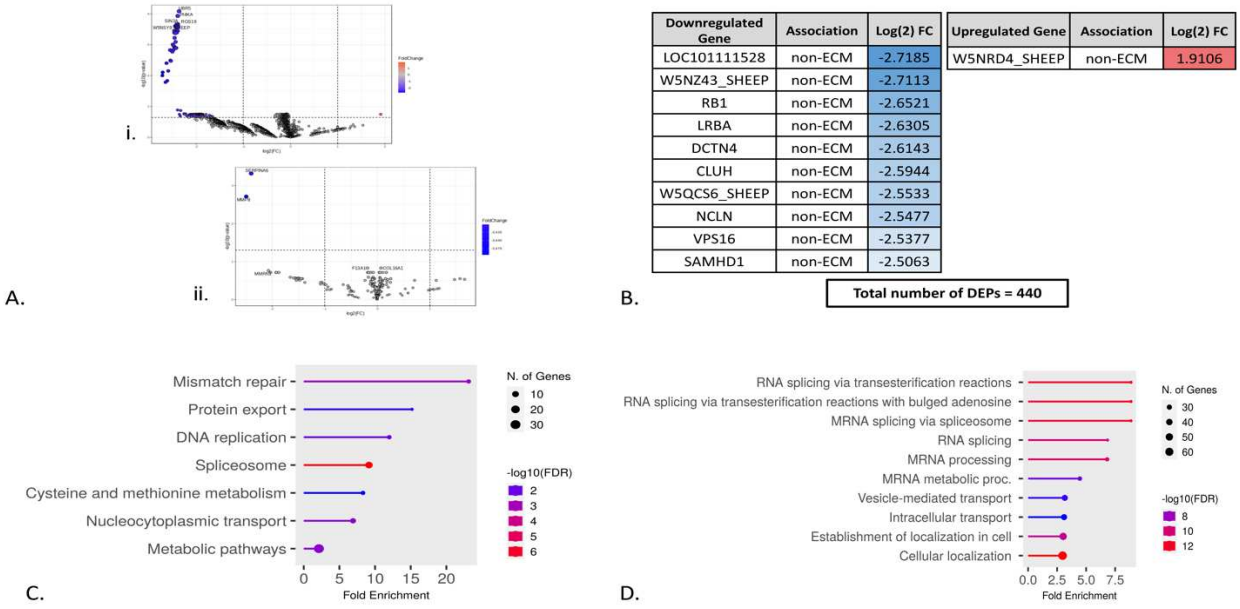

Figure 4.9. Figure. Control group baseline vs. 12-months protein analysis. A total of 438 non-ECM associated DEPs were identified (437 downregulated, 1 upregulated), and 2 ECM DEPs were identified (2 downregulated, 0 upregulated). A) Volcano plots of (i) non-ECM associated proteins and (ii) ECM proteins using a paired one-way ANOVA in MetaboAnalyst. B) Top 10 downregulated and all upregulated proteins in MetaboAnalyst with log(2) fold change. C) Top enriched KEGG pathways. D) Top 10 GO Biological Processes.

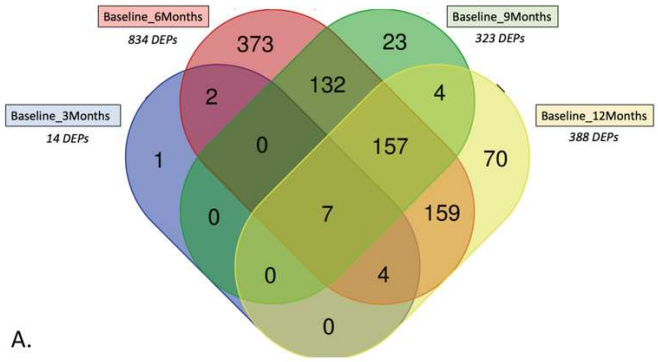

A.

B.

Gene	Protein
CTR9	CTR9 homolog, Paf1/RNA polymerase II complex component
INPP5D	phosphatidylinositol 3,4,5-trisphosphate 5-phosphatase 1
CDK6	cyclin dependent kinase 6
PPP2R5C	protein phosphatase 2 regulatory subunit B'gamma
NUP133	nucleoporin 133
ITPRIPL1	Condensin complex subunit 2
W5PH60_SHEEP	tRNA-binding domain-containing protein

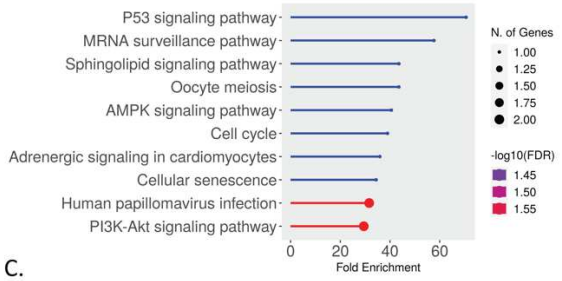

C.

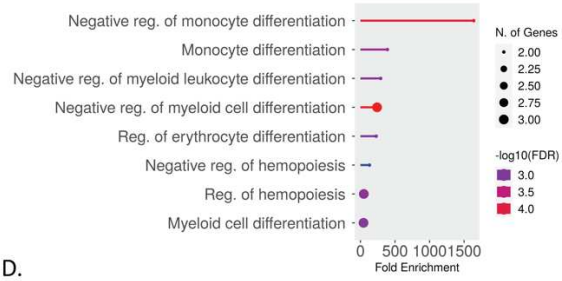

D.

Figure 4.10. Venn diagram of OP group differentially expressed proteins (DEPs) at all time points compared to baseline. B) Protein identifications of the 7 DEPs shared across all OP group time point comparisons. C) Top 10 enriched KEGG pathways of the 7 shared OP group DEPs. D) Top 10 enriched GO Biological Processes of the 7 shared OP group DEPs.

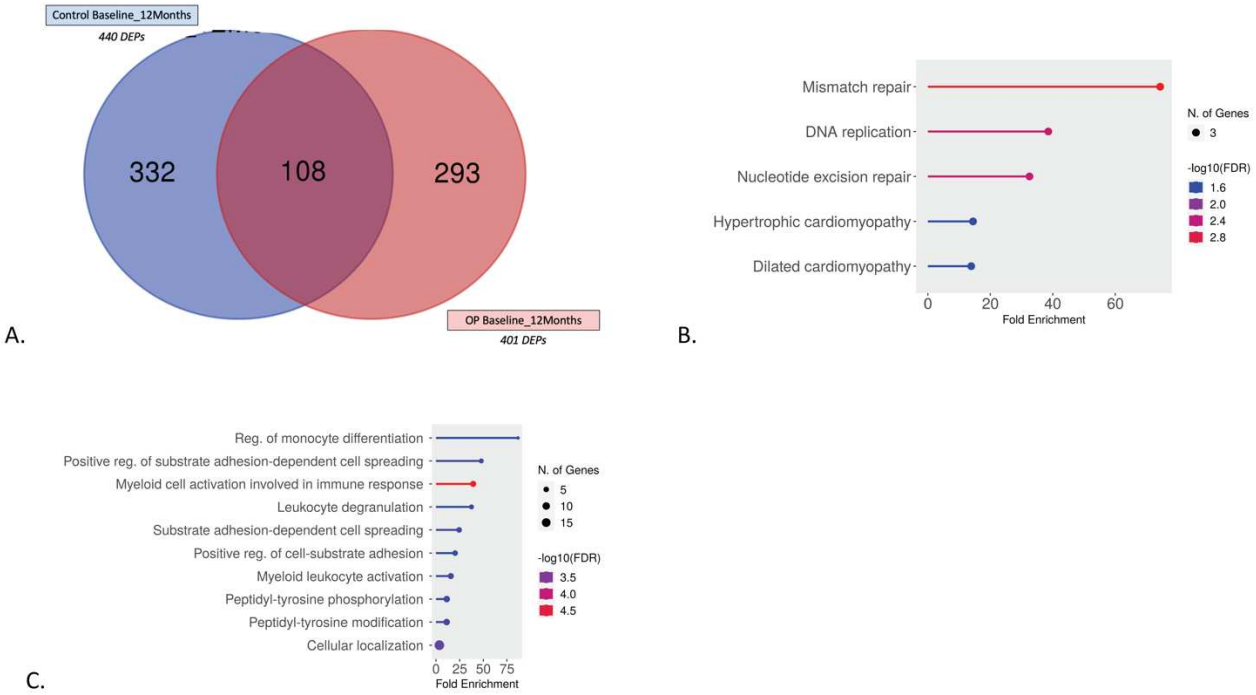

Figure 4.11. Venn diagram of OP group and control group differentially expressed proteins (DEPs) at 12-months to baseline. B) Top 10 enriched KEGG pathways of the 108 shared DEPs between OP and control groups at 12-months. C) Top 10 enriched GO biological processes of the 108 shared DEPs between OP and control groups at 12-months.

4.6 References

1. Feng, X., *Chemical and biochemical basis of cell-bone matrix interaction in health and disease.* Current chemical biology, 2009. **3**(2): p. 189-196.
2. Aibar-Almazán, A., et al., *Current status of the diagnosis and management of osteoporosis.* International journal of molecular sciences, 2022. **23**(16): p. 9465.
3. Liu, D., et al., *Local Treatment of Osteoporotic Sheep Vertebral Body With Calcium Sulfate for Decreasing the Potential Fracture Risk: Microstructural and Biomechanical Evaluations.* Clin Spine Surg, 2016. **29**(7): p. E358-64.
4. Alcorta-Sevillano, N., et al., *Deciphering the relevance of bone ECM signaling.* Cells, 2020. **9**(12): p. 2630.
5. Licini, C., C. Vitale-Brovarone, and M. Mattioli-Belmonte, *Collagen and non-collagenous proteins molecular crosstalk in the pathophysiology of osteoporosis.* Cytokine & growth factor reviews, 2019. **49**: p. 59-69.
6. Dole, N.S., et al., *Osteocyte-intrinsic TGF-β signaling regulates bone quality through perilacunar/canalicular remodeling.* Cell reports, 2017. **21**(9): p. 2585-2596.
7. Visweswaran, M., et al., *Multi-lineage differentiation of mesenchymal stem cells–To Wnt, or not Wnt.* The international journal of biochemistry & cell biology, 2015. **68**: p. 139-147.
8. Jiang, X., et al., *Development of efficient protein extraction methods for shotgun proteome analysis of formalin-fixed tissues.* Journal of proteome research, 2007. **6**(3): p. 1038-1047.

9. Al-Ansari, M.M., et al., *Proteomics profiling of osteoporosis and osteopenia patients and associated network analysis.* International Journal of Molecular Sciences, 2022. **23**(17): p. 10200.

10. Chaput, C.D., et al., *A proteomic study of protein variation between osteopenic and age-matched control bone tissue.* Experimental Biology and Medicine, 2012. **237**(5): p. 491-498.

11. Mellacheruvu, D., et al., *The CRAPome: a contaminant repository for affinity purification–mass spectrometry data.* Nature methods, 2013. **10**(8): p. 730-736.

12. Shao, X., et al., *MatrisomeDB: the ECM-protein knowledge database.* Nucleic acids research, 2020. **48**(D1): p. D1136-D1144.

13. Willforss, J., A. Chawade, and F. Levander, *NormalyzerDE: online tool for improved normalization of omics expression data and high-sensitivity differential expression analysis.* Journal of proteome research, 2018. **18**(2): p. 732-740.

14. Chong, J. and J. Xia, *MetaboAnalystR: an R package for flexible and reproducible analysis of metabolomics data.* Bioinformatics, 2018. **34**(24): p. 4313-4314.

15. Ge, S.X., D. Jung, and R. Yao, *ShinyGO: a graphical gene-set enrichment tool for animals and plants.* Bioinformatics, 2020. **36**(8): p. 2628-2629.

16. Rupp, M., et al., *Large Animal Model of Osteoporotic Defect Healing: An Alternative to Metaphyseal Defect Model.* Life (Basel), 2021. **11**(3).

17. Coelho, C.A., et al., *Evaluation of hematology, general serum biochemistry, bone turnover markers and bone marrow cytology in a glucocorticoid treated ovariectomized sheep model for osteoporosis research.* An Acad Bras Cienc, 2020. **92**(4): p. e20200435.

18. Osterhoff, G., et al., *Bone mechanical properties and changes with osteoporosis.* Injury, 2016. **47 Suppl 2**(Suppl 2): p. S11-20.

19. Zebaze, R.M., et al., *Intracortical remodelling and porosity in the distal radius and post-mortem femurs of women: a cross-sectional study.* The Lancet, 2010. **375**(9727): p. 1729-1736.

20. Cabrera, D., et al., *Effects of short-and long-term glucocorticoid-induced osteoporosis on plasma metabolome and lipidome of ovariectomized sheep.* BMC musculoskeletal disorders, 2020. **21**: p. 1-13.

21. Yu, T., et al., *p53 plays a central role in the development of osteoporosis.* Aging (Albany NY), 2020. **12**(11): p. 10473.

22. Ogasawara, T., et al., *Role of cyclin-dependent kinase (Cdk) 6 in osteoblast, osteoclast, and chondrocyte differentiation and its potential as a target of bone regenerative medicine.* Oral Science International, 2011. **8**(1): p. 2-6.

23. Wang, L., et al., *Protein phosphatase 2A as a new target for downregulating osteoclastogenesis and alleviating titanium particle-induced bone resorption.* Acta Biomaterialia, 2018. **73**: p. 488-499.

24. Xi, J.C., et al., *The PI3K/AKT cell signaling pathway is involved in regulation of osteoporosis.* J Recept Signal Transduct Res, 2015. **35**(6): p. 640-5.

25. Qian, G.F., et al., *PPWD1 is associated with the occurrence of postmenopausal osteoporosis as determined by weighted gene co-expression network analysis.* Molecular medicine reports, 2019. **20**(4): p. 3202-3214.

26. Hong, J., et al., *Identification of the specific microRNAs and competitive endogenous RNA mechanisms in osteoporosis.* J Int Med Res, 2020. **48**(10): p. 300060520954722.

27. Broersen, L.H., et al., *Adrenal insufficiency in corticosteroids use: systematic review and meta-analysis.* The Journal of Clinical Endocrinology & Metabolism, 2015. **100**(6): p. 2171-2180.

28. Yang, K., J. Li, and L. Tao, *Purine metabolism in the development of osteoporosis.* Biomed Pharmacother, 2022. **155**: p. 113784.

29. Wei, Z., et al., *Metabolomics coupled with pathway analysis provides insights into sarco-osteoporosis metabolic alterations and estrogen therapeutic effects in mice.* Biomolecules, 2021. **12**(1): p. 41.

30. Pignolo, R.J., S.F. Law, and A. Chandra, *Bone aging, cellular senescence, and osteoporosis.* Journal of Bone and Mineral Research Plus, 2021. **5**(4): p. e10488.

31. Li, T., et al., *Proteome Informatics in Tibetan Sheep (Ovis aries) testes suggest the crucial proteins related to development and functionality.* Frontiers in Veterinary Science, 2022. **9**: p. 923789.

32. Wang, X., et al., *Proteomic analyses of sheep (ovis aries) embryonic skeletal muscle.* Scientific Reports, 2020. **10**(1): p. 1750.

CHAPTER 05: CONCLUSIONS AND FUTURE DIRECTIONS

Osteoporosis poses a significant burden to our worldwide community. Strategies to adequately prevent and treat fragility fractures are in high demand as the aging population continues to grow. With new pharmacologic interventions comes the need for appropriate and clinically relevant preclinical animal models. While both small and large animals have been shown to be effective models for osteoporosis, the sheep offers researchers the ability to perform long-term and robust studies to evaluate bone quality and strength. We performed a multi-aim *in vivo* study to fill in knowledge gaps of bone loss pathophysiology in the sheep model of osteoporosis. Through these aims, we comprehensively characterized the bone, systemic, and molecular changes associated with osteoporosis induction in a sheep model.

While all the three study aims differed in objectives, their results were ultimately linked together by our sixteen study animals. Initially, we observed clinical bone loss in the lumbar spine and tibia of our osteoporotic group compared with controls through use of DXA bone scanning. We also observed changes to bone microarchitecture, through microCT scanning of iliac crest biopsies, indicative of osteoporotic bone loss in the experimental group, including trabecular thinning and a decrease in bone volume. Subsequently, we also were able to confirm the use of QCT as an alternative method to DXA to measure bone density in our sheep model, which was able to provide a more targeted assessment of trabecular bone than capable on DXA. We were then finally able to observe the iliac crest bone at a more microscopic level through histology, noting decreasing trabecular area in our osteoporotic animals, which was in line with our microCT findings of the same biopsies. Concurrent with all these changes to the bone density

and microarchitecture, we observed clinical systemic changes occurring in these animals, as well. At the time point when animals had received the longest duration of high-dose corticosteroids (~3-months), several differences in hematology and serology values were noted to be impacted in the osteoporotic group compared to controls. These animals showed clinical pathology levels indicating dysregulation to white blood cells, platelets, electrolyte levels, kidney proteins, phosphorus levels, and liver enzymes. Once the final taper dose of steroids was administered (~6-months), we saw changes in red blood cells and iron levels. We also noted continued increases in serum phosphorus, kidney, and liver enzymes that had carried over from the 3-month time point. As all of these dysregulations leveled out to comparable control levels by the completion of the study, we attributed these acute systemic changes primarily to the administration of high dose corticosteroids. Finally, after being able to see both the impact of osteoporosis development on the bone and systemically in the animals, we began the process of uncovering a molecular answer to these osteoporotic changes using proteomics. We revealed significant protein changes in the bone of our osteoporotic animals across time over the course of model progression. While we observed changes in phosphorus and white blood cell levels in the blood, we simultaneously saw enrichment of signaling pathways involved in phosphate metabolism, monocyte and leukocyte differentiation at the same time points (3 and 6-months). When comparing proteins between all time points, we observed changes in pathways associated with aging and cell cycle. These may be key mechanisms driving long-term changes in our sheep model on a molecular level.

Several findings from this study provoked additional questions that require further investigation in the future. One of the oddities we observed in this study was the minimal change

in circulating estradiol levels as compared to healthy controls. While we would expect that removal of the ovaries would prevent further significant endogenous estrogen synthesis, this did not appear to be the case in the sheep. Since other studies have also reported on this finding in sheep, we would like to further investigate why estradiol does not decrease following ovariectomy in the sheep. In particular, we would like to explore other sources of extragonadal estrogen and how they might impact bone turnover without the presence of ovarian production. The proteomic results from this study are just the tip of the iceberg when it comes to uncovering the mechanism of bone loss we observed in our osteoporotic animals. In the future, we will plan to investigate pathway changes briefly touched upon in Chapter 4. For example, we would like to understand how the dysregulation of chromosome condensation and DNA replication pathways connect to the bone changes observed in the same animals at the same time points. We have now opened the door to possibilities of future experimentation, whether through *in vitro* experimentation to investigate one of the seven shared proteins presented in Chapter 4, or through *in vivo* mouse knockout studies to investigate the impact of inflammatory pathway dysregulation on bone loss. If we and others continue to add to the field of sheep -omics, we could one day even develop a transgenic large animal model that more clinically manifests the human condition of osteoporosis, allowing researchers to continue to run robust bone quality and toxicity studies for the advancement of novel therapeutics to treat and prevent osteoporosis.

In keeping with our overall objective to report on the effects of osteoporosis development more comprehensively in sheep, one of the other categories that has been severely underrepresented in the literature is the exploration of co-morbidities associated with osteoporosis, as discussed in Chapter 1. Utilizing tissues explanted from animals on this study,

we will plan to perform preliminary *in vitro* research to determine the impact of our model on the development of other associated conditions, including intervertebral disc degeneration, osteoarthritis, and tendinopathy. Any potential findings could inform future use of this sheep model and extend its use into other age-associated pathologies.

In summary, results from this study both confirmed the work of previous preclinical osteoporosis studies as well as further characterized certain novel aspects of our large animal model of osteoporosis. A more comprehensive understanding of our animal models will inform appropriate study design and result in more advanced scientific inquiry.

Appendix 1 – Hematology Values and Comparisons

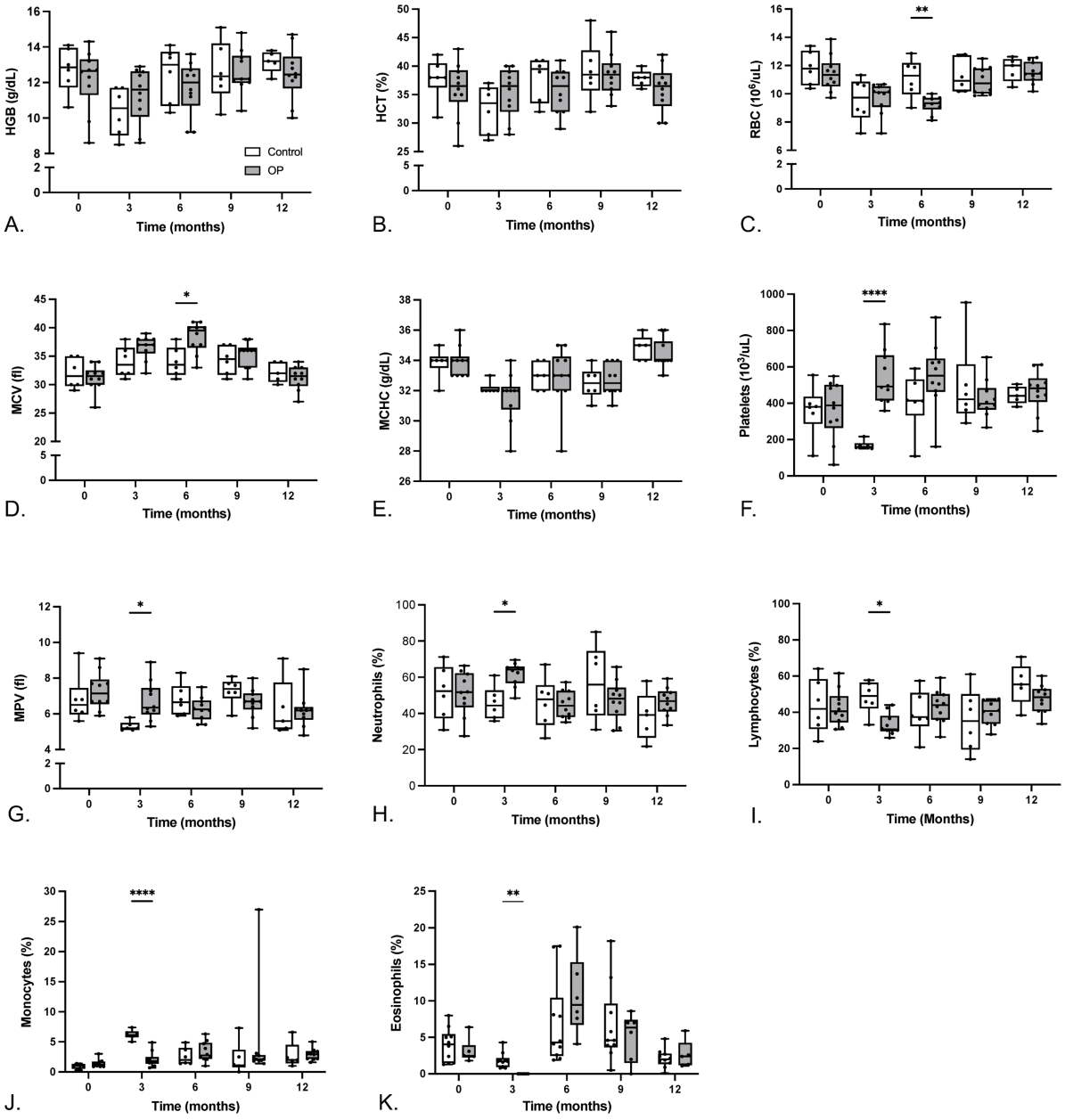

Hematology results for all study animals at baseline, 3, 6, 9, and 12 months. A) Hemaglobin (HGB). B) Hematocrit (HCT). C) Red blood cells (RBC). D) Mean corpuscular volume (MCV). E) Mean corpuscular hemoglobin concentration (MCHC). F) Platelet count. G) Mean platelet volume (MPV). H) Percentage of neutrophils. I) Percentage of lymphocytes. J) Percentage of monocytes. K) Percentage of eosinophils. Significance indicators: *$p<0.05$, **$p<0.01$, ****$p<0.0001$.

Appendix 2 – Serology Values and Comparisons

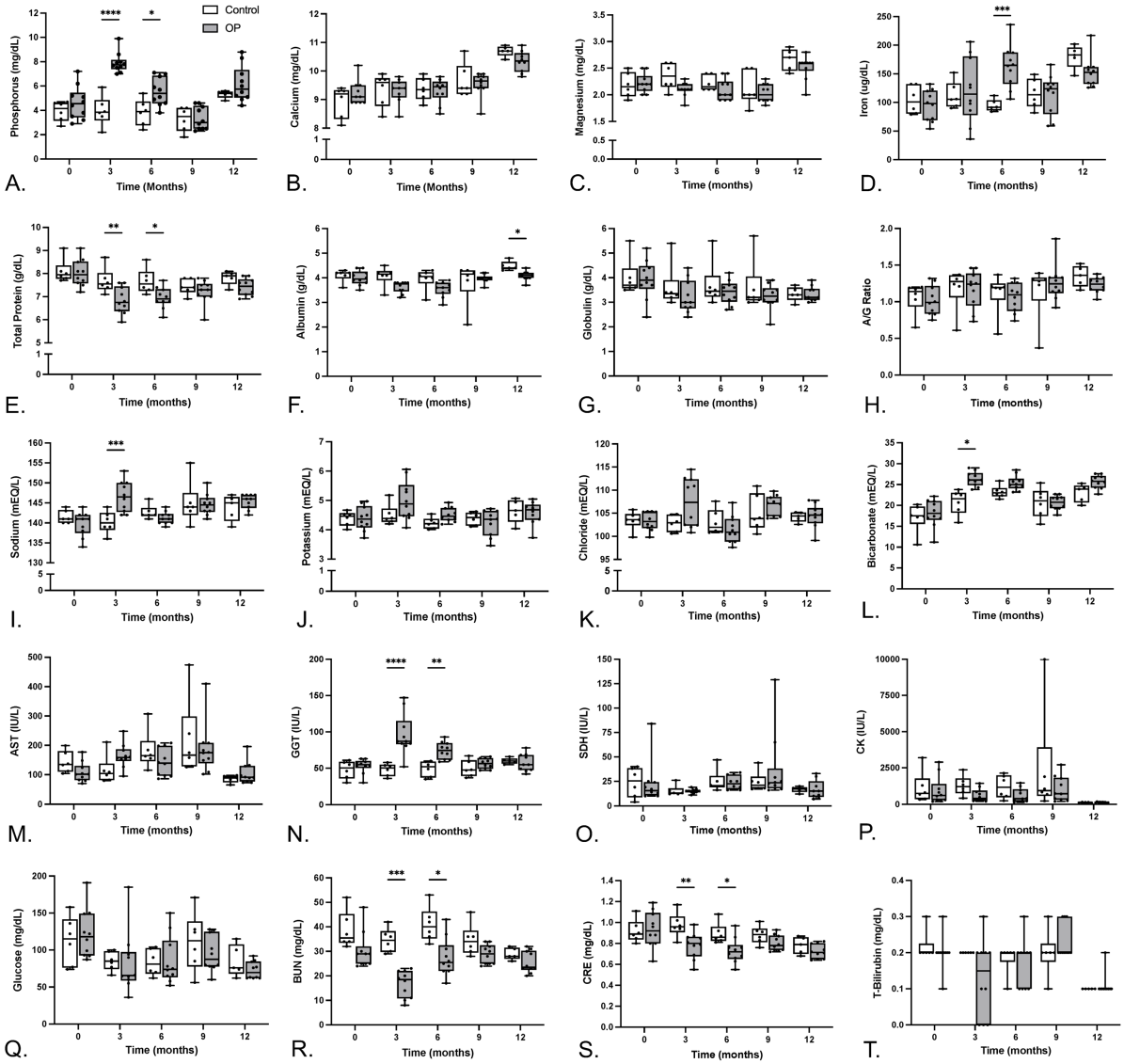

Serology results for all study animals at baseline, 3, 6, 9, and 12 months. A) Phosphorus. B) Calcium. C) Magnesium. D) Iron. E) Total protein. F) Albumin. G) Globulin. H) Albumin/globulin ratio (A/G). I) Sodium. J) Potassium. K) Chloride. L) Bicarbonate. M) Aspartate transferase (AST). N) Gamma-glutamyl transferase (GGT). O) sorbitol dehydrogenase (SDH). P) Creatinine kinase (CK). Q) Glucose. R) Blood urea nitrogen (BUN). S) Creatinine (CRE). T) Total bilirubin (T-bilirubin). Significance indicators: *p<0.05, **p<0.01, ***p<0.001, ****p<0.0001.